Targeting the Cell Cycle in Oral, Head, and Neck Squamous Cell Carcinoma

Hakan Y. Gem

A dissertation

submitted in partial fulfillment of the

requirements for the degree of

Doctor of Philosophy

University of Washington

2022

Reading Committee:

Bruce E. Clurman, Chair

Raymond J. Monnat Jr.

Dolphine Oda

Program Authorized to Offer Degree:

Oral Health Sciences

University of Washington

Abstract

Targeting the Cell Cycle in Oral, Head, and Neck Squamous Cell Carcinoma

Hakan Y. Gem

Chair of the Supervisory Committee:

Dr. Bruce E. Clurman, M.D., Ph.D.

Executive Vice President and Deputy Director

Professor, Divisions of Clinical Research and Human Biology

Fred Hutchinson Cancer Center

Professor, Departments of Medicine & Oral Health Sciences

University of Washington

A fundamental hallmark of cancer is the cell's ability to sustain proliferative signaling thereby deregulating the cell cycle. Uncovering the molecular changes that inappropriately drive proliferation has allowed researchers to specifically target cancer cell vulnerabilities related to cell cycle control. An important class of proteins that contribute to this control are the cyclins and cyclin-dependent kinases (CDKs). Cancer cell mutations that lead to aberrant activation of cyclin-CDKs are common in many cancers including oral, head, and neck squamous cell carcinomas (OHNSCCs). As the sixth most common cancer worldwide, OHNSCC represents a

key opportunity for researchers to study the application of targeted inhibitors to cell cycle control. In my dissertation, I explore the diverse roles that cyclin-CDKs play not only in driving cancer cell proliferation, but also in how they might contribute to therapeutic resistance of targeted inhibitors. Specifically, we employed a genome-wide CRISPR-Cas9 screen to reveal mediators of replication stress failure in cells with constitutively active CDK2 complexes. Data from this screen implicated CDK2 in activating apoptotic signaling. However, rather than contributing to apoptosis, CDK2 may instead activate non-canonical functions of apoptotic signaling molecules to initiate senescence. While our screen level data strongly suggested the involvement of apoptotic signaling in constitutively active CDK2 cells experiencing replication stress, validation of individual hits were unable to confirm this finding. We also investigated the role of cyclin E in conferring CDK4/6 inhibitor resistance in OHNSCC. Our data show that contrary to the established view that high cyclin E activity serves as a bypass mechanism to this class of drug, it is actually insufficient on its own phosphorylate pRb in lieu of CDK4/6 activity. Finally, we applied a chemical genetic approach refined in our lab to conduct a proteomic screen for the discovery of novel CDK6 substrates. With this technique, we found a host of novel candidate CDK substrates and validated one of these candidates, CDC45, in-vitro. Together, these studies have expanded our knowledge of cyclin-CDK biology while also providing an essential clarification in how these complexes contribute to therapeutic resistance. These insights will serve as the basis for future investigations on cell cycle deregulation and the appropriate application of targeted therapies.

Table of Contents

List of Figures

List of Tables

Acknowledgements

I would first like to acknowledge my mentor, Bruce Clurman, for providing me the opportunity to work in his lab as a graduate student. Despite my inexperience in the field, Bruce put his trust in me while also providing the critical guidance necessary for any graduate student to succeed. As deputy director of the Fred Hutch Cancer Center, Bruce is constantly in demand, however, his dedication to science, mentorship, and the success of his lab members has been resolute the entire time I've known him. I am grateful for the projects he guided me through and even more appreciative of the unwavering support he has shown for my career goals and ambitions.

I am honored to have been co-mentored by an outstanding dissertation advisory committee. Denise Galloway is a pioneer in many respects, and she was incredibly generous with her time, thoughtful with her questions during our meetings, and pushed me to become a more meticulous and detail-oriented scientist. Patrick Paddison was critical for my development during my first year in the Clurman lab and provided extensive resources and time to help guide me through a complex genomic screen. Raymond Monnat provided many insightful comments during our committee meetings and email exchanges while always maintaining a positive outlook and an emphasis on how my work fits into the "big picture" – a critical skill for all young scientists to develop. I am also thankful for his involvement in our collaborations with Julia Sidorova and Hee Yeon Kim. Finally, Dolphine Oda served as my graduate student representative and as always demonstrated her tireless dedication to the success of her students. I feel beyond fortunate to have had such an incredible group of scientists guiding me on this journey.

I cannot say enough about the amazing people of the Clurman lab who have been a joy to work with over the last four years. A huge thank you to Jherek Swanger who taught me many fundamental lab techniques while patiently answering my seemingly endless list of questions. My brilliant bay mate, Markus Welcker, was a boundless source of information and inspiration for so many of my experiments, and I will dearly miss our conversations and time spent together in the lab. I am so thankful to have met our post-doctoral fellow, Ahmed Diab, who I consider the older brother I never had. Ahmed was the first person I worked closely with at the Hutch, and I am forever in his debt for the skills, theory, and lessons he has so generously shared with me over the years. Another big thank you to our staff scientists Shlomo Handeli and Yong Chi for their great insights and helpful feedback on my work in and out of lab meetings, particularly to Yong who

helped me through one of the major projects in my dissertation. Thank you to Nayanga Thirimanne who graduated from our lab just last year for fearlessly showing me how to achieve the major milestones that every PhD student must eventually face. Thank you to Yasser Hussaini for always willing to lend me a helping hand on my experiments. Finally, thank you to all the administrators and past members of the Clurman lab who all played instrumental roles in my development including Stuart Tenney, Will Hallauer, Bonnie Kraskouskas, Alyssa Michaels, Heuijoon Park, Kaleb Smith, and Grace Zhou.

I would also like to thank all of the wonderful people who make up the Oral Health Sciences department at the University of Washington School of Dentistry. First and foremost, I would like to acknowledge our former director, Richard Presland, for encouraging me to pursue the DDS/PhD route and for providing all of the necessary guidance and insights to help me through it. Thank you to Kathy Hobson who always demonstrated the utmost professionalism with her timely responses to my barrage of emails and questions over the years. And a big thank you to our new leadership, both Robert Cornell and Lora Brewsaugh, who flawlessly guided me through the final six to eight months of my time in the program.

I am so grateful for all the talented folks who work in the shared resources cores at the Hutch. Thank you to those in the genomics and bioinformatics core including Elizabeth Jensen, Andy Marty, and Ryan Bassom. Thank you to Brian Raden, Amira Davis, Ben Janoschek, Rebecca Reeves, and Nate Colven for your incredible patience and help with my flow cytometry experiments. And finally, a big thank you to Lena Schroeder and particularly Jin Meng in cellular imaging for her amazing contributions in our live imaging project.

I would be remiss if I did not express my gratitude for the brilliant surgeon-scientists, Eddie Mendez, who tragically passed away in 2018. Eddie was a young, up-and-coming PI who gave me my first opportunity to work here at the Hutch as a summer intern in his lab. Despite his busy schedule, he agreed to take me in, and it is safe to say that I would not be here if it weren't for his generosity and willingness to help a budding scientist find his footing in this competitive field.

Finally, thank you to my incredible cast of friends and family who have energized and supported me throughout every step of my career. Thank you to my incredible partner, Jennifer Tran, who never hesitated to provide words of encouragement and was an endless source of positivity and motivation even in the most difficult of times. I would not be the man I am today

without my stepfather, Tuna Ertemalp, and my father, Ilhan Yagiz. I am so thankful for both of these role models who have taught me the importance of hard work, perseverance, and accountability. And of course, my deepest gratitude for the single most important individual in my life, my mother, Dr. Tulay Kent, DDS. As the only constant since I was born, she was the light who guided me through my childhood and into adulthood with poise, love, and compassion. Even after she passed away from cancer in 2015, she continues to be my biggest inspiration, and for that I am forever grateful.

Dedication

In memory of my loving mother, Tülay Kent

Chapter 1. Introduction

1.1 Cell Cycle Overview

The eukaryotic cell cycle is a series of highly coordinated molecular events that ensures the production of two genetically identical daughter cells from a single mother cell (Figure 1.1)[1,2]. The cell cycle is composed of two discrete stages: interphase and M phase (mitosis). Within interphase there are three further subdivisions: G1 (Gap 1), S (DNA Synthesis), and G2 (Gap 2). In G1, the cell grows in size while producing the necessary proteins required for DNA synthesis. In the subsequent S phase, cellular DNA is accurately replicated to ensure identical copies for both daughter cells. Finally, in G2, the newly replicated DNA is checked for damage, repaired as needed, and the cell continues to grow prior to entry into M phase. Once the cell enters M phase, chromosomes are tightly condensed, aligned, and segregated to opposite ends of the cell which is followed by cytokinesis, the separation of two identical daughter cells thus marking the end of the cell cycle.

1.2 Cyclins, Cyclin-Dependent Kinases, and Cell Cycle Checkpoints

Between each of the cell cycle phases exists a checkpoint (also referred to as a restriction point) to guard against aberrant cell cycle progression[3–5]. The primary mediators of the cell cycle are a family of proteins known as the cyclins and cyclin-dependent kinases (CDKs), and they act on or in between these checkpoints to coordinate cell cycle kinetics[6–8].

1.2.1 Cyclins and CDKs

There are four primary types of cyclins (A, B, D, & E), and their expression is modulated throughout the cycle[6–8]. Transcription of the D-type cyclins begins in G1, followed by the expression of cyclin E in late G1 and through the G1/S transition. As cells progress through S-phase and into G2, cyclin A becomes the predominant cyclin followed by cyclin B once cells

transition to mitosis. Each cyclin exerts its effect by binding to its respective CDK to form an active complex which can then phosphorylate its specific substrates. In general, expression of the different CDKs is kept constant throughout the cell cycle while cyclin levels fluctuate through transcriptional activation and targeted degradation at the points specified above. These are the canonical cyclin-CDK complexes: cyclin D-CDK4, cyclin D-CDK6, cyclin E-CDK2, cyclin A-CDK2, cyclin A-CDK1, and cyclin B-CDK1[8].

Several layers of regulation act upon cyclin-CDK complexes to ensure they are activated and inactivated at the appropriate times. For example, for full activation of CDK1 and/or CDK2, the CDK-activating complex (CAK) must phosphorylate the CDK on a threonine residue, T160, found in the surface activation loop[6–9]. Furthermore, inhibitory phosphorylations on T14 and Y15 by the Wee1 and Myt1 kinases, respectively, must be removed by the Cdc25 phosphatase[10]. It is in this state when A) the CDK is in complex with its cyclin, B) the CDK is phosphorylated on T160, and C) inhibitory phosphorylations on T14 and Y15 are removed that the cyclin-CDK complex is active and may target its own substrates for phosphorylation.

Another layer of regulation is found within the family of CDK inhibitors (CKIs) known as the INK4 and CIP/KIP family of proteins[7,11,12]. The INK4 family consists of the proteins $p15^{INK4a}$, $p16^{INK4b}$, $p18^{INK4c}$, and $p19^{INK4d}$ whose roles are to specifically inhibit CDKs 4 and 6 in the event that a G1 arrest is initiated[13]. The CIP/KIP family consists of the proteins $p21^{cip1/waf1}$, $p27^{kip1}$, and $p57^{kip2}$ which are capable of inhibiting a wider array of CDKs including CDK1 and CDK2[14,15]. Interestingly the CIP/KIP proteins have also been shown to stabilize and activate cyclin D-CDK4/6 complexes during G1. The expression of these inhibitors is typically induced when the cell cycle must be arrested in the event of, for example, excessive DNA damage requiring repair. Specific inhibitors and their actions on cyclin-CDK complexes will be discussed in further detail below.

1.2.2 G1/S checkpoint

The classical model for the G1/S transition first reported in 1974 defines a restriction point in late G1 where the cell is irreversibly committed to enter and complete S phase, even upon discontinuation of mitogen stimulation[3]. This restriction point relies on the assumption that all cells entering G1 have unphosphorylated pRb through the action of protein phosphatase 1 (PP1) in the previous round of mitosis[4,16]. As cells approach the G1/S transition, CDKs 4 and 6 partner with one of three D-type cyclins, cyclin D1-3, to form an active complex whose primary role is to phosphorylate pRb. This initial pRb phosphorylation releases the E2F transcription factor resulting in the transcription of S-phase promoting genes such as *CCNE1/2* (Figure 1.2). The subsequent increase in cyclins E1 and E2 promotes the formation of active cyclin E-CDK2 complexes, which go on to further phosphorylate pRb pushing the cell into S-phase. This positive feedback loop results in the hyperphosphorylation and complete inactivation of pRb thereby allowing the E2F family of transcription factors to express their full array of S-phase promoting genes. If, for example, CDKs 4 and 6 are inhibited pharmacologically or by the native INK4 family of CDK inhibitors, cells will typically fail to reach the restriction point and exit the cell cycle into a state of quiescence or senescence. Technological advances since the 1970s have allowed researchers to elaborate on the classical G1/S restriction point resulting in many proposed updates to this model[17–21]. These updates include new three new "commitment points" that can extend as far back as mother cell mitosis and impact daughter cell G1/S transition (Figure 1.3).

1.2.3 Intra-S checkpoints

To ensure accurate DNA replication, cells may activate checkpoints during S-phase in order to prevent excessive damage formation[22]. DNA damage can occur from both intrinsic and extrinsic sources such as reactive oxygen species or UV radiation. Depending on the type of lesion

and extent of damage, cells initiate specific repair pathways including base excision repair (BER), nucleotide excision repair (NER), and mismatch repair for single-strand defects and non-homologous end joining (NHEJ) or homologous recombination (HR) for double-strand breaks[23,24]. There are two primary S-phase kinases responsible for initiating intra-S checkpoints and coordinating DNA damage response (DDR): ataxia telangiectasia mutated (ATM) and ATM/Rad3-related protein (ATR). ATM is typically activated in response to double-strand breaks while ATR is activated in response to a more diverse set of DNA lesions often resulting in replication protein A (RPA) coated single-stranded DNA. When either of these kinases are activated, they subsequently phosphorylate and activate the two effector kinases, Chk1 and Chk2. These two proteins have many overlapping roles in mammalian cells, however, Chk1 activation is primarily mediated by ATR and Chk2 activation is primarily mediated by ATM[22–24]. Upon activation, Chk1 and Chk2 target multiple substrates for phosphorylation such as Cdc25, p53, Rad51, among others to inhibit cell cycle progression and promote DDR. Cdc25 is a phosphatase responsible for maintaining CDK1/2 activity during S-phase by removing inhibitory phosphorylations on those kinases[10]. Chk1 phosphorylation of Cdc25 targets the protein for ubiquitin-mediated degradation thereby resulting in the accumulation of inhibitory phosphorylations on CDK1/2. Once the cell is arrested through the action of Chk1 and/or Chk2, the cell either repairs DNA damage and completes S-phase or initiates apoptosis in cases of excessive damage thus preventing the propagation of faulty DNA to future generations.

1.2.4 S/G2 checkpoint

Recently, an S/G2 checkpoint was described implicating ATR in regulating entry into G2 from S phase, distinct from its role as an intra-S phase checkpoint kinase[25]. By measuring ATR activity and pFOXM1 levels throughout S-phase and into G2, Saldivar *et al*. demonstrate a distinct

and causative relationship between the two. When ATR activity naturally dropped at the end of S-phase, this resulted in a switch-like phosphorylation of FOXM1 by CDK1 suggestive of a regulatory checkpoint that defines the transition from S to G2. ATR inhibition (ATRi) of S-phase cells demonstrated increasing levels of phospho-FOXM1 and experienced accelerated mitotic entry while ATR inhibition during G2 did not affect the rate of mitotic entry. Furthermore, ATRi cells experienced under-replicated DNA along with increased DNA damage. Thus, the activity of ATR was shown to protect cells from premature entry into G2 and M from S-phase.

1.2.5 G2/M checkpoint

The G2/M checkpoint represents a critically important step that ensures DNA damage is sufficiently repaired prior to mitosis, and this step relies heavily on cyclin B-CDK1 activity[26,27]. Throughout G2, cyclin B slowly accumulates and forms a complex with CDK1. These cyclin B-CDK1 complexes are actively exported from the nucleus until the cell is ready to transition into M phase. Cyclin B-CDK1 is also rendered inactive by inhibitory phosphorylations at Y15 and T14 by the Wee1 and Myt1 kinases, respectively. To surpass the G2/M checkpoint, cyclin B-CDK1 must be localized to the nucleus, dephosphorylated at Y15 and T14 by the Cdc25 phosphatase, and activated by phosphorylation at T161 by the CDK-activating kinase (CAK). Once active in the nucleus, cyclin B-CDK1, also referred to as the mitosis-promoting factor (MPF), may phosphorylate its substrates to promote progression through mitosis. If, however, DNA damage is detected during G2, the cell cycle is momentarily delayed while DNA damage response (DDR) pathways are activated. One way in which this is accomplished is through the activation of the DNA damage sensing kinases ATM and ATR, as discussed previously. However, if DNA damage is extensive, cells will initiate apoptosis to prevent the propagation of faulty DNA to subsequent daughter cells.

1.3 Cell Cycle Deregulation in Cancer

One of the fundamental hallmarks of cancer is the capacity for unrestrained cell proliferation[28]. Therefore, many of the most frequently mutated genes are related to cell cycle regulation. For example, the gene encoding the tumor suppressor p53 (*TP53*), which has a wide array of effects on cell cycle modulation, is the most commonly mutated gene across all cancers[29,30]. p53 is responsible for many regulatory effects including cell cycle arrest at the G1/S transition upon DNA damage detection, activation of DNA damage repair pathways, reinitiation of the cell cycle upon successful DNA repair, activation of apoptosis in cases of irreparable DNA damage, among many others. Therefore, inactivating mutations in *TP53* impair a cell's ability to control proliferative rate, and this becomes particularly problematic as cells accumulate other mutations and DNA lesions that go unchecked.

Cyclins and CDKs are the primary mediators of several cell cycle checkpoints, and common mutations in genes like *PIK3CA*, *BRCA*, or *KRAS* contribute to oncogenic signaling in part by converging on cyclin/CDK activation[29]. In addition to upstream mutations, copy number changes like *CDK4* and/or *CDK6* amplifications that inappropriately drive the G1/S transition have been observed in glioblastomas and in squamous cell carcinomas of the lung and esophagus[31]. Overexpression of *CDK1* and/or *CDK2* which can drive all aspects of the cell cycle has been reported in some colon adenocarcinomas, lymphomas, and advanced melanomas[31]. In addition to CDKs, amplifications in *CCND* and *CCNE* have been observed in OHNSCC, breast cancers, colon cancers, AML, and other cancers thus highlighting the critical need to understand how these molecules could be targeted in treatments. Of course, the natural CKIs are also often mutated or deleted in cancer, thus adding to the complexity of cell cycle deregulation. Deletion of *CDKN2A* (p16) can be seen in up to 50% of gliomas and 40-60% of OHNSCC and pancreatic cancers[13].

Consequently, deletions to *CDKN2B* (p15) which is closely located to *CDKN2A*, and changes to *CDKN2D* (p19) which shares the *CDKN2A* locus following an alternative reading frame are often co-observed in instances of *CDKN2A* deletion[32]. In addition, low p27 expression has been associated with poor prognosis in some cancers such as renal cell carcinoma and astrocytoma[33,34]. All in all, the cell cycle deregulation represents a fundamental aspect of cancer cell biology and targeting specific components for the treatment of specific cancer types remains an active and fruitful area of scientific research.

1.4 Oral, Head, and Neck Squamous Cell Carcinoma

As the sixth most common cancer worldwide (890,000 new cases and 450,000 deaths in 2018), OHNSCC represents a growing and significant public health concern[35]. Incidence of this disease continues to rise globally and is projected to surpass one million new cases annually by the year 2030[36]. In the US, over 54,000 new cases of oral cancer will be diagnosed each year, and approximately 10% of cases will be fatal[37]. The overall 5-year survival rate is 65% but can range as high as 84% if diagnosed early or as low as 39% if the cancer has metastasized to a distant site within the body.

OHNSCC typically arises in the mucosal epithelia that line the oral cavity, pharynx, or larynx and is broadly grouped into two major categories: human papilloma virus (HPV)-positive or HPV-negative. HPV-positive OHNSCC is primarily caused by high-risk strains such as HPV-16 and HPV-18 whose oncoproteins E6 and E7 deregulate the cell cycle by abrogating the host tumor suppressors p53 and pRb, respectively. HPV-negative OHNSCC is most commonly caused by exposure to tobacco products, alcohol, and other carcinogenic substances which place a high mutational burden on the epithelial cells lining the mucosa. Men are generally two to four times more likely to develop OHNSCC, which largely reflects differences in sex-specific modifiable risk

behaviors. Cultural differences at the population level help explain a striking difference in etiology for the rising incidence of OHNSCC by geographical region. For example, the prevalence of areca nut chewing products in Southeast Asia and India likely explains the high incidence of HPV-negative OHNSCC in those regions, while increasing rates of HPV infection explain the higher incidence of HPV-positive OHNSCC in places like the USA and Western Europe. The general use of tobacco products and alcohol consumption are global contributors to OHNSCC incidence[36].

1.4.1 Genomic landscape of OHNSCC and disease progression

Some of the most common genomic changes in HPV-negative OHNSCC are in cell cycle genes such as *TP53*, *CDKN2A*, *FAT1*, *NOTCH1*, and *CCND1*, among others[38–41]. Up to 84% of HPV-negative OHNSCCs harbor a mutation in *TP53* making it the most commonly mutated gene and often one of the earliest driving mutations for this disease. Other early and common genomic alterations such as homozygous loss of *CDKN2A* and amplification of *CCND1* work together to deregulate the G1/S transition of the cell cycle.

In OHNSCC, progression of disease from hyperplasia to dysplasia to invasive carcinoma is centered around key genetic events. Progression from normal mucosa to hyperplasia typically occurs with loss of the chromosomal region 9p21 which includes the tumor suppressor genes *CDKN2A* and *ARF*[36]. Progression from hyperplasia to dysplasia is typically marked by the loss of 3p21 and 17p13 which includes the site for *TP53*. And finally, progression to carcinoma in situ and invasive carcinoma relies on the loss of additional regions such as 11q13 and 10q23 while frequently being driven by amplifications to genes such as *CCND1* and *EGFR*. While the prevalence of these events has been gleaned from genomic and histologic data out of The Cancer Genome Atlas (TCGA), disease progression need not always rely on the specific sequence outline above. Mutations, amplifications, and deletions may indeed progress differently based on unique

factors from individual to individual. The prevalence, however, of *CDKN2A* mutation/loss (up to 45% of cases) and *CCND1* amplification (up to 30% of cases) point to the critical role of G1/S deregulation for the development of HPV-negative OHNSCC[38–40].

1.4.2 Standard treatments, targeted therapies, and clinical trials for OHNSCC

Surgery remains the primary method of treatment for OHNSCC as techniques have improved considerably in recent decades[42]. For advanced-stage cancers, microvascular reconstruction following tumor resection has become the standard treatment modality allowing for more favorable outcomes. However, radiotherapy and cytotoxic chemotherapy are often required prior to surgical intervention, especially in cases of advanced disease. Recent advancements in radiation oncology have led to the development of intensity-modulated radiotherapy, adaptive radiotherapy, and proton beam therapy which have all served to improve disease prognosis and reduce treatment-related morbidities[43]. Induction chemotherapy often precedes radiotherapy and includes some combination of the cytotoxic drugs docetaxel, cisplatin, and/or 5-fluorouracil. It has been argued that the application of these drugs may serve as radiosensitizers prior to surgery, but opposing studies have challenged this notion as cytotoxic treatment regimens have been shown to provide modest benefit to overall survival rates while significantly increasing acute toxicities[44,45]. This has led many scientists and oncologists to consider immunotherapies and targeted therapies as the next generation of systemic treatment.

Epidermal growth factor receptor (EGFR) inhibitors like cetuximab and anti-programmed cell death protein (PD)-1 agents like pembrolizumab have shown enough promise to garner FDA approval for the treatment of certain OHNSCCs as recently as 2006 and 2016, respectively. Clinical trials to determine the most effective combination of these drugs with existing treatments have been underway since the mid 2000s and 2010s[46,47]. As with many immunotherapies and

targeted therapies, however, resistance to these drugs has emerged as a serious problem[48,49]. A more recent addition to the list of targeted therapy candidates for OHNSCC includes the CDK4/6 inhibitor, palbociclib (PD-0332991 or PD). Palbociclib was first approved by the FDA in 2015 in combination with letrozole for the treatment of ER+ advanced breast cancer. It's primary mechanism of action is to inhibit CDK4 and CDK6 thus preventing phosphorylation of the tumor suppressor, pRb, during G1 of the cell cycle (Figure 1.4A). As a result, these cells are unable to pass the restriction point to enter S phase and instead exit the cell cycle into a state of quiescence or senescence[50]. Cancers with genomic changes that deregulate the G1/S transition (e.g., *CCND1/2/3* amplification or *CDKN2A* loss) are the primary candidates for treatment with this class of drug. To date, one phase I and two phase II clinical trials have been completed using palbociclib for the treatment of OHNSCC, and six additional trials are currently active or recruiting (ClinicalTrials.gov). Related CDK4/6 inhibitors such as abemaciclib and ribociclib are also being studied in over eight phase I and II clinical trials, but the focus of this project will remain on the more prevalent inhibitor, palbociclib. While many pre-clinical and clinical data have supported the use of palbociclib in the treatment of HPV-negative OHNSCC, innate and acquired resistance is emerging as a serious and growing obstacle for the widespread application of this drug[51–55].

The first phase I clinical trial of palbociclib for the treatment of OHNSCC was published in 2016[56]. The drug was combined with cetuximab to treat recurrent and/or metastatic OHNSCC and included patients with cetuximab- or platinum-resistant disease. For all nine patients involved in the study, none experienced dose limiting toxicity and a maximum tolerated dose of palbociclib was not reached. Two patients experienced partial response, six had stable disease, and only one had progressive disease. Thus, the combination with cetuximab was deemed safe and a recommended dose of palbociclib for a phase II clinical trial was made (125mg/day for days 1-21

of each 28-day cycle). Following this study, several phase II clinical trials including palbociclib were initiated, but they have produced mixed results thus far. In one study, the combination of palbociclib and cetuximab against cetuximab- or platinum-resistant OHNSCC showed favorable outcomes with limited adverse events[57]. In another study, however, the combination of palbociclib with carboplatin for the treatment of unresectable recurrent or metastatic OHNSCC was associated with significant treatment related toxicity and insufficient anti-tumor activity[58]. In yet another study, the combination of palbociclib and cetuximab did not meet the prespecified statistical threshold to outperform the combination of placebo and cetuximab in platinum-resistant tumors[59]. These data indicated that further study of the combination of palbociclib and cetuximab for patients with platinum-resistant disease was unwarranted. Conclusions from these phase II trials must be evaluated carefully as the participants typically entered the studies with some degree of advanced disease. Nonetheless, these studies highlight the issue of innate or acquired palbociclib resistance, a phenomenon readily observed in a growing number of breast cancer cases, and the lack of solid data to predict when or how resistance may occur.

1.4.3 CDK4/6 inhibitor resistance

Several mechanisms of palbociclib resistance have been described for different cancers, but they most commonly include *RB1* downregulation or loss, *CDK4/6* amplification, and *CCNE1* upregulation or amplification[51,52,55,60]. There is strong preclinical and clinical evidence to support the idea that pRb loss indeed renders cancer cells resistant to CDK4/6 inhibition, especially in the context of HPV-positive OHNSCC[61,62]. The ultimate effect of palbociclib – to reduce pRb phosphorylation and force cells into G0 – is offset by the HPV-E7 oncoprotein as it abrogates host pRb. Consequently, neither HPV-positive cells in vitro nor patients with HPV-positive OHNSCC are responsive to the drug. *CDK4/6* amplifications have also been described as a common pathway

to resistance in various cancers[63,64]. As the specific target of palbociclib, overexpressed CDK4 and CDK6 in amplified tumors may simply outcompete circulating drug and promote cell cycle progression even in its presence. There is also some discussion with respect to the kinase independent activities of CDK6 and the role its overexpression may play in conferring resistance, but the findings are inconclusive at this time[60].

The theoretical rationale for cyclin E mediated palbociclib resistance is strong, but pre-clinical evidence to support this idea is mixed[51,55,65–68]. According to the classical model of the G1/S restriction point, cyclin E-CDK2 complexes are responsible for pRb hyperphosphorylation during late G1. Therefore, in the presence of palbociclib, increased cyclin E-CDK2 activity could in principle bypass the effects of CDK4/6 inhibition and phosphorylate pRb (Figure 1.4B). Furthermore, a recent study by Guiley *et al.* demonstrated that the primary mechanism through which cell cycle arrest is achieved by palbociclib is due to the downstream inhibition of cyclin E-CDK2 complexes as a result of CIP/KIP inhibitor (i.e., p21 and p27) redistribution[69]. In short, palbociclib can only bind and inactivate monomeric CDK4, and to a lesser extent, dimeric cyclin D-CDK4 complexes. But the active trimeric complex which includes cyclin D, CDK4, and Y74-phosphorylated p27 physically blocks the drug from interacting with the kinase. This binding was shown to be mutually exclusive as p27 showed no affinity for monomeric CDK4 saturated with palbociclib. As a result, when palbociclib is bound to and inhibiting CDK4, the CIP/KIP inhibitors that are no longer able to interact with the kinase are instead redistributed to cyclin E-CDK2 complexes where their primary effect is inhibitory. It is important to note that these results were only reported for CDK4, and this effect has not yet been demonstrated for CDK6. The authors of this study argue that this redistribution and indirect inhibition of CDK2 is the true mediator of cell cycle arrest after palbociclib treatment. Whether the arrest is occurring due to direct CDK4/6

inhibition by palbociclib or due to indirect CDK2 inhibition by p21/p27, cyclin E hyperactivity could bypass these inhibitions and phosphorylate pRb to promote cell cycle progression. Indeed, multiple studies demonstrate some upregulation of cyclin E associated with palbociclib resistance, but these studies often fail to demonstrate cyclin E *activity* as the primary mediator [65,66,68]. In other words, cyclin E abundance is often correlated with palbociclib resistance, but whether cyclin E is driving the phenotype or is simply the passenger of another genetic change has not been determined conclusively.

In HPV-negative OHNSCC, *CCNE1* amplification is relatively rare as compared to other mutations that may deregulate cyclin E activity. Specifically, the E3 ubiquitin ligase Fbw7, which is known to regulate the degradation of cyclin E among a host of other substrates, is mutated or lost (4q31.3 deletion) in up to 10% of OHNSCC cases[70–73]. Knowing that cyclin E activity would be deregulated in Fbw7 null OHNSCC, we hypothesize that *FBXW7* loss predicts resistance to CDK4/6 inhibitors such as palbociclib (Figure 1.4C).

1.5 Dissertation Overview

Though the cell cycle has been a fertile area of research for decades, many questions remain unanswered and new questions have been raised as novel therapeutics have entered the market. The specific roles and responses of cyclins and CDKs to these new therapies inform much of the work found in this dissertation. Starting with Chapter 2, I use a genome-wide CRISPR-Cas9 knockout screen to find candidate mediators of replication stress failure in constitutively active CDK2 colon cancer cells. In Chapter 3, I explore the role of cyclin E in mediating resistance to CDK4/6 inhibition in HPV-negative OHNSCC. *CCNE1* amplification is frequently cited as a bona fide resistance mechanism to CDK4/6 inhibition, however my data challenge this paradigm by demonstrating the limited effects of cyclin E hyperactivity on palbociclib treated cells.

Furthermore, I hypothesize *FBXW7* loss as a novel resistance mechanism to CDK4/6 inhibition, though similar to cyclin E activity, I demonstrate its limitation in conferring robust resistance to palbociclib. Finally in Chapter 4, I employ an analog sensitive CDK6 molecule for an in-situ proteomic screen to identify novel CDK substrates. Our screen reveals a pool of novel CDK substrate candidates, one of which I successfully validate in vitro, and lays the foundation for future in-vivo studies. Overall, the work outlined below expands our understanding of the diverse roles that cyclins and CDKs play in the context of human cancers and their treatments.

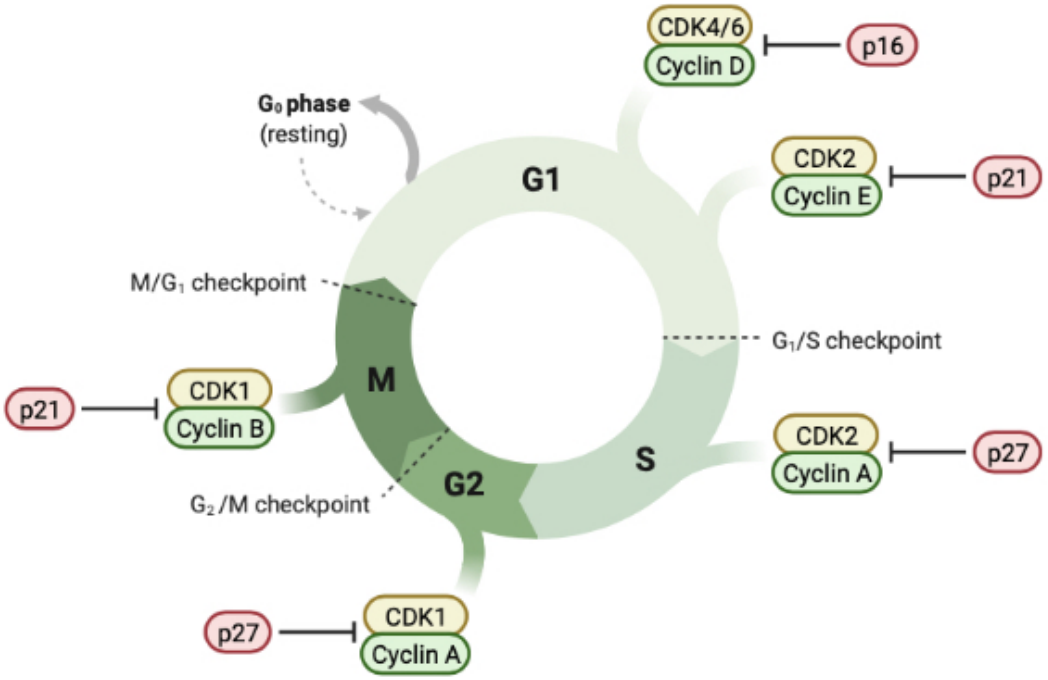

Figure 1.1 Cell cycle overview
The cell cycle is a series of highly coordinated molecular events that eventually gives rise to two genetically identical daughter cells from one mother cells. Here, each phase of the cell cycle is shown with the relevant cyclin-CDK complexes and their inhibitors which can either drive or regulate the checkpoints between each phase (created with BioRender.com).

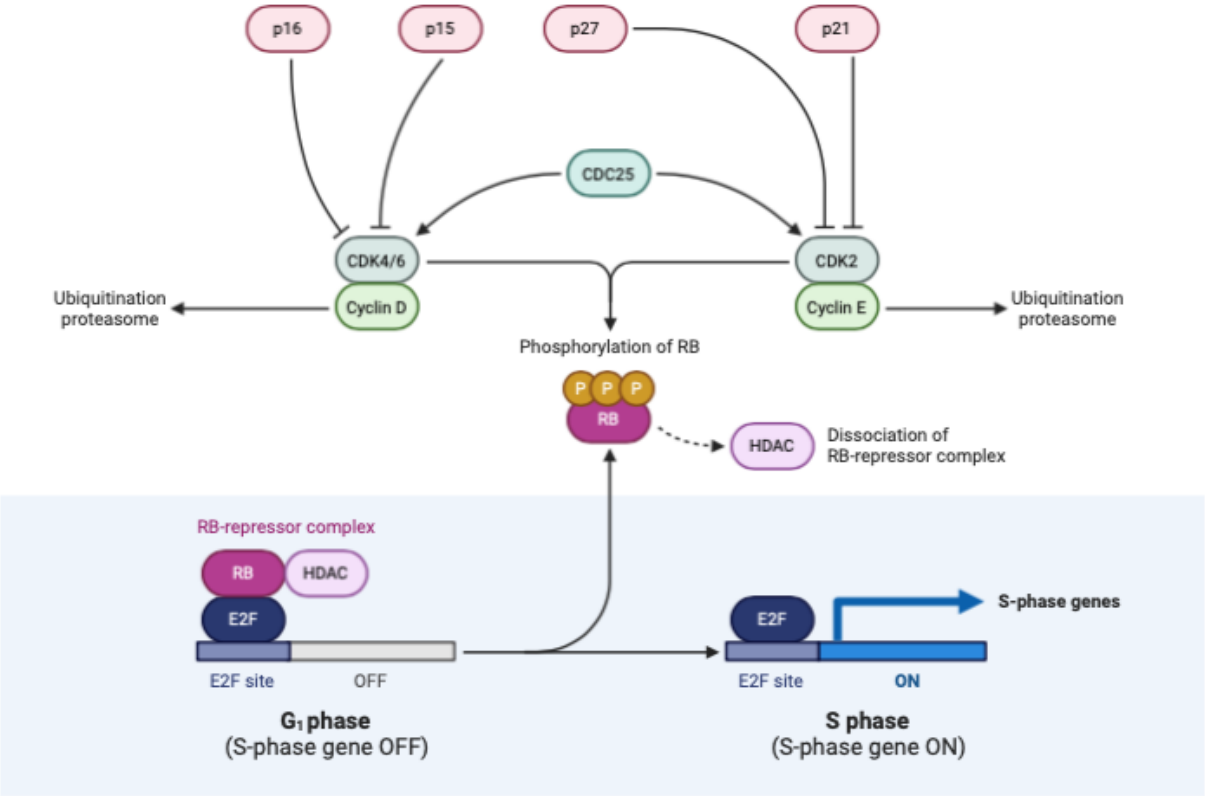

Figure 1.2 Classical G1/S restriction point
In the classical model of the G1/S restriction point, increasing cyclin D-CDK4/6 activity through G1 leads to the hypophosphorylation of pRb. This allows for the initial release of the E2F family of transcription factors and thus an increase in cyclin E transcription. Rising cyclin E levels and cyclin E-CDK2 activity leads to the hyperphosphorylation and full release of E2F. Once initiated, this positive feedback mechanism ensures full commitment to S-phase entry as the full array of S-phase promoting genes are transcribed (created with BioRender.com).

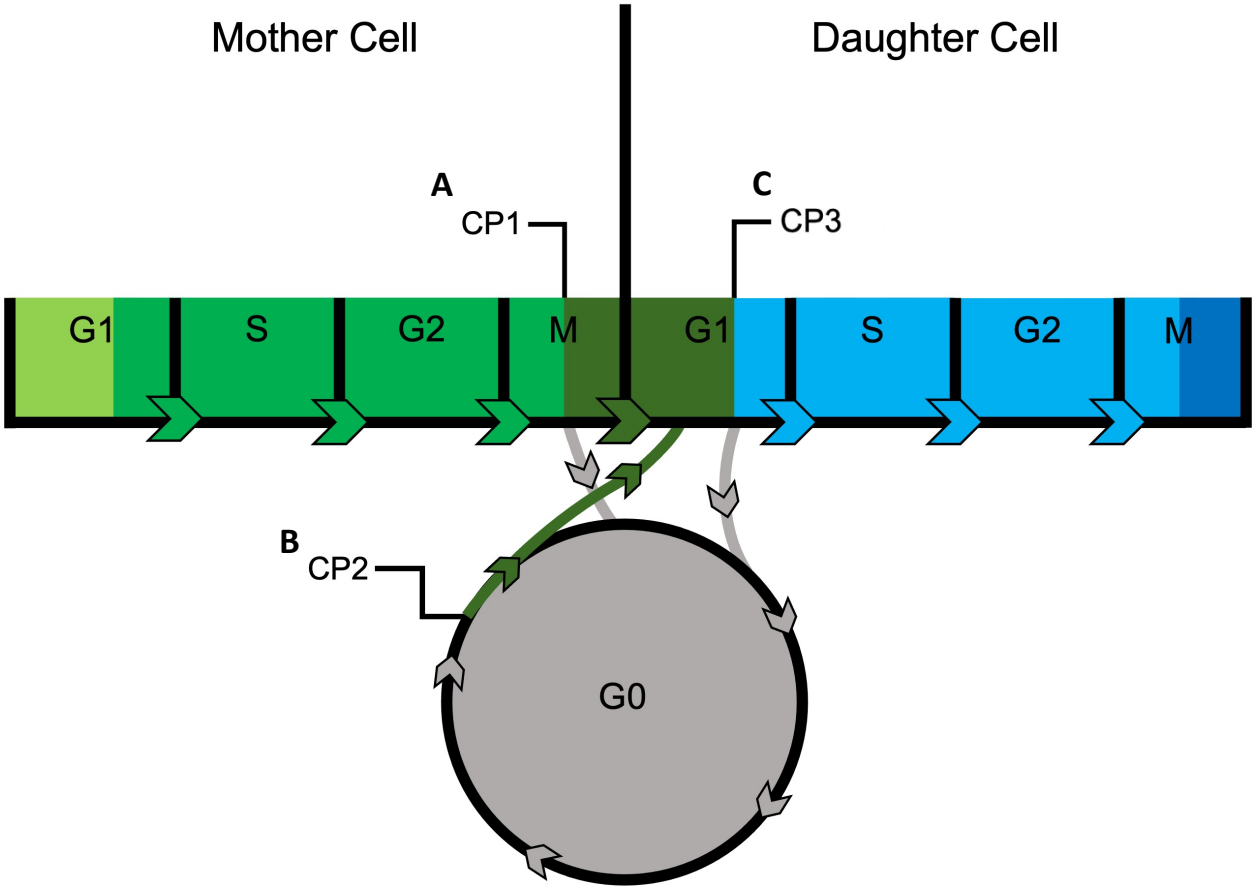

Figure 1.3 Proposed updates to the G1/S transition
The updated model for the G1/S transition identifies three commitment points rather than a single restriction point. Note that this model has not necessarily replaced the old paradigm (schematic was adapted with modifications from the 2020 review of the G1/S transition by Hume, Dianov, and Ramadan[18]. **(A)** 1st major departure from the classical model is that cells enter G1 phase with Rb already phosphorylated, and the job of cyclin D-CDK4/6 is to maintain phosphorylation through G1 while cyclin E/A-CDK2 takes over in S-phase. This pushes the first commitment point (CP1) back from daughter cell G1 to mother cell mitosis. If all is well during mother cell mitosis, PP1 activity is limited and Rb remains phosphorylated. Alternatively, if mitogens are absent and/or DNA damage is sensed during mother cell mitosis, pRb phosphorylation is prevented, and cells exit the cell cycle. **(B)** CP2 occurs in cells that are unable to pass CP1 and have therefore dephosphorylated Rb during mother cell mitosis. If mitogen signals return and DNA damage is sufficiently repaired, Rb is once again phosphorylated by cyclinD-CDK4/6 and re-entry to the cell cycle is achieved. **(C)** CP3 is the final commitment point determined entirely by daughter cell G1 DNA damage detection and APC/C-CDH1 inactivation (heavily dependent on E2F). If APC remains active through G1 due to DNA damage (p53 induces p21 which represses cyclin D-CDK4/6 & cyclin E-CDK2), S-phase promoting proteins are degraded and the cell can still back out of the cell cycle. Initial release of E2F and activation of cyclinE-CDK2 results in partial inhibition of APC/C-CHD1.

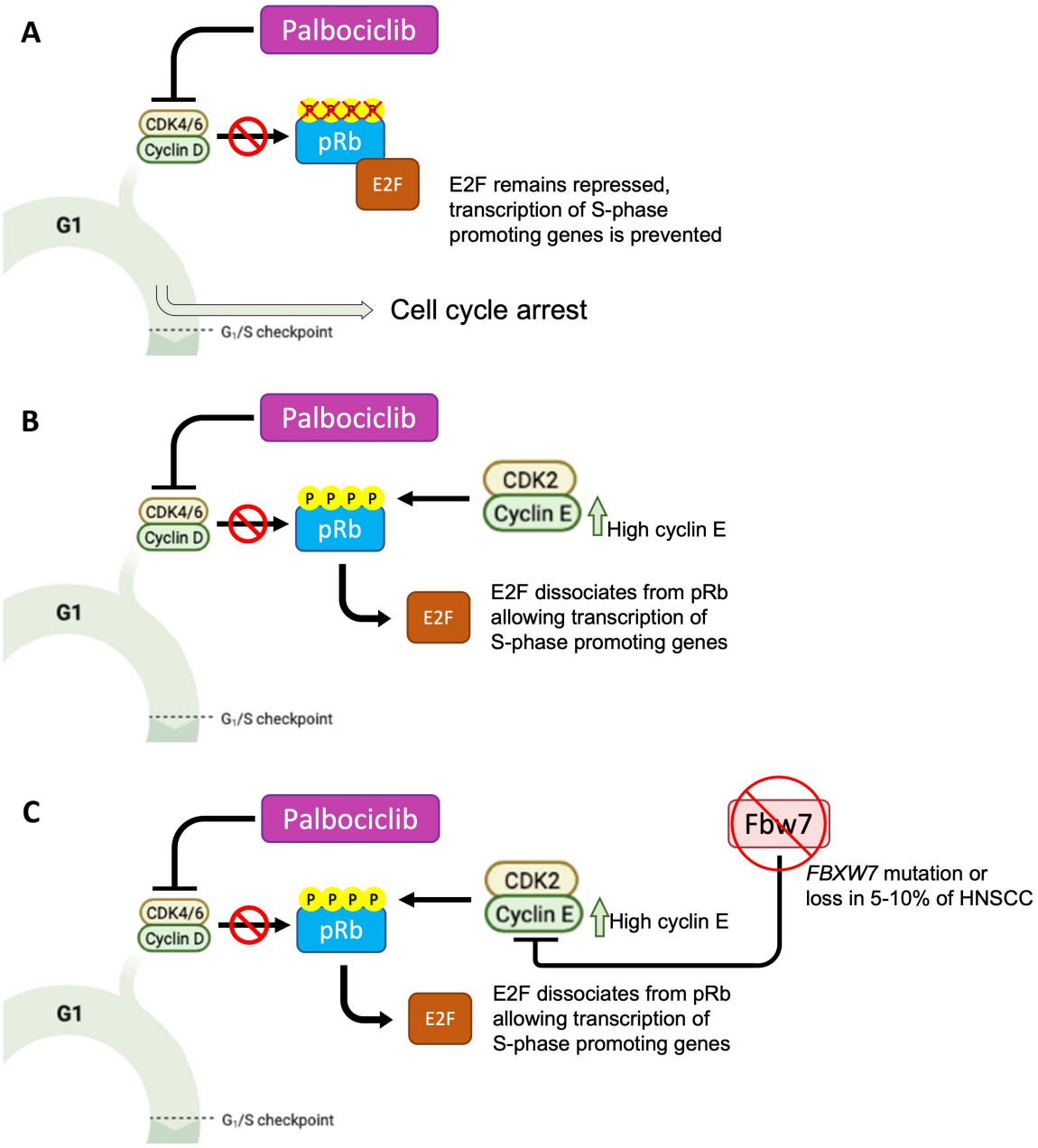

Figure 1.4 Mechanisms of action and resistance to palbociclib
(A) Palbociclib is a highly selective CDK4/6 inhibitor that promotes cell cycle arrest during G1 by preventing CDK4/6 phosphorylation of pRb. The arrest can either be transient (i.e., quiescence) or permanent (i.e., senescence) depending on several factors such as tumor type, concentration of drug, length of treatment, co-treatment with other drugs, among others still under investigation. **(B)** Several mechanisms of palbociclib resistance have been described including amplification/overexpression of cyclin E. It is thought that cyclin E-CDK2 complexes can bypass CDK4/6 inhibition by directly phosphorylating pRb in lieu of the D-type cyclins leading to E2F release and S-phase progression. **(C)** Because cyclin E amplification is rare in OHNSCC, we propose a novel mechanism of palbociclib resistance in OHNSCC, namely *FBXW7* mutation or deletion, which would result in cyclin E deregulation and bypass of CDK4/6 inhibition.

Chapter 2. Genome-Wide CRISPR-Cas9 Screen to Identify Mediators of Replication Stress Failure in CDK2AF Cells

2.1 Introduction

The cell cycle is regulated by cyclin-CDK complexes, and they are in turn regulated by activating and inhibitory phosphorylations on specific amino acid residues[6–8]. For example, once CDK1 or CDK2 is bound to its partner cyclin, they must be phosphorylated on T160 by the CDK-activating kinase (CAK) to become fully active[9]. To inhibit activity, CDK1 and CDK2 are phosphorylated on Y15 and T14 by the Wee1 and Myt1 kinases, respectively (Figure 2.1A). CDK1 inhibitory phosphorylation by Wee1 is best understood at the G2/M transition where cyclin B-CDK1 activity is suppressed until the onset of mitosis when the Cdc25 family of phosphatases oppose the action of Wee1 and Myt1[10,26,27]. These inhibitory phosphorylation sites, found on both CDK1 and CDK2, can also be utilized when DNA damage is sensed, and the cell cycle must be paused to initiate DNA repair.

In 2014, Moser/Xu *et al*. revealed Wee1 as a therapeutic target in OHNSCC using an RNAi functional kinomics viability screen, and they discovered that p53 deficient OHNSCC demonstrated the greatest sensitivity to the small-molecule Wee1 inhibitor, AZD-1775[74]. One byproduct of Wee1 inhibition is the prevention of inhibitory phosphorylation on CDK2, and further analysis revealed that p53 deficient cells treated with AZD-1775 underwent premature mitotic entry/catastrophe and apoptosis (Figure 2.1B)[75,76]. Thus, a synthetic lethal model of Wee1 inhibition in p53 deficient OHNSCC was created and a phase I clinical trial combining AZD-1775 with docetaxel and cisplatin was launched. Initial data from the trial were first published in 2018 and they revealed 4 extreme responders, 3 partial responders, and 1 patient with progressive disease out of 8 patients eligible for analysis at the end of the study[77]. Further investigations of

Wee1 inhibition have revealed additional mechanisms of action such as the exacerbation of replication stress by slowing replication forks in cells treated with AZD-1775 and FOXM1 driving hypersensitivity to AZD-1775 in HPV+ OHNSCC[78,79]. These studies collectively highlight the importance of regulating CDK2 activity, particularly in the context of p53 deficient OHNSCC.

Because CDK1 and CDK2 are similarly regulated on T14/Y15, it has historically been difficult to study the regulation of one specific kinase over the other. To address the specific impact of CDK2 inhibitory phosphorylation, the Clurman lab previously engineered a colon cancer cell line (HCT-116) to express CDK2 lacking the two inhibitory phosphorylation sites (herein named CDK2AF) (Figure 2.1C)[80]. As a result, CDK2AF cells had constitutively active CDK2 and exhibited aberrant cell cycle kinetics such as premature S-phase entry, increased origin firing, and decreased fork speed. Furthermore, CDK2AF cells were hypersensitive to S-phase agents that cause replication stress such as hydroxyurea (HU) and aphidicolin (APH). Low dose treatment with either of these agents resulted in excess accumulation of DNA damage measured by γH2AX, S-phase exit, and failure to return to the cell cycle resulting in senescence (Figure 2.2A). While the repercussions of constitutive CDK2 activity were clearly outlined, one question remained: what were the downstream targets of CDK2 that were mediating such dramatic sensitivity to replication stress? We hypothesized that CDK2 would have downstream targets that, when phosphorylated, would become active and contribute to the dramatic S-phase agent hypersensitivity observed in CDK2AF cells.

To test this hypothesis, we employed a genome-wide CRISPR-Cas9 knockout screen in HU treated CDK2AF cells (Figure 2.2B). The objective was to find downstream targets of CDK2 that when knocked out, would restore proliferation in CDK2AF cells treated with HU. We conducted the screen in collaboration with the Paddison lab using the Brunello CRISPR library[81].

Three independent screen replicates were designed with slight variations in each one. In the first screen, we treated cells with 1mM HU and allowed four days of growth following drug washout. In the second and third screens, we allowed fourteen days of growth following drug washout while treating one replicate with 1mM HU and the other with 100μM HU. To confirm the theoretical and technical success of the screen, guides targeting CDK2 would serve as positive controls since previous work had shown a reversal of HU hypersensitivity in CDK2 knocked down CDK2AF cells[80]. For bioinformatics, we utilized Model-based Analysis of Genome-wide CRISPR/Cas9 Knockout (MAGeCK) to score positively selected sgRNAs at the end of outgrowth[82]. Indeed, the top hit from the screen demonstrating the most robust recovery and proliferation following HU treatment was CDK2, thus affirming the presence of our positive control (Figure 2.3A). Including CDK2, we collated the top 150 up represented genes from each screen and found an overlap of seven hits shared between all three. Gene ontology analysis of our top hits showed an enrichment for genes involved in several different pathways, most notably in apoptotic signaling (Figure 2.3C). Following the screens, siRNAs and sgRNAs were used to validate our top hits. While modest recovery from HU treatment was observed in most of the validated hits, none displayed the same degree of recovery as sg*CDK2* indicating that either 1) no single downstream target of CDK2 was responsible for the observed hypersensitivity, or 2) that the action of CDK2 in this context is inactivating, in which case the screen would be unable to identify the downstream target. One of our candidate hits, FAM122A, did reveal a reduction in γH2AX levels when knocked out of HU treated CDK2AF cells thus laying a foundation for future work studying the relationship between FAM122A and CDK2.

2.2 Materials and Methods

2.2.1 Cell lines, plasmids, and drug treatments

HCT-116 (WT and CDK2AF) cells were grown in Dulbecco's Modified Eagle Medium (DMEM) supplied with 10% fetal bovine serum (Gibco) and penicillin-streptomycin (Gibco). To generate individual knockouts, the lentiCRISPRv2 vector backbone was obtained from the Paddison lab (originally from the Feng Zhang lab, MIT)[83]. For drug treatments, HU (Sigma) was used at the indicated concentrations, either 100μM or 1mM.

2.2.2 CRISPR-Cas9 screening

The human genome-wide Brunello CRISPR-Cas9 pooled library was used in a lentiviral format to transduce HCT-116 WT and CDK2AF cells. In each replicate of the screen, we aimed for 500-fold representation of the library at 30% infection efficiency. Cells were washed the morning after library transduction, and puromycin selection was initiated at 1μg/mL the morning after for 48 hours. A fraction of cells was harvested for the day 0 control timepoint, and 120 million cells were divided and plated in 15cm plates for three experimental replicates (40 million cells/replicate). The remainder of the cells were frozen down for the two future screen repeats. The plated cells were allowed to grow and were passaged as needed for seven days to allow CRISPR knockouts to take full effect. The treatment protocol for screen #1 called for 24-hour treatment with 1mM HU, wash and replace with drug-free media for 24 hours, another round of 24-hour treatment with 1mM HU, and wash and grow in drug-free media for four days. At the end of the growth period, genomic DNA was extracted from each replicate using the DNeasy Blood and Tissue Kit (Qiagen), and a two-step nested PCR was conducted to amplify sgRNA sequences and incorporate deep sequencing barcodes on the sgRNA amplicons (full primer sequences can be found in Table 2.4). Purified PCR products were submitted for next generation sequencing (NGS)

using the HiSeq 2500 (Illumina) platform in the Fred Hutchinson Cancer Center Genomics Shared Resources. For screens #2 and #3, the treatment protocols were changed in the following ways:

Screen #2: 24-hour treatment with 1mM HU, wash and replace with drug-free media for 24 hours, another round of 24-hour treatment with 1mM HU, and wash and grow in drug-free media for 14 days.

Screen #3: 24-hour treatment with 100μM HU, wash and replace with drug-free media for 24 hours, another round of 24-hour treatment with 100μM HU, and wash and grow in drug-free media for 14 days.

NGS reads were aligned to the Brunello library using Bowtie v1.0.0 and counts were tallied using the R/Bioconductor packages edgeR v3.20.9 and MAGeCK v0.5.7. For MAGeCK analysis, data were collapsed so as to represent each gene with 4 guides, and values for logFC(log2 ratio), logCPM(average log2 counts per million), false discovery rate (FDR), normalized guide counts, raw guide counts, and positive/negative composite ranks (taking into consideration logFC & FDR) were generated by the MAGeCK algorithm. Using the positive ranks to order the significantly up represented genes, we restricted our candidate validations to the top 150 hits per screen as determined by the MAGeCK ranking algorithm.

2.2.3 siRNA

FlexiTube products containing 4 preselected siRNAs per gene of interest were purchased from Qiagen for initial validation studies. Sequences of each siRNA product are provided in Table 2.2. All siRNA transfections were completed using Lipofectamine RNAiMAX Reagent according to manufacturer's protocol (Invitrogen). Target protein knockdown was confirmed via western blot, and all follow up assays were completed within five to ten days of siRNA delivery.

2.2.4 sgRNA assembly

sgRNA sequences were designed using the online Synthego Knockout Guide Design tool and the online Broad Institute GPP sgRNA Design/CRISPick tool. Two guide sequences (20 base pairs in length) were selected per gene between the two online platforms. Guide sequences for each gene are provided in Table 2.3. DNA oligonucleotides were ordered from Integrated DNA Technologies (IDT) with the following sequences flanking the 20bp guide sequences on either side:

5'- GTGGAAAGGACGAAACACCG - 20bp sequence - GTTTTAGAGCTAGAAATAGC - 3'

PCR was then performed with the following primers to generate ~200bp guide sequence:

F: TAACTTGAAAGTATTTCGATTTCTTGGCTTTATATATCTTGTGGAAAGGACGAAACACCG

R: ACTTTTTCAAGTTGATAACGGACTAGCCTTATTTTAACTTGCTATTTCTAGCTCTAAAAC

The PCR product was run on a 2% TBE gel and its presence was confirmed using the Bio-Rad ChemiDoc Imaging system. DNA was purified using the Zymoclean Gel DNA Recovery Kit (Zymo Research) according to manufacturer's protocol. The lentiCRISPRv2 vector was subject to a vector digest reaction using the BsmBI restriction endonuclease (NEB) and also gel purified using the Zymoclean Kit. The purified PCR product was then cloned into the cut backbone using Gibson Assembly Master Mix (NEB) by a one-hour incubation at 50°C. The ligated plasmid was then electroporated into Stbl3 competent *E. coli* cells, spread over agar plates containing 50µg/mL ampicillin, and left to grow overnight in 37°C. The following morning, two to four colonies of each guide were selected and dropped into tubes containing 3mL LB Broth (Miller) also containing 50µg/mL ampicillin. Tubes were left to allow overnight growth in a shaker at 37°C. The following morning, approximately 2mL of the culture was used for plasmid extraction using the PureLink Quick Plasmid Miniprep Kit (Invitrogen). A sequencing PCR was conducted on the isolated

plasmid using the "24 master mix" (Fred Hutch) with the following sequencing primer: 5'-GAGGGCCTATTTCCCATGAT-3'. Once sequence was confirmed with the appropriate CRISPR guide in the lentiCRISPRv2 backbone, the remaining liquid culture was used to inoculate 250mL LB Broth (Miller) for larger scale plasmid preparation using PureLink HiPure Plasmid Filter Maxiprep Kit (Invitrogen).

2.2.5 Lentivirus generation

2-3 million Lenti-X 293T cells were seeded into 10cm plates and left to settle and grow overnight. The following afternoon, cells were transfected using 10µg CRISPR vector along with 6.5µg pSPAX2 and 6.0µg pMD2.G packaging vectors using the traditional calcium-phosphate transfection protocol. Media was changed the following morning and lentivirus containing media was filtered and harvested the morning after. Viral transduction was completed immediately upon harvest and any excess viral media was stored in -80°C for future use.

2.2.6 Generating individual knockouts

HCT-116 WT and CDK2AF target cells were plated at approximately 25% confluency in 6cm plates for next day lentivirus infection. Lentivirus was delivered to target cells with 4µg/µL polybrene and left to incubate overnight. Cells were washed the following morning, and puromycin selection was initiated the morning after at 1µg/mL. Once cells in the control plates had completely died off (approximately two to four days), surviving cells in the target plates were pelleted and successful gene knockout was confirmed by western blot. Remaining cells were frozen down in 10% DMSO + DMEM in liquid N_2 for future use.

2.2.7 Immunoblotting

Cells were harvested by trypsinization, pelleted, washed with PBS, and lysed in 0.5% NP-40 lysis buffer (50 mM Tris pH 8.0, 150 mM NaCl, and 0.5% (vol/vol) NP-40) supplemented with

protease and phosphatase inhibitors. Lysates were sonicated, cleared, and protein concentrations were normalized using Bradford assay. Lysates were prepared in Laemmli buffer, boiled at 95°C for 10 minutes, loaded into Bolt 4-12% Bis-Tris (Invitrogen) gradient gels, and electrophoresed for approximately 1 hour at 125 volts. Gel contents were then transferred to a PVDF membrane using the iBlot 2 Gel Transfer Device (Invitrogen). Equal protein loading and successful gel transfer were confirmed with Ponceau staining and the membrane was blocked for at least 30 minutes in 5% milk/TBST shaking at room temperature. The membrane was then incubated with the appropriate primary antibody shaking at 4°C overnight. The following morning, the membrane was washed with TBST and incubated with the appropriate HRP-conjugated anti-mouse or anti-rabbit secondary antibody at 1:10,000 for at least 1 hour shaking at room temperature. Proteins were then visualized on the membrane using ECL (Thermo Fisher Scientific) with the Bio-Rad ChemiDoc Imaging system.

2.2.8 Growth assays (CellTiter-Glo, colony formation, and pooled qPCR outgrowth)

For CellTiter-Glo assays, cells were seeded in 96-well plates on day 0 at 1,000 cells per well. Following the treatment protocol of the CRISPR screen, HU was added on day 1 at either 100μM or 1mM, washed out on day 2, applied once again on day 3, washed out on day 4, and cells were allowed to grow for 4 days or longer until control wells were nearing confluence. At the end of outgrowth, plates were removed from the incubator and allowed to reach room temperature along with the CellTiter-Glo reagent (Promega). 15μL of reagent was added to each well and put on the shaker at room temperature covered from light for 2-3 minutes. The plates were then removed from the shaker and allowed to sit in darkness at room temperature to allow stabilization of the luminescence signal. The final luminescence readout was conducted in The Synergy HT microplate reader (BIO-TEK).

For colony formation assays, cells were seeded in 6-well plates on day 0 at 5,000 cells per well. Following the treatment protocol of the CRISPR screen, HU was added on day 1 at either 100μM or 1mM, washed out on day 2, applied once again on day 3, washed out on day 4, and cells were allowed to grow for up to 10 days. At the end of outgrowth, cells were washed with PBS and fixed on the plates with a 1:7 mixture of acetone and methanal at room temperature for 2 minutes. The methanal mixture was recovered, and cells were stained with 0.5% crystal violet solution for 20 minutes on the shaker at room temperature. After recovery of the crystal violet solution, the wells were washed with diH_2O and allowed to dry overnight.

For pooled qPCR outgrowth assays, we designed the following experiment to replicate the CRISPR screen conditions and results as accurately as possible: Control vs knockout cells were pooled together at a known ratio (10,000:1) and plated in three replicates within 15cm plates. A day 0 batch was frozen down to serve as the no treatment control condition. Following the treatment protocol of the CRISPR screen, HU was added on day 1 at either 100μM or 1mM, washed out on day 2, applied once again on day 3, washed out on day 4, and cells were allowed to grow for either 4 or 14 days. 14-day outgrowth plates were split 1:4 as they neared confluence so as to prevent contact inhibition and to maintain representation. At the end of outgrowth, cells were harvested by trypsinization, and genomic DNA was extracted. qPCR primers were designed against sgRNA guide sequences (details found in Table 2.5), and the assay was run on ABI QuantStudio5 Real Time PCR Systems. Primers targeting the sgCTRL sequence were treated as our housekeeping gene and ΔΔCt analysis was used to detect changes in knockout vs control cell ratios between Day 0 and Day 4/14.

2.2.9 Cell cycle analysis and flow cytometry

Growing cells were pulsed with 3μg/mL bromodeoxyuridine (BrdU) for one hour prior to harvest. At the end of one hour, cells were washed, harvested by trypsinization, and fixed in 4% paraformaldehyde at room temperature for 15 minutes. Once fixed, cells were washed with PBS and stored in ice cold methanol for at least 24 hours at -20°C. To prepare samples for flow cytometry, fixed cells were washed twice with flow wash buffer (0.3% bovine serum albumin (BSA) and 0.1% tween in PBS) and centrifuged at 300g for 3 minutes in between washes. After the second wash, the pellet was resuspended in 500μL of 2M HCl and incubated at room temperature for 20 minutes. HCl was washed out with flow wash buffer, centrifuged, and aspirated. The pellet was resuspended in 500μL 0.1M sodium borate to neutralize any residual acid and once again washed, centrifuged, and aspirated. The pellet was resuspended for 15 minutes in blocking buffer (3% BSA, 3% normal goat serum in PBS). Once washed out, the pellet was incubated with the appropriate primary antibodies overnight at 4°C. The following morning, primary antibody was washed out, and the pellet was incubated with propidium iodide (0.5μg/mL) for 10 minutes, washed, resuspended in FBS Stain Buffer (BD Biosciences), and taken to the flow cytometry core at the Fred Hutch Cancer Center for analysis. Flow cytometry was conducted on a BD LSRFortessa X-50 cytometer and data was analyzed using FlowJo software.

2.2.10 Antibodies

Antibodies were purchased from suppliers and used as follows: Abnova: FAM122A (3E9, mouse monoclonal, 1:1,000); BD Biosciences: γH2AX Ser139 (N1-431, mouse monoclonal Alexa 647 conjugated, 1:500 for flow cytometry); Cell Signaling Technology: Actin (13E5, rabbit monoclonal HRP-conjugated, 1:1,000), CASP8 (1C12, mouse monocloncal, 1:1,000), DR4 (D9S1R, rabbit monoclonal, 1:1,1000), DR5 (#3696, rabbit polyclonal, 1:1,000), γH2AX Ser139

(20E3, rabbit monoclonal, 1:1,000), MAPK14 (#9212, rabbit polyclonal, 1:1,000), MAP2K3 (#9238, rabbit polyclonal, 1:1,000); Invitrogen: p-CDK2 Tyr15 (A700-101, rabbit monoclonal, 1:1,1000); Santa Cruz Biotechnology: CDK2 (M2, rabbit polyclonal, 1:250 for IP, 1:1,000 for IB), PCNA (PC10, mouse monoclonal HRP-conjugated, 1:1,000).

2.3 Results

2.3.1 CRISPR-Cas9 screen reveals diverse array of candidate mediators that modestly rescue growth during replication stress in CDK2AF cells

We performed three independent CRISPR-Cas9 screens to identify genes contributing to HU hypersensitivity in HCT-116 CDK2AF cells. As expected, guides targeting CDK2 were consistently up represented across all screens (Figure 2.3A). Gene set enrichment of the top 150 hits (scored by MAGeCK analysis) revealed several interesting pathways involved in rescuing CDK2AF cells upon HU treatment, most notably the TRAIL-activated apoptotic signaling pathway, replicative senescence, and DNA damage response (Figure 2.3C). Seven of the top 150 hits shared by all three screens included *AKT1*, *CDK2*, *CEBPB*, *FAM122A*, *MAPK14*, *TNFRSF10A*, and *TNFRSF10B* (Figure 2.3B). In addition to these hits, *CASP8* and *MAP2K3* were hits shared by at least two of the screens guiding us toward the apoptotic and MAPK signaling pathways for our validation studies. As a result, we chose to include the following candidates in our validations: *CASP8*, *TNFRSF10A*, *TNFRSF10B*, *MAP2K3*, and *MAPK14*. *CDK2* was included during validation as a benchmark for HU treatment rescue. A full list of the top 150 hits from each screen can be found in Table 2.1. Note: the genes *TNFRSF10A* and *TNFRSF10B* are alternatively

named *DR4* and *DR5* as they encode the proteins death receptor 4 (DR4) and death receptor 5 (DR5), respectively, and will herein be referred to as *DR4* and *DR5*.

2.3.2 siRNA knockdown of primary candidates fails to validate screen results

For our initial validation studies, we used siRNAs against our candidate hits and attempted to recapitulate screen results through growth assays after drug treatment. Successful knockdown of each protein was confirmed via western blot and cells were seeded into 96-well plates for completion of the growth assay (Figure 2.4A). Cells were treated with 1mM HU, washed, and allowed to for 4 days before analyzing outgrowth by CellTiter-Glo (CTG). CTG values of HU-treated siCTRL wells were not significantly different from CTG values of HU-treated siRNA wells targeting our screen hits (Figure 2.4B). Treated vs. untreated CTG ratios also failed to show growth rescue in drug, however, we were surprised to see that siCDK2 cells also failed to outgrow siCTRL after treatment. We concluded that incomplete knockdown of target proteins might be preventing robust rescue, and thus siRNA was not an ideal tool for validation experiments. As a result, we proceeded to generate individual knockouts of each target from CDK2AF cells using CRISPR-Cas9.

2.3.3 CRISPR-Cas9 knockout of primary candidates fails to validate screen results

To knockout each gene, we cloned sgRNA sequences targeting our screen candidates into the lentiCRISPRv2 vector backbone and confirmed successful gene knockouts by western blot (Figure 2.5A). To replicate our screen results, we designed an outgrowth assay to mimic the conditions of the screen as closely as possible. Briefly, we spiked a growing population of CDK2AF sgCTRL cells with a small fraction of sg*CDK2* cells and determined the initial ratio of sg*CDK2*:sgCTRL cells by qPCR using primers specific to the CRISPR guide sequences for each knockout (detailed protocol in materials and methods). We then exposed the growing pool of cells

to HU (100μM and 1mM), washed out the drug, allowed cells to recover over the predetermined outgrowth period (4 or 14 days), and measured the final sg*CDK2*:sgCTRL ratio using the same qPCR protocol. Log_2 fold change (log_2FC) could then be calculated between initial and final sg*CDK2*:sgCTRL values along with each of the other screen candidates.

Data from these qPCR outgrowth assays revealed strong proliferation of sg*CDK2* cells within the HU-treated pooled sg*CDK2*:sgCTRL population demonstrating the validity of this assay. In the 1mM HU, 4-day outgrowth validation, sg*CDK2* cells had an average log_2FC of 3.65 meaning the population of sg*CDK2* within the pool increased 12.5X during outgrowth (Figure 2.5C). In line with this finding, average log_2FC of sg*CDK2* cells in the 1mM HU/14-day outgrowth was 6.38, and in the 100μM HU/14-day outgrowth was 2.1. The lower log_2FC value in the 100μM outgrowth assay may reflect the enhanced growth capacity of sgCTRL cells in lower concentrations of HU thus rendering a lower fold-change value for sg*CDK2* cells.

Individual knockouts of our screen candidates unfortunately failed to rescue growth after drug treatment to the same degree as *CDK2* knockouts (Figure 2.5C). Nearly all knockouts in all treatment and outgrowth conditions demonstrated positive log_2FC values, however, the degree of rescue was modest at best. The highest observed log_2FC was seen in sg*DR5* cells in the 1mM/4-day outgrowth assay ($log_2FC = 2.6$), though these cells failed to show the same degree of outgrowth in the two 14-day assays.

In parallel with our qPCR outgrowth assays, we also set up colony formation assays for two of our candidate hits (*CASP8* and *MAPK14*). Briefly, 5,000 cells were seeded in each well, treatments were given at either 100μM or 1mM HU, and cells were allowed to grow for 10 days. Once again, we observed growth rescue only in our sg*CDK2* cells while sg*CASP8* and sg*MAPK14* failed to rescue growth in this setting (Figure 2.5B).

In addition to outgrowth, we wanted to assay changes in DNA damage in knockout cells treated with HU. The Clurman lab had previously shown that eliminating CDK2 from CDK2AF cells dramatically reduces γH2AX after HU treatment[80]. Indeed, when we analyze cells by flow cytometry, we observe a 56% reduction in γH2AX for HU-treated sgCDK2 cells (Figure 2.5D). In contrast, none of our other knockout cells experienced a reduction in γH2AX when treated with HU as compared to our sgCTRL line, and in some cases even increased γH2AX upon treatment (Figure 2.5E).

2.3.4 CRISPR-Cas9 knockout of *FAM122A* prevents HU-induced DNA damage

After conducting growth and γH2AX assays for our initial screen candidates, we revisited the master list of candidates and selected *FAM122A* for additional study. Very little had been known about the function of this protein, but a publication from Li *et al*. in 2020 demonstrated its role in regulating Wee1 degradation and thus prompted us to revisit this candidate from our screen. In the model proposed by Li *et al*., FAM122A normally inhibits the phosphatase PP2A which is responsible for dephosphorylating and thus stabilizing the Wee1 kinase. When a cell experiences replication stress or DNA damage, ATR activates Chk1, and Chk1 phosphorylates a number of substrates to initiate DNA damage response, including FAM122A. Upon phosphorylation, FAM122A localizes in the cytoplasm where it binds to the protein 14-3-3 and is prevented from reentering the nucleus. The absence of FAM122A in the nucleus allows Wee1 dephosphorylation by PP2A thus stabilizing the protein and enabling an appropriate G2/M checkpoint. When FAM122A is absent, Wee1 degradation is prevented by continuous PP2A activity, and Li *et al*. show that FAM122A can therefore be an acquired resistance mechanism to ATR and Chk1 inhibitors. Since our screen induced DNA damage through the application of HU, sg*FAM122A*

cells may have gained a slight replicative advantage by enhancing DNA damage response and thus becoming one of our top hits.

To test this idea, we once again used CRISPR-Cas9 to generate sg*FAM122A* CDK2AF cells (Figure 2.5F). We measured sg*FAM122A* outgrowth after HU treatment by CTG but saw no difference in proliferation when compared to HU-treated sgCTRL cells (Figure 2.5H). However, when we assayed DNA damage by western blot, we did observe a notable drop in γH2AX levels in sg*FAM122A* cells treated with HU (Figure 2.5G). This outcome, though not our outgrowth data, was consistent with the model proposed by Li *et al*.

2.4 Discussion

In this study, we employed a genome wide CRISP-Cas9 screen to find mediators of HU hypersensitivity in CDK2AF cells. These cells were previously engineered in our lab to express constitutively active CDK2 so that the effects of CDK2 inhibitory phosphorylations during S-phase could be studied directly. While it wase shown that these cells exhibited excessive amounts of DNA damage and senesced after HU treatment, the downstream targets of CDK2 that were mediating this phenotype were still unidentified. Our goal was to identify these mediators by knocking them out with the Brunello CRISPR-Cas9 library and screening for those cells that were able to grow after HU treatment. Initial data from the three versions of our screen showed an enrichment for genes involved in the apoptotic signaling pathway (*CASP8*, *DR4*, *DR5*, *FADD*, and *BIDD*) and the MAPK signaling pathway (*MAP2K3* and *MAPK14*). The identification of multiple genes in the apoptotic signaling pathway was intriguing given the lack of apoptosis seen in HU-treated CDK2AF cells in previous experiments[80]. Rather than initiating apoptosis, CDK2AF cells were shown to exit the cell cycle by senescence when treated with HU and assayed for senescence-associated beta-galactosidase activity. One possible explanation for this apparent disparity might

be that caspase-8 is performing one of its non-apoptotic functions in response to HU treatment in these cells. More specifically, in addition to its role in apoptosis, caspase-8 has been described in recent years as having a role as a scaffolding protein to promote NF-κB-dependent expression of pro-inflammatory cytokines and chemokines such as IL-6 and IL-8[84,85]. Interestingly, IL-6 and IL-8 are among the most commonly found cytokines in microenvironments surrounding senescent cells, otherwise known as the senescence-associated secretory phenotype (SASP)[86]. Furthermore, MAPKs have also been shown to contribute to cell senescence under conditions of oxidative stress and/or DNA damage[87]. It's therefore conceivable that the MAPK and apoptotic genes found in our screen actually contribute to CDK2 driven senescence in HU-treated CDK2AF cells.

Of note from the MAGeCK analysis of our screens were the particularly modest gene logFC values, especially in conditions of higher drug concentration (1mM HU) and shorter outgrowth (4 days) (Table 2.1). It was only in our 100μM, 14-day outgrowth screen that we observed a large positive logFC value (5.7) for our strongest expected hit, CDK2. Most other genes that scored highly in the analysis exhibited logFC values between 0.5-1.5 depending on screen conditions. Nonetheless, we moved forward with validation and prioritized *CASP8*, *DR4*, *DR5*, *MAPK14*, and *MAP2K3* because these hits were shared between at least two of our three screens, ranked in the top 10 of their respective screens by the MAGeCK algorithm, and occupied roles in shared pathways (i.e., apoptotic signaling or MAPK signaling).

After generating individual knockouts of each hit in CDK2AF cells, we assayed DNA damage and cell outgrowth after HU treatment to recapitulate our screen results. However, with the exception of *CDK2* knockout cells, all of our aforementioned hits failed to strongly rescue growth after HU treatment (Figure 2.5C). Furthermore, DNA damage was either unchanged or slightly increased in our hits when measuring for γH2AX+ cells by flow cytometry (Figure 2.5E).

A colony formation assay with sg*CDK2*, sg*MAPK14*, and sg*CASP8* cells also confirmed the inability of individual hits (besides *CDK2*) to rescue growth after HU treatment (Figure 2.5B). These results may suggest that the modest growth rescue seen from these hits in our screen may be secondary to the DNA damage induced by HU rather than participating in the formation of that damage directly. Following these initial validation experiments, we revisited another hit, *FAM122A*, after a recent publication implicated this protein in regulating Wee1 stability[88,89]. We created an individual knockout of this gene in CDK2AF cells, but once again failed to see strong growth rescue after HU treatment. However, HU-treated sg*FAM122A* CDK2AF cells did exhibit a noticeable reduction in γH2AX levels measured both by western blot and by flow cytometry. In concert with the model proposed by Li *et al*, the reduction in γH2AX observed in our cells may be the result of proper G2/M checkpoint activation by Wee1 stabilization. While CDK2 in this setting could not be inactivated by Wee1 due to the AF mutation, the phosphorylation of other Wee1 substrates including CDK1 may be enough to override the activity of CDK2 and initiate some amount of DNA repair.

Because our screen data and our validation experiments were unable to show strong growth rescue, we could eliminate the following explanations for the observed HU hypersensitivity phenotype in CDK2AF cells: 1) CDK2 has a single downstream target that is activated upon phosphorylation and responsible for HU hypersensitivity. It is possible that the observed HU hypersensitivity is the result of multiple downstream targets being activated by CDK2 which might explain why none of our individual knockouts could rescue growth after HU treatment on their own. It is also possible that the downstream target is an essential gene, so we would be unable to find it in a knockout screen. 2) If CDK2 does have a single downstream target that is responsible for the HU hypersensitivity phenotype, then the effect of CDK2 phosphorylation is activating. One

of the assumptions made in our screen is that the downstream target responsible for HU hypersensitivity would be activated upon CDK2 phosphorylation and readily contribute to γH2AX+ accumulation and senescence. If the opposite is true, then our knockout screen would fail to find such a target since the act of knocking out that gene would be equivalent to an inactivating phosphorylation by CDK2. Thus, a CRISPR activation screen would be a logical next step to find such a substrate.

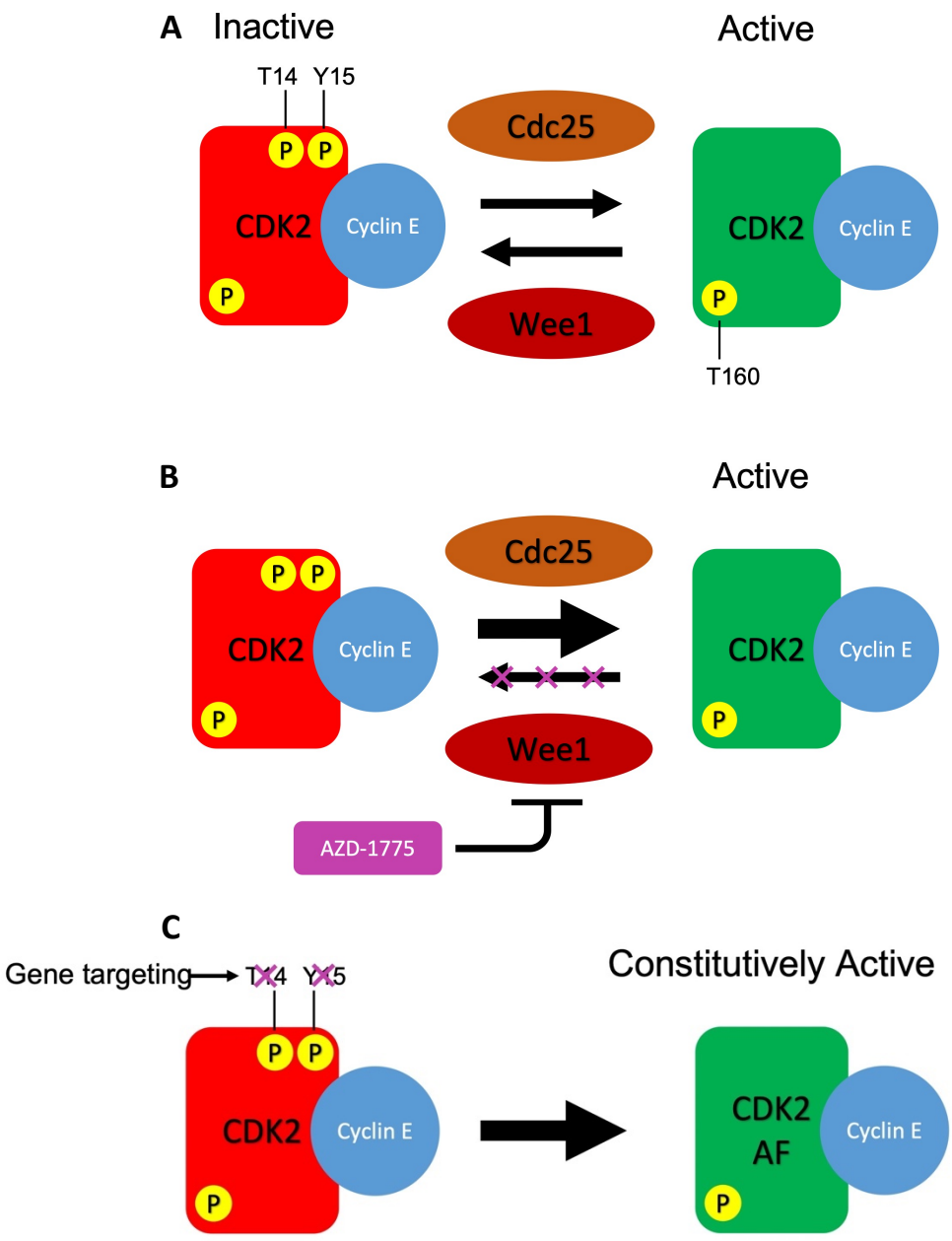

Figure 2.1 Regulation of CDK2 activity

(A) For full cyclin E-CDK2 activation, Cdc25 must dephosphorylate CDK2 at the two inhibitory phosphorylation sites, T14 and Y15, which are regulated by the Wee1 and Myt1 kinases, respectively. **(B)** The Wee1 kinase can be targeted by AZD1175 so as to prevent inhibitory phosphorylation of CDK2. This treatment results in overactive cyclin E/A-CDK2 complexes and promotes synthetic lethality in *TP53* mutant cancers by driving replication catastrophe, premature mitotic entry, and apoptosis. **(C)** In order to study the specific effects of CDK2 hyperactivity, the Clurman lab generated a mutant form of CDK2 lacking the two phosphorylation sites at T14/Y15. Thus, these "CDK2AF" cells possess constitutively active CDK2 and display several unique phenotypes including hypersensitivity to S-phase agents.

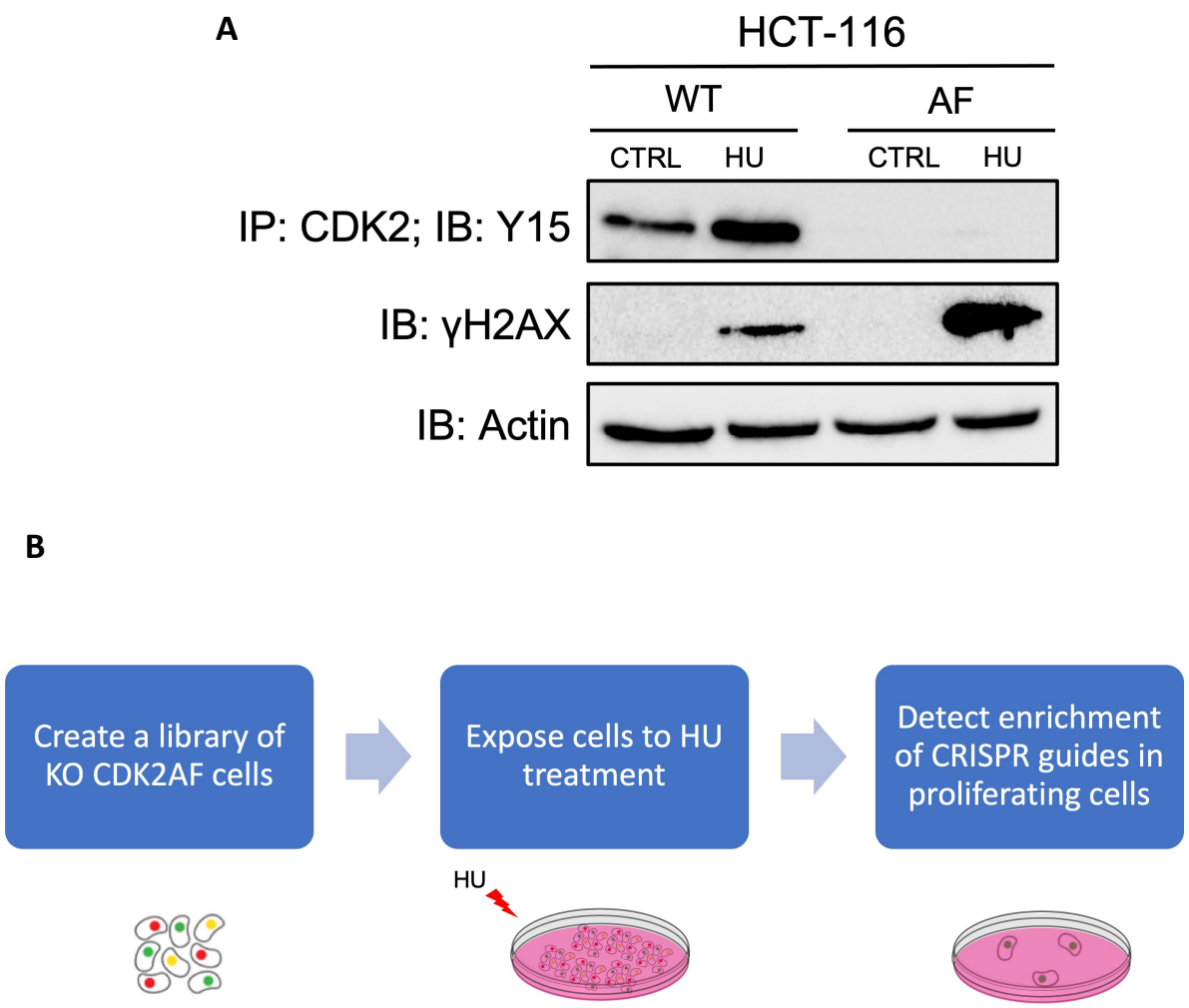

Figure 2.2 CDK2AF HU hypersensitivity and CRISPR screen design
(A) HCT-116 WT and CDK2AF cells were treated with 1mM HU overnight and assayed for DNA damage by γH2AX western blot. CDK2AF cells were confirmed to be missing inhibitory phosphorylation by immunoprecipitating CDK2 and blotting for phospho-Y15. **(B)** A schematic depicting the genome-wide CRISPR-Cas9 knockout screen in CDK2AF cells. A population of CDK2AF knockout cells would be created using the Brunello CRISPR library, exposed to various HU treatments, and then allowed to grow out. Enrichment of specific knockouts can then be detected by isolating genomic DNA of surviving cells and submitting samples for deep sequencing.

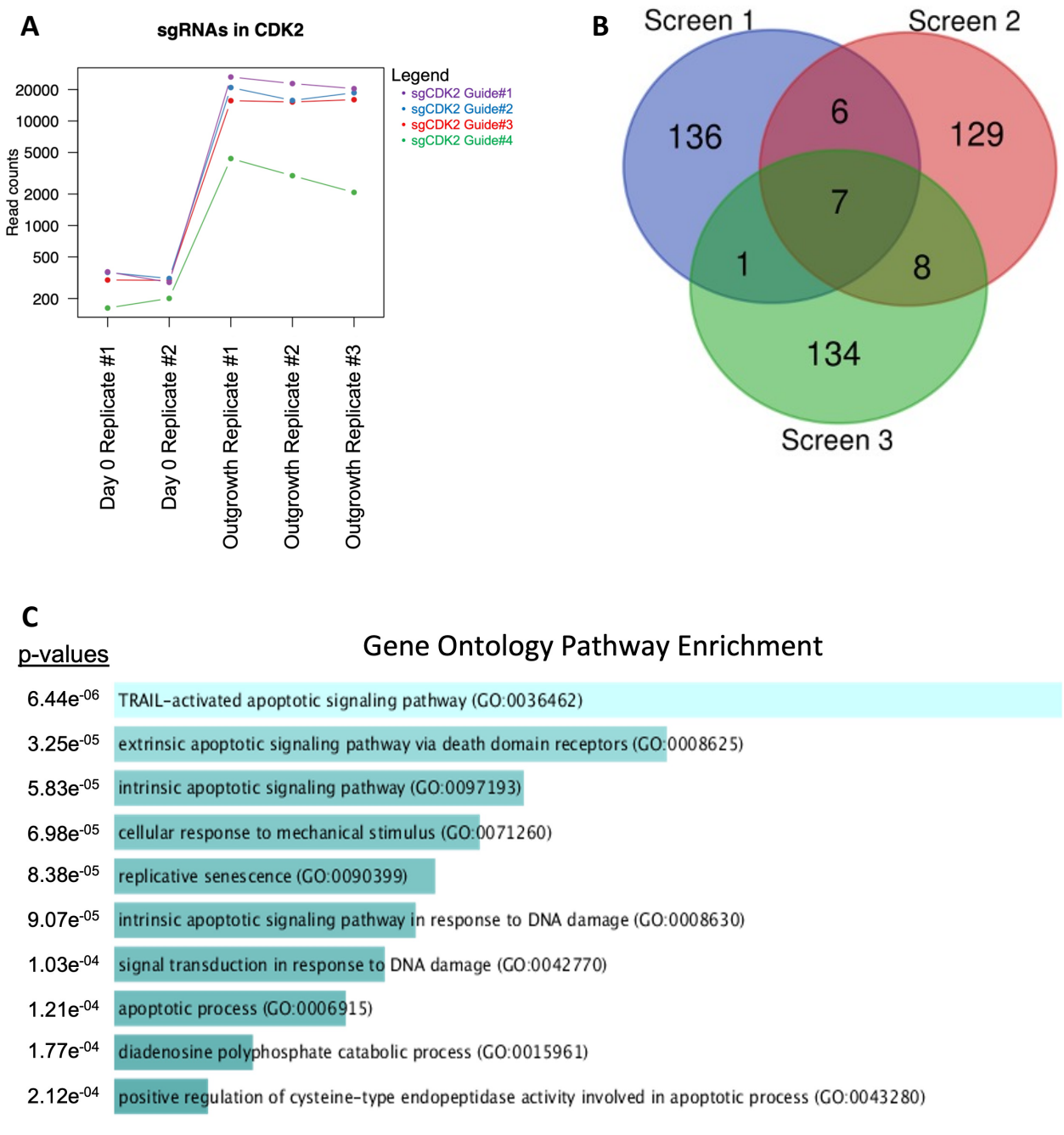

Figure 2.3 CDK2AF CRISPR-Cas9 screen results

(A) An example readout of sg*CDK2* enrichment from one of the screens. All four guides in the Brunello library targeting *CDK2* (seen in different colors) show an increase in read counts i.e., enrichment) between the two day 0 replicates and three outgrowth replicates submitted for deep sequencing. **(B)** Venn diagram showing overlap of the top 150 up represented hits between each of the three screens. **(C)** Gene ontology terms that were enriched for specific pathways in the top 150 hits from each screen ranked in order by decreasing p-value.

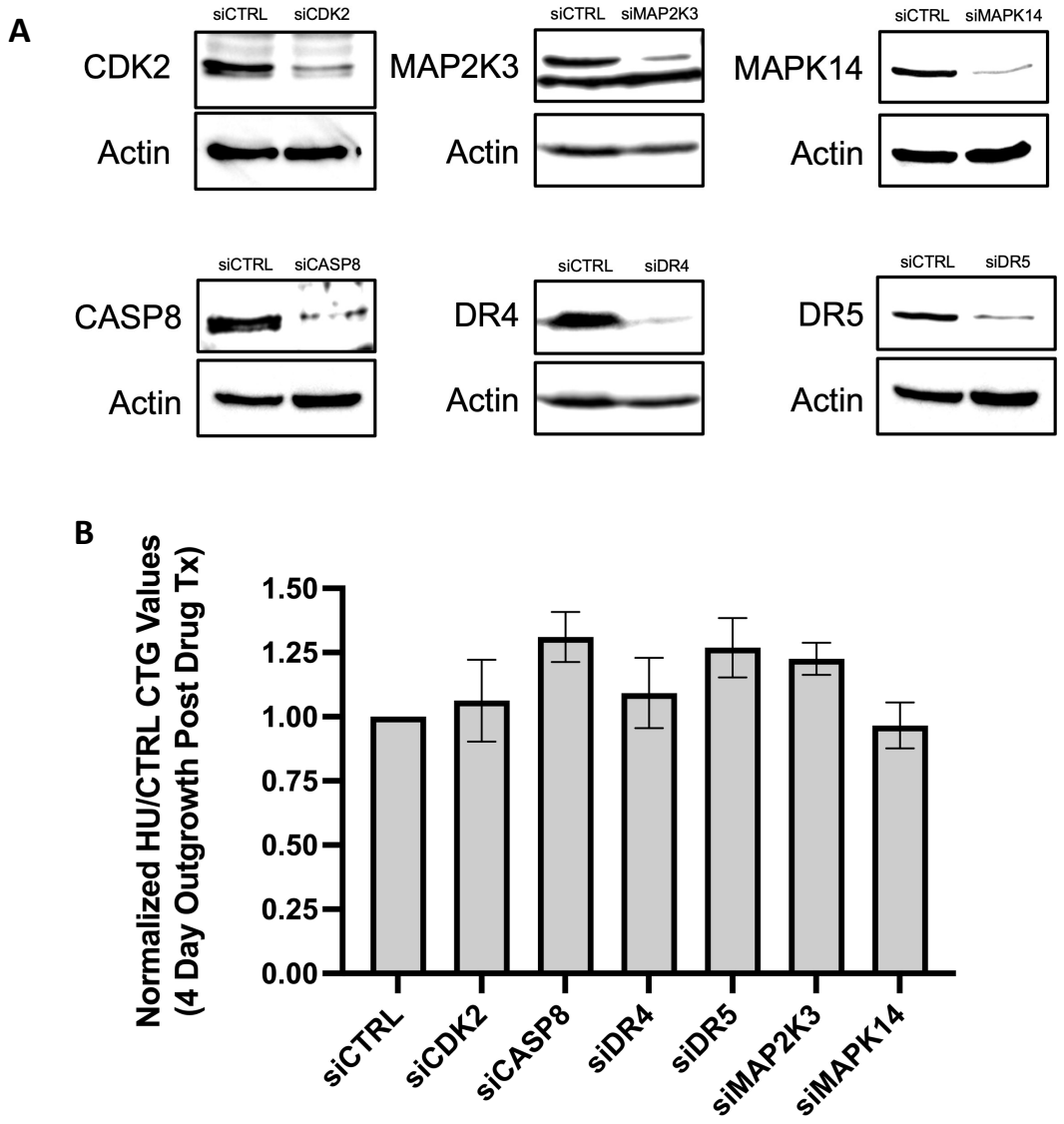

Figure 2.4 siRNA validation of selected screen hits
(A) Successful knockdowns of selected hits were confirmed by treating CDK2AF cells with siRNAs targeting *CDK2*, *MAP2K3*, *MAPK14*, *CASP8*, *DR4*, and *DR5*. AllStars Negative Control siRNA (Qiagen) was used as our siCTRL. **(B)** Each knockdown was seeded in triplicate into 96-well plates, treated with two rounds of 1mM HU for 24 hours each round, washed with PBS, and allowed to grow for four days. Post-treatment outgrowth of each knockdown was measured by CellTiter-Glo and normalized to siCTRL.

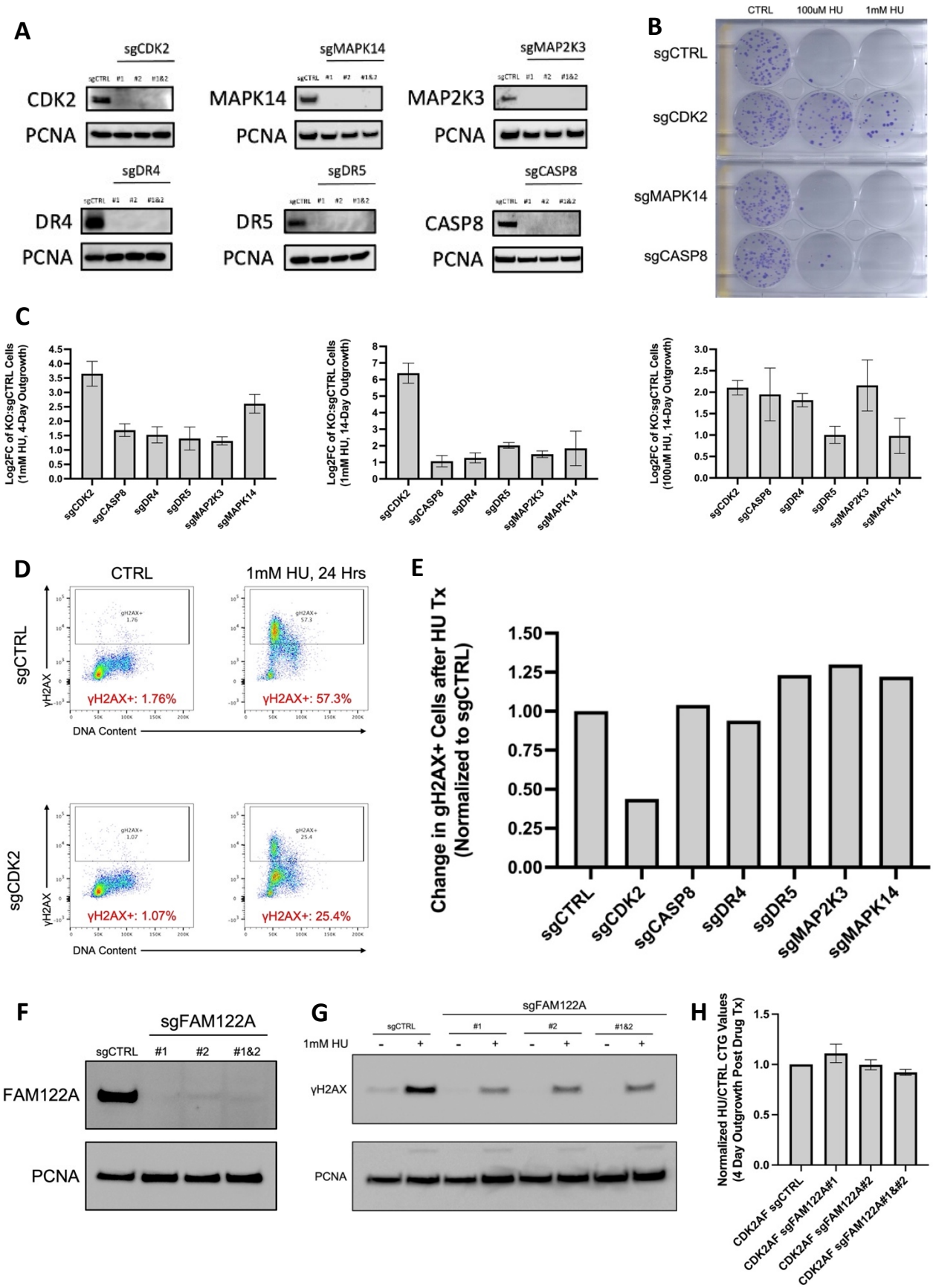
A
sgCDK2
CDK2
PCNA
sgMAPK14
MAPK14
PCNA
sgMAP2K3
MAP2K3
PCNA
sgDR4
DR4
PCNA
sgDR5
DR5
PCNA
sgCASP8
CASP8
PCNA
B
CTRL
100uM HU
1mM HU
sgCTRL
sgCDK2
sgMAPK14
sgCASP8
C
Log2FC of KO:sgCTRL Cells (1mM HU, 4-Day Outgrowth)
Log2FC of KO:sgCTRL Cells (1mM HU, 14-Day Outgrowth)
Log2FC of KO:sgCTRL Cells (100uM HU, 14-Day Outgrowth)
sgCDK2
sgCASP8
sgDR4
sgDR5
sgMAP2K3
sgMAPK14
D
CTRL
1mM HU, 24 Hrs
sgCTRL
sgCDK2
γH2AX
DNA Content
γH2AX+: 1.76%
γH2AX+: 57.3%
γH2AX+: 1.07%
γH2AX+: 25.4%
E
Change in gH2AX+ Cells after HU Tx (Normalized to sgCTRL)
sgCTRL
sgCDK2
sgCASP8
sgDR4
sgDR5
sgMAP2K3
sgMAPK14
F
sgFAM122A
sgCTRL
#1
#2
#1&2
FAM122A
PCNA
G
sgFAM122A
sgCTRL
#1
#2
#1&2
1mM HU
γH2AX
PCNA
H
Normalized HU/CTRL CTG Values (4 Day Outgrowth Post Drug Tx)
CDK2AF sgCTRL
CDK2AF sgFAM122A#1
CDK2AF sgFAM122A#2
CDK2AF sgFAM122A#1&#2

Figure 2.5 sgRNA validation of selected screen hits
(A) Western blots depicting successful knockout of each target in CDK2AF cells. Two sgRNA sequences were designed for each gene and delivered alone or in combination to generate knockouts. All subsequent validation experiments proceeded with sg#1 for each gene. **(B)** Colony formation assay of select hits treated with HU and allowed to grow for 10 days. **(C)** Pooled qPCR outgrowth assays measuring fold change of KO to sgCTRL cells after corresponding HU treatments and outgrowth periods. This assay was completed three times so as to replicate the conditions of each of the three original CRISPR screens: 1mM HU, 4-day outgrowth (n=3); 1mM HU, 14-day outgrowth (n=3); 100μM HU, 14-day outgrowth (n=3). **(D)** DNA damage assayed by flow cytometry in CDK2AF sgCTRL vs. sg*CDK2* cells. Cells were treated with 1mM HU for 24 hours, fixed, stained, and analyzed by flow cytometry gating for γH2AX+ cells. **(E)** Quantification of flow cytometry plots for each hit showing change in γH2AX+ cells between treated and untreated cells, normalized to sgCTRL. **(F)** Western blot depicting successful knockout of *FAM122A* in CDK2AF cells. Two sgRNAs were designed and delivered alone or in combination to generate knockouts. **(G)** CDK2AF sgCTRL and sg*FAM122A* cells were treated with 1mM HU for 24 hours and assayed for DNA damage by γH2AX western blot. **(H)** Each sg*FAM122A* line was seeded in triplicate into 96-well plates, treated with two rounds of 1mM HU for 24 hours each round, washed with PBS, and allowed to grow for four days. Post-treatment outgrowth of each knockout was measured by CellTiter-Glo and normalized to sgCTRL.

Table 2.1 Top 150 hits from each screen ranked by MAGeCK algorithm

Screen 1 (1mM HU, 4 days)					
pos|rank	gene id	pos|score	pos|p-value	pos|fdr	pos|lfc
1	TNFRSF10B	1.27E-06	4.35E-06	4.70E-02	6.30E-01
2	DNAH5	1.42E-06	4.86E-06	4.70E-02	8.15E-01
3	CASP8	2.09E-06	7.41E-06	4.79E-02	7.67E-01
4	ENPP7	3.42E-06	1.25E-05	6.06E-02	5.63E-01
5	EFCAB13	2.58E-05	1.01E-04	2.41E-01	2.13E-01
6	MAPK14	2.89E-05	1.11E-04	2.41E-01	5.50E-01
7	OR9A4	3.22E-05	1.24E-04	2.41E-01	5.51E-01
8	TNFRSF10A	3.25E-05	1.25E-04	2.41E-01	5.51E-01
9	AKT1	3.48E-05	1.33E-04	2.41E-01	4.37E-01
10	CTSB	3.70E-05	1.41E-04	2.41E-01	4.44E-01
11	EDA2R	3.92E-05	1.49E-04	2.41E-01	4.38E-01
12	BAX	5.02E-05	1.95E-04	2.90E-01	4.74E-01
13	KRTAP19-4	7.11E-05	2.81E-04	3.54E-01	7.02E-01
14	APOH	7.73E-05	3.10E-04	3.54E-01	5.02E-01
15	SFMBT1	7.75E-05	3.11E-04	3.54E-01	5.99E-01
16	TCF7L2	9.24E-05	3.65E-04	3.74E-01	4.06E-01
17	CCDC28A	9.26E-05	3.67E-04	3.74E-01	4.24E-01
18	CSRP3	1.03E-04	4.09E-04	3.85E-01	3.47E-01
19	LAMB3	1.06E-04	4.17E-04	3.85E-01	3.70E-01
20	CEBPB	1.14E-04	4.47E-04	3.94E-01	5.98E-01
21	NDUFS1	1.21E-04	4.75E-04	3.94E-01	6.03E-01
22	RGS7	1.25E-04	4.89E-04	3.94E-01	4.40E-01
23	DCBLD1	1.47E-04	5.85E-04	4.51E-01	5.54E-01
24	DCAF7	1.56E-04	6.13E-04	4.51E-01	4.19E-01
25	LRP12	1.60E-04	6.29E-04	4.51E-01	3.03E-01
26	DLL4	1.81E-04	6.92E-04	4.79E-01	1.27E-01
27	OR2AK2	1.97E-04	7.48E-04	4.81E-01	5.74E-01
28	MRPL41	2.10E-04	7.94E-04	4.81E-01	4.82E-01
29	DCAF8	2.24E-04	8.47E-04	4.82E-01	4.61E-01
30	DEFA5	2.30E-04	8.72E-04	4.82E-01	4.17E-01
31	PDE9A	2.33E-04	8.78E-04	4.82E-01	3.68E-01
32	ATM	2.41E-04	9.03E-04	4.82E-01	4.62E-01
33	ZNF709	2.54E-04	9.51E-04	4.82E-01	4.09E-01
34	PAPOLB	2.56E-04	9.60E-04	4.82E-01	3.54E-01
35	TBC1D22A	2.62E-04	9.76E-04	4.82E-01	4.65E-01
36	NT5C1A	2.67E-04	9.95E-04	4.82E-01	2.70E-01
37	FN3K	2.76E-04	1.03E-03	4.85E-01	2.48E-01
38	CACNA1F	2.84E-04	1.05E-03	4.85E-01	1.50E-01
39	OR5M8	3.10E-04	1.15E-03	5.06E-01	4.40E-01
40	CRIP1	3.26E-04	1.20E-03	5.18E-01	5.39E-01
41	FAM122A	3.36E-04	1.24E-03	5.19E-01	1.37E-01
42	TH	3.49E-04	1.28E-03	5.19E-01	6.89E-01
43	B3GAT1	3.65E-04	1.34E-03	5.30E-01	3.52E-01
44	TMSB4Y	3.76E-04	1.38E-03	5.30E-01	5.39E-01
45	ITM2B	3.83E-04	1.41E-03	5.30E-01	4.11E-01
46	IL37	3.88E-04	1.42E-03	5.30E-01	2.47E-02
47	L3MBTL3	4.13E-04	1.52E-03	5.51E-01	6.58E-01
48	HDAC5	4.18E-04	1.54E-03	5.51E-01	3.30E-01
49	STK36	4.39E-04	1.60E-03	5.56E-01	2.91E-02
50	CDNF	4.48E-04	1.64E-03	5.56E-01	5.10E-01
51	ZNF660	4.56E-04	1.68E-03	5.56E-01	3.47E-01
52	RAD51AP2	4.61E-04	1.70E-03	5.56E-01	4.19E-01
53	CYP11B1	4.67E-04	1.72E-03	5.56E-01	4.33E-01
54	VNN3	4.77E-04	1.76E-03	5.58E-01	4.44E-01
55	LOC100505841	4.91E-04	1.81E-03	5.64E-01	2.36E-01
56	CSMD3	5.29E-04	1.94E-03	5.78E-01	3.87E-01
57	PLXNC1	5.31E-04	1.95E-03	5.78E-01	2.79E-01
58	CAP2	5.43E-04	1.99E-03	5.78E-01	1.13E-01
59	NKAIN2	5.47E-04	2.01E-03	5.78E-01	5.50E-01
60	KLHL18	5.59E-04	2.05E-03	5.78E-01	4.60E-01
61	HTR5A	5.65E-04	2.09E-03	5.78E-01	4.49E-01
62	LRRC14B	5.81E-04	2.14E-03	5.78E-01	3.54E-01
63	GPM6B	5.92E-04	2.17E-03	5.78E-01	4.44E-01
64	FGF14	5.94E-04	2.18E-03	5.78E-01	9.83E-02
65	MSC	6.25E-04	2.29E-03	5.78E-01	5.79E-01
66	PDE10A	6.40E-04	2.34E-03	5.78E-01	4.65E-01
67	SLC26A2	6.46E-04	2.36E-03	5.78E-01	1.99E-01
68	EN2	6.59E-04	2.41E-03	5.78E-01	4.23E-01
69	CCDC15	6.60E-04	2.41E-03	5.78E-01	2.59E-01
70	PLA2G4C	6.65E-04	2.43E-03	5.78E-01	2.64E-01
71	TADA3	6.70E-04	2.45E-03	5.78E-01	4.58E-01
72	UGT1A4	6.81E-04	2.49E-03	5.78E-01	3.84E-01
73	RNASE3	6.92E-04	2.53E-03	5.78E-01	5.32E-01
74	EPHA7	6.98E-04	2.55E-03	5.78E-01	2.19E-01
75	CLEC1B	7.25E-04	2.65E-03	5.78E-01	5.99E-01
76	MGAM	7.34E-04	2.68E-03	5.78E-01	2.97E-01
77	DNAJC27	7.44E-04	2.71E-03	5.78E-01	4.69E-01
78	TBX3	7.49E-04	2.73E-03	5.78E-01	-4.61E-01
79	TBXAS1	7.50E-04	2.73E-03	5.78E-01	4.59E-01
80	LPAR6	7.55E-04	2.75E-03	5.78E-01	4.54E-01
81	SLC25A14	7.63E-04	2.78E-03	5.78E-01	3.28E-01
82	OR2A2	7.77E-04	2.83E-03	5.78E-01	5.17E-01
83	EDARADD	7.78E-04	2.83E-03	5.78E-01	6.13E-01
84	RAP1A	7.95E-04	2.89E-03	5.78E-01	3.22E-01
85	FHIT	8.01E-04	2.91E-03	5.78E-01	2.50E-01
86	SPATA31D3	8.34E-04	3.02E-03	5.78E-01	6.04E-01
87	FSHB	8.39E-04	3.04E-03	5.78E-01	3.96E-01
88	SPAG16	8.53E-04	3.09E-03	5.78E-01	1.03E-01
89	CD244	8.57E-04	3.11E-03	5.78E-01	3.97E-01
90	RPS4Y1	8.80E-04	3.20E-03	5.78E-01	4.62E-01
91	FAM160A2	8.96E-04	3.25E-03	5.78E-01	7.52E-01
92	GAGE2A	9.04E-04	3.27E-03	5.78E-01	5.30E-02
93	SYN1	9.24E-04	3.35E-03	5.78E-01	3.43E-01
94	PGK2	9.24E-04	3.35E-03	5.78E-01	3.90E-01
95	TMEM55A	9.29E-04	3.37E-03	5.78E-01	4.14E-01
96	SLC22A3	9.34E-04	3.38E-03	5.78E-01	2.62E-01
97	OR6B2	9.35E-04	3.39E-03	5.78E-01	4.04E-01
98	PGPEP1L	9.56E-04	3.46E-03	5.78E-01	1.82E-01
99	SH3D19	9.57E-04	3.47E-03	5.78E-01	4.12E-01
100	MAPKAP1	9.64E-04	3.49E-03	5.78E-01	3.71E-01

Screen 2 (1mM HU, 14 days)					
pos|rank	gene id	pos|score	pos|p-value	pos|fdr	pos|lfc
1	CASP8	8.68E-10	2.56E-07	9.90E-04	9.30E-01
2	CDK2	1.64E-09	2.56E-07	9.90E-04	1.30E+00
3	TNFRSF10A	3.88E-09	2.56E-07	9.90E-04	6.46E-01
4	MAPK14	2.69E-08	2.56E-07	9.90E-04	5.66E-01
5	TNFRSF10B	3.90E-08	2.56E-07	9.90E-04	6.63E-01
6	MIDN	3.13E-07	1.28E-06	4.13E-03	5.99E-01
7	FAM122A	1.26E-06	4.35E-06	1.18E-02	8.80E-01
8	DDIT3	1.43E-06	4.86E-06	1.18E-02	5.55E-01
9	MAP2K3	5.56E-06	2.02E-05	4.35E-02	5.58E-01
10	EIF4B	8.56E-06	3.30E-05	6.39E-02	5.25E-01
11	CHRM2	1.67E-05	6.62E-05	1.17E-01	3.41E-01
12	CCNE1	1.97E-05	7.70E-05	1.24E-01	3.71E-01
13	CCDC96	3.06E-05	1.17E-04	1.74E-01	5.34E-01
14	IRGC	3.26E-05	1.26E-04	1.74E-01	3.80E-01
15	CKS2	3.57E-05	1.35E-04	1.75E-01	6.42E-01
16	MID1IP1	4.52E-05	1.73E-04	1.95E-01	3.03E-01
17	FAM120C	5.08E-05	1.97E-04	1.95E-01	4.40E-01
18	KLHL9	5.17E-05	2.00E-04	1.95E-01	5.80E-01
19	NUDT10	5.17E-05	2.01E-04	1.95E-01	3.58E-01
20	IER2	5.30E-05	2.06E-04	1.95E-01	2.97E-01
21	PDE12	6.06E-05	2.39E-04	2.10E-01	7.74E-01
22	ANKRD9	6.40E-05	2.56E-04	2.15E-01	3.70E-01
23	BID	8.13E-05	3.26E-04	2.54E-01	6.99E-01
24	AVPR1A	8.24E-05	3.29E-04	2.54E-01	3.60E-01
25	LOC101927572	8.79E-05	3.46E-04	2.56E-01	4.41E-01
26	COX8A	9.05E-05	3.58E-04	2.56E-01	4.34E-01
27	KRTAP9-8	9.55E-05	3.82E-04	2.56E-01	2.78E-01
28	FADD	9.73E-05	3.91E-04	2.56E-01	6.24E-01
29	SLC5A10	1.39E-04	5.50E-04	3.26E-01	5.10E-01
30	CELF1	1.40E-04	5.55E-04	3.26E-01	5.43E-01
31	PYGO2	1.45E-04	5.77E-04	3.28E-01	3.92E-01
32	TMEM221	1.49E-04	5.92E-04	3.28E-01	3.85E-01
33	RAVER1	1.81E-04	6.92E-04	3.72E-01	4.58E-01
34	GAREM	2.01E-04	7.60E-04	3.96E-01	2.68E-01
35	PDE10A	2.05E-04	7.77E-04	3.96E-01	5.58E-01
36	ISM1	2.17E-04	8.20E-04	4.07E-01	3.66E-01
37	CSF3	2.31E-04	8.76E-04	4.20E-01	3.01E-01
38	OR52I2	2.68E-04	9.99E-04	4.57E-01	3.57E-01
39	JPH1	2.84E-04	1.05E-03	4.62E-01	7.14E-01
40	EMD	3.02E-04	1.12E-03	4.83E-01	3.12E-01
41	FGF11	3.15E-04	1.17E-03	4.89E-01	2.80E-01
42	BAX	3.25E-04	1.20E-03	4.89E-01	5.92E-01
43	C7orf43	3.34E-04	1.23E-03	4.89E-01	3.47E-01
44	IER5L	3.36E-04	1.24E-03	4.89E-01	-7.50E-02
45	ADGRL3	3.53E-04	1.30E-03	4.93E-01	3.09E-01
46	PDZD3	3.62E-04	1.33E-03	4.93E-01	4.98E-01
47	TBRG4	3.81E-04	1.40E-03	4.93E-01	2.94E-01
48	FOXK1	3.83E-04	1.41E-03	4.93E-01	5.51E-01
49	OR2L8	3.98E-04	1.46E-03	4.93E-01	2.53E-01
50	GIMD1	3.99E-04	1.46E-03	4.93E-01	4.46E-01
51	GPR27	4.02E-04	1.48E-03	4.93E-01	3.49E-01
52	KRTAP17-1	4.25E-04	1.55E-03	4.98E-01	4.94E-01
53	TMEM170A	4.39E-04	1.60E-03	4.98E-01	1.03E-01
54	GIT1	4.58E-04	1.69E-03	4.98E-01	4.09E-01
55	SSNA1	4.61E-04	1.70E-03	4.98E-01	4.41E-01
56	CEACAM3	4.89E-04	1.80E-03	4.98E-01	3.13E-01
57	NBPF3	4.91E-04	1.81E-03	4.98E-01	-1.40E-01
58	PAX1	4.94E-04	1.82E-03	4.98E-01	4.14E-01
59	PFKM	5.02E-04	1.85E-03	4.98E-01	3.72E-01
60	SPANXB1	5.13E-04	1.89E-03	4.98E-01	3.65E-01
61	FAM175B	5.15E-04	1.90E-03	4.98E-01	2.77E-01
62	SCRN1	5.17E-04	1.90E-03	4.98E-01	4.28E-01
63	DOCK5	5.21E-04	1.92E-03	4.98E-01	2.76E-01
64	OR4Q3	5.24E-04	1.93E-03	4.98E-01	4.25E-01
65	TMCO4	5.32E-04	1.95E-03	4.98E-01	5.91E-01
66	SLC27A3	5.43E-04	1.99E-03	4.99E-01	2.57E-02
67	TMEM223	5.60E-04	2.06E-03	4.99E-01	1.67E-01
68	ZNF853	5.61E-04	2.06E-03	4.99E-01	4.38E-01
69	USP48	5.90E-04	2.16E-03	4.99E-01	5.03E-01
70	KRT23	5.94E-04	2.18E-03	4.99E-01	1.51E-01
71	CKS1B	6.07E-04	2.23E-03	4.99E-01	3.33E-01
72	AKT1	6.17E-04	2.26E-03	4.99E-01	4.26E-01
73	NR2F1	6.19E-04	2.27E-03	4.99E-01	4.37E-01
74	SYTL5	6.20E-04	2.28E-03	4.99E-01	3.05E-01
75	KIAA1109	6.27E-04	2.30E-03	4.99E-01	3.82E-01
76	TMEM213	6.35E-04	2.33E-03	4.99E-01	4.74E-01
77	TFDP2	6.46E-04	2.36E-03	4.99E-01	-1.09E-01
78	NRTN	6.48E-04	1.86E-03	4.98E-01	4.02E-01
79	USP24	6.51E-04	1.87E-03	4.98E-01	6.05E-01
80	FAM19A5	6.59E-04	2.41E-03	4.99E-01	3.29E-01
81	PCOLCE2	6.65E-04	2.43E-03	4.99E-01	2.74E-01
82	TMEM9B	6.75E-04	2.46E-03	4.99E-01	4.91E-01
83	RAB25	6.77E-04	2.47E-03	4.99E-01	3.21E-01
84	LVRN	6.81E-04	2.49E-03	4.99E-01	2.50E-01
85	EXD3	6.84E-04	2.50E-03	4.99E-01	4.42E-01
86	COL9A2	6.93E-04	2.53E-03	4.99E-01	3.67E-01
87	GJB1	6.98E-04	2.55E-03	4.99E-01	3.87E-01
88	CD52	7.25E-04	2.64E-03	5.04E-01	3.94E-01
89	TUBB3	7.33E-04	2.68E-03	5.04E-01	2.96E-01
90	ZNF749	7.48E-04	2.73E-03	5.04E-01	4.32E-01
91	MSH2	7.49E-04	2.73E-03	5.04E-01	3.15E-02
92	OR4C11	7.63E-04	2.78E-03	5.04E-01	2.62E-01
93	GGT1	7.74E-04	2.82E-03	5.04E-01	4.51E-01
94	ADAMTS2	7.77E-04	2.83E-03	5.04E-01	1.11E-01
95	RPS6KA3	7.83E-04	2.85E-03	5.04E-01	2.56E-01
96	WNT16	8.01E-04	2.91E-03	5.04E-01	1.26E-01
97	YBX1	8.02E-04	2.91E-03	5.04E-01	2.51E-01
98	TP53	8.23E-04	2.98E-03	5.04E-01	7.54E-01
99	EDNRB	8.27E-04	2.99E-03	5.04E-01	2.93E-01
100	C19orf12	8.30E-04	3.01E-03	5.04E-01	4.83E-01

Screen 3 (100µM HU, 14 days)					
pos|rank	gene id	pos|score	pos|p-value	pos|fdr	pos|lfc
1	CDK2	2.63E-11	2.56E-07	2.48E-03	5.76E+00
2	FAM122A	3.19E-09	2.56E-07	2.48E-03	1.57E+00
3	GTPBP6	2.31E-07	1.28E-06	8.25E-03	9.03E-01
4	TAZ	7.39E-07	2.81E-06	1.36E-02	1.07E+00
5	MAP2K3	7.53E-06	2.94E-05	1.14E-01	8.73E-01
6	GTPBP8	1.03E-05	3.86E-05	1.25E-01	5.84E-01
7	TMEM8C	1.33E-05	5.19E-05	1.32E-01	6.74E-01
8	MAPK14	2.22E-05	8.92E-05	1.81E-01	5.54E-01
9	KLF10	2.34E-05	9.33E-05	1.81E-01	4.32E-01
10	SLC4A1AP	2.75E-05	1.08E-04	1.90E-01	4.33E-01
11	FURIN	3.96E-05	1.50E-04	2.41E-01	5.25E-01
12	MCAT	4.86E-05	1.87E-04	2.58E-01	6.41E-01
13	NRBP1	5.05E-05	1.96E-04	2.58E-01	7.91E-01
14	YME1L1	5.30E-05	2.06E-04	2.58E-01	9.27E-01
15	DAPP1	5.54E-05	2.13E-04	2.58E-01	4.40E-01
16	HLA-A	5.92E-05	2.34E-04	2.66E-01	6.55E-01
17	TNFRSF10B	6.93E-05	2.77E-04	2.79E-01	4.32E-01
18	HTRA2	7.69E-05	3.07E-04	2.79E-01	8.66E-01
19	TMEM50B	7.75E-05	3.11E-04	2.79E-01	4.77E-01
20	STT3A	7.92E-05	3.16E-04	2.79E-01	3.22E-01
21	NDUFB7	7.94E-05	3.17E-04	2.79E-01	4.20E-01
22	NDUFAF6	9.21E-05	3.64E-04	3.04E-01	4.51E-01
23	GCSAM	9.58E-05	3.84E-04	3.04E-01	3.20E-01
24	CA2	9.80E-05	3.92E-04	3.04E-01	3.35E-01
25	THAP11	1.12E-04	4.38E-04	3.18E-01	6.36E-01
26	AKR1E2	1.13E-04	4.43E-04	3.18E-01	3.18E-01
27	PCGF5	1.25E-04	4.91E-04	3.21E-01	6.85E-01
28	ZDHHC19	1.27E-04	5.02E-04	3.21E-01	3.83E-01
29	FARP1	1.29E-04	5.10E-04	3.21E-01	2.66E-01
30	SGK223	1.33E-04	5.26E-04	3.21E-01	6.37E-01
31	TNFRSF10A	1.36E-04	5.39E-04	3.21E-01	4.93E-01
32	TSC22D2	1.39E-04	5.50E-04	3.21E-01	1.24E+00
33	BCL3	1.42E-04	5.65E-04	3.21E-01	3.45E-01
34	ZBTB17	1.47E-04	5.85E-04	3.21E-01	8.70E-01
35	DCAF7	1.51E-04	5.99E-04	3.21E-01	3.12E-01
36	MIDN	1.59E-04	6.24E-04	3.21E-01	6.10E-01
37	PAPOLA	1.61E-04	6.29E-04	3.21E-01	4.64E-01
38	OR10K2	1.81E-04	6.92E-04	3.21E-01	4.33E-02
39	KCNMB4	1.87E-04	7.06E-04	3.21E-01	4.18E-01
40	SETD2	1.88E-04	7.13E-04	3.21E-01	5.24E-01
41	RFFL	1.89E-04	7.13E-04	3.21E-01	4.90E-01
42	GNA13	1.89E-04	7.13E-04	3.21E-01	2.90E-01
43	CEBPB	2.01E-04	7.59E-04	3.31E-01	5.73E-01
44	MTRF1L	2.12E-04	8.03E-04	3.31E-01	4.41E-01
45	UBOX5	2.13E-04	8.04E-04	3.31E-01	4.20E-01
46	ROMO1	2.19E-04	8.32E-04	3.33E-01	5.01E-01
47	PRAMEF2	2.25E-04	8.51E-04	3.33E-01	4.21E-01
48	USP48	2.28E-04	8.61E-04	3.33E-01	6.88E-01
49	ANO4	2.33E-04	8.78E-04	3.33E-01	5.13E-02
50	PPFIA4	2.54E-04	9.52E-04	3.54E-01	2.82E-01
51	ANKRD16	2.60E-04	9.70E-04	3.54E-01	5.43E-01
52	DSP	2.72E-04	1.01E-03	3.61E-01	4.71E-01
53	SEMA4F	2.84E-04	1.05E-03	3.70E-01	-3.34E-01
54	BRD8	2.95E-04	1.10E-03	3.70E-01	9.93E-01
55	JAGN1	2.99E-04	1.11E-03	3.70E-01	3.88E-01
56	SLC2A1	3.04E-04	1.13E-03	3.70E-01	1.07E+00
57	TMEM242	3.07E-04	1.14E-03	3.70E-01	5.65E-01
58	ATG4B	3.12E-04	1.16E-03	3.70E-01	5.52E-01
59	LRFN1	3.29E-04	1.22E-03	3.70E-01	4.60E-01
60	AKT1	3.34E-04	1.23E-03	3.70E-01	3.90E-01
61	OPHN1	3.36E-04	1.24E-03	3.70E-01	-6.38E-01
62	VHL	3.44E-04	1.27E-03	3.70E-01	3.79E-01
63	SAMHD1	3.45E-04	1.27E-03	3.70E-01	6.57E-01
64	TARDBP	3.53E-04	1.30E-03	3.70E-01	1.76E-01
65	CKS1B	3.65E-04	1.34E-03	3.70E-01	1.40E+00
66	ATPAF2	3.70E-04	1.37E-03	3.70E-01	5.13E-01
67	NPBWR1	3.72E-04	1.37E-03	3.70E-01	5.33E-01
68	TMEM200C	3.81E-04	1.40E-03	3.70E-01	3.74E-01
69	PROP1	3.81E-04	1.41E-03	3.70E-01	3.62E-01
70	GPI	3.83E-04	1.41E-03	3.70E-01	8.03E-01
71	CNN2	3.89E-04	1.43E-03	3.70E-01	3.93E-01
72	SLC7A7	3.93E-04	1.45E-03	3.70E-01	3.83E-01
73	UBAP2L	3.94E-04	1.45E-03	3.70E-01	4.73E-01
74	MTX2	4.09E-04	1.50E-03	3.78E-01	5.50E-01
75	OPA1	4.14E-04	1.52E-03	3.78E-01	9.98E-01
76	PCYT2	4.40E-04	1.61E-03	3.95E-01	4.89E-01
77	IER5L	4.91E-04	1.81E-03	4.32E-01	-1.80E-01
78	NUDCD1	4.91E-04	1.81E-03	4.32E-01	5.03E-01
79	KRTAP10-10	5.26E-04	1.93E-03	4.32E-01	5.18E-01
80	ZNF7	5.31E-04	1.95E-03	4.32E-01	4.32E-01
81	SLC16A2	5.35E-04	1.96E-03	4.32E-01	3.86E-01
82	MTOR	5.44E-04	1.99E-03	4.32E-01	7.10E-01
83	GATA3	5.57E-04	2.05E-03	4.32E-01	2.20E-01
84	CPQ	5.68E-04	2.10E-03	4.32E-01	2.67E-01
85	EIF4B	5.75E-04	2.12E-03	4.32E-01	6.43E-01
86	C1orf185	5.82E-04	2.14E-03	4.32E-01	6.63E-01
87	ARMT1	5.94E-04	2.18E-03	4.32E-01	2.11E-01
88	AMT	5.99E-04	2.20E-03	4.32E-01	2.89E-01
89	EEF1D	6.02E-04	2.21E-03	4.32E-01	2.67E-01
90	CLPB	6.09E-04	2.24E-03	4.32E-01	1.24E+00
91	GJB7	6.12E-04	2.24E-03	4.32E-01	4.90E-01
92	MRPL54	6.17E-04	2.26E-03	4.32E-01	4.12E-01
93	SLC17A1	6.17E-04	2.27E-03	4.32E-01	4.18E-01
94	ACTRT1	6.21E-04	2.28E-03	4.32E-01	4.79E-01
95	FER1L6	6.23E-04	2.29E-03	4.32E-01	3.15E-01
96	HLA-DPA1	6.28E-04	2.30E-03	4.32E-01	7.38E-01
97	GPR174	6.30E-04	2.31E-03	4.32E-01	3.35E-01
98	SPON2	6.36E-04	2.33E-03	4.32E-01	3.41E-01
99	EFCAB6	6.41E-04	2.34E-03	4.32E-01	3.51E-01
100	MPP1	6.66E-04	2.43E-03	4.35E-01	5.68E-01

101	NIN	9.75E-04	3.53E-03	5.78E-01	3.24E-01
102	KCNAB3	9.78E-04	3.54E-03	5.78E-01	2.44E-01
103	SCUBE1	9.81E-04	3.54E-03	5.78E-01	3.14E-01
104	HEPHL1	1.00E-03	3.62E-03	5.78E-01	5.06E-01
105	GREM2	1.01E-03	3.66E-03	5.78E-01	3.76E-01
106	FOXA1	1.03E-03	3.74E-03	5.78E-01	2.72E-01
107	GABRA5	1.04E-03	3.77E-03	5.78E-01	2.96E-01
108	UQCR10	1.06E-03	3.84E-03	5.78E-01	2.40E-01
109	IDH3B	1.06E-03	3.86E-03	5.78E-01	4.69E-01
110	CHD5	1.09E-03	3.96E-03	5.78E-01	4.58E-01
111	FLYWCH2	1.10E-03	3.99E-03	5.78E-01	3.83E-01
112	C16orf58	1.10E-03	3.99E-03	5.78E-01	4.21E-01
113	PLP1	1.10E-03	4.00E-03	5.78E-01	2.56E-01
114	BICC1	1.12E-03	4.06E-03	5.78E-01	3.79E-01
115	ADRA1A	1.12E-03	4.07E-03	5.78E-01	2.77E-01
116	KCNK13	1.14E-03	4.11E-03	5.78E-01	4.76E-01
117	PLIN5	1.14E-03	4.13E-03	5.78E-01	4.00E-01
118	SIX1	1.15E-03	4.16E-03	5.78E-01	1.27E-01
119	HIST1H4L	1.16E-03	4.19E-03	5.78E-01	3.95E-01
120	LY6D	1.16E-03	4.20E-03	5.78E-01	5.13E-01
121	NEK9	1.16E-03	4.21E-03	5.78E-01	3.81E-02
122	BCKDHB	1.18E-03	4.26E-03	5.80E-01	4.84E-01
123	CDK2	1.19E-03	4.30E-03	5.80E-01	5.47E-01
124	WRAP73	1.19E-03	4.32E-03	5.80E-01	5.79E-01
125	RNF220	1.21E-03	4.39E-03	5.84E-01	2.24E-01
126	KCNK2	1.24E-03	4.47E-03	5.84E-01	3.39E-01
127	C9orf3	1.24E-03	4.49E-03	5.84E-01	4.81E-01
128	CCSAP	1.24E-03	4.49E-03	5.84E-01	2.11E-01
129	GRAMD1B	1.27E-03	4.57E-03	5.90E-01	1.50E-01
130	MC5R	1.28E-03	4.63E-03	5.90E-01	3.63E-01
131	WNT10A	1.31E-03	4.73E-03	5.90E-01	4.08E-01
132	MAGEA4	1.32E-03	4.75E-03	5.90E-01	2.77E-01
133	CLVS2	1.34E-03	4.81E-03	5.90E-01	5.90E-01
134	SERAC1	1.35E-03	4.87E-03	5.90E-01	3.83E-01
135	NEMF	1.36E-03	4.88E-03	5.90E-01	4.72E-01
136	JAK2	1.36E-03	4.88E-03	5.90E-01	5.02E-01
137	GATA4	1.36E-03	4.90E-03	5.90E-01	3.44E-01
138	FCGR2A	1.37E-03	4.92E-03	5.90E-01	6.64E-02
139	KRTAP22-2	1.38E-03	4.95E-03	5.90E-01	1.37E-01
140	CDC42BPA	1.41E-03	5.06E-03	5.90E-01	4.32E-01
141	C19orf35	1.42E-03	5.09E-03	5.90E-01	5.13E-01
142	TRIM51	1.42E-03	5.10E-03	5.90E-01	3.59E-01
143	KRTAP21-2	1.42E-03	5.11E-03	5.90E-01	2.70E-01
144	PCDHGB6	1.43E-03	5.14E-03	5.90E-01	3.73E-01
145	ELOVL1	1.44E-03	5.16E-03	5.90E-01	5.58E-01
146	MRPL18	1.44E-03	5.18E-03	5.90E-01	3.01E-01
147	NDUFB4	1.45E-03	5.20E-03	5.90E-01	4.78E-01
148	SPATA16	1.46E-03	5.24E-03	5.90E-01	2.48E-01
149	GPM6A	1.47E-03	5.25E-03	5.90E-01	4.30E-01
150	LDOC1	1.47E-03	5.27E-03	5.90E-01	5.67E-01

101	RASSF10	8.31E-04	3.01E-03	5.04E-01	3.83E-01
102	TMEM97	8.38E-04	3.03E-03	5.04E-01	2.98E-01
103	PROK2	8.53E-04	3.09E-03	5.08E-01	1.34E-01
104	NDUFS6	8.70E-04	3.16E-03	5.14E-01	4.08E-01
105	RLIM	9.00E-04	3.26E-03	5.19E-01	2.49E-01
106	PLEKHA4	9.15E-04	3.31E-03	5.20E-01	4.84E-01
107	CYB561A3	9.30E-04	3.37E-03	5.20E-01	3.40E-01
108	PVRIG	9.33E-04	3.38E-03	5.20E-01	3.73E-01
109	GAS6	9.36E-04	3.39E-03	5.20E-01	1.92E-01
110	L3MBTL2	9.45E-04	3.42E-03	5.20E-01	4.85E-01
111	VCY	9.61E-04	3.48E-03	5.20E-01	2.62E-01
112	OXSR1	9.68E-04	3.51E-03	5.20E-01	3.60E-01
113	BHLHE23	9.82E-04	3.55E-03	5.20E-01	3.64E-01
114	DUSP23	9.87E-04	3.57E-03	5.20E-01	3.32E-01
115	MAP4K2	9.92E-04	3.59E-03	5.20E-01	3.62E-01
116	APLP1	1.01E-03	3.64E-03	5.20E-01	3.33E-01
117	NMT2	1.01E-03	3.65E-03	5.20E-01	2.49E-01
118	PLA2G4C	1.03E-03	3.72E-03	5.20E-01	5.21E-01
119	KRTAP12-3	1.04E-03	3.75E-03	5.20E-01	2.73E-01
120	RAB43	1.04E-03	3.77E-03	5.20E-01	4.46E-01
121	SLC9A3R1	1.06E-03	3.84E-03	5.20E-01	3.30E-01
122	SLC28A1	1.06E-03	3.85E-03	5.20E-01	3.02E-01
123	ICAM4	1.06E-03	3.85E-03	5.20E-01	2.60E-01
124	PPP1R37	1.06E-03	3.86E-03	5.20E-01	3.06E-01
125	LELP1	1.06E-03	3.86E-03	5.20E-01	3.62E-01
126	RAD51AP2	1.10E-03	3.98E-03	5.31E-01	1.30E-01
127	TREX2	1.11E-03	4.01E-03	5.31E-01	3.76E-01
128	ADGRL4	1.11E-03	4.03E-03	5.31E-01	1.41E-01
129	GADD45A	1.13E-03	4.09E-03	5.31E-01	3.99E-01
130	SPRN	1.14E-03	4.14E-03	5.35E-01	3.17E-01
131	CNN2	1.16E-03	4.21E-03	5.35E-01	2.25E-01
132	PPP1R13L	1.17E-03	4.23E-03	5.35E-01	2.87E-01
133	IRGQ	1.21E-03	4.38E-03	5.39E-01	3.46E-01
134	WEE2	1.21E-03	4.39E-03	5.39E-01	8.02E-03
135	RFXANK	1.22E-03	4.42E-03	5.39E-01	4.62E-01
136	B3GALT6	1.23E-03	4.44E-03	5.39E-01	2.82E-01
137	GATA4	1.24E-03	4.48E-03	5.39E-01	2.45E-01
138	GDF10	1.24E-03	4.49E-03	5.39E-01	2.88E-01
139	TTC7A	1.25E-03	4.51E-03	5.39E-01	3.34E-01
140	RYR2	1.27E-03	4.57E-03	5.40E-01	4.22E-01
141	RAB33B	1.28E-03	4.61E-03	5.41E-01	6.41E-01
142	ATP1A4	1.29E-03	4.65E-03	5.41E-01	3.59E-01
143	CCER2	1.29E-03	4.66E-03	5.41E-01	1.32E-01
144	CEBPB	1.34E-03	4.83E-03	5.51E-01	4.44E-01
145	ANKRD55	1.35E-03	4.86E-03	5.51E-01	3.79E-01
146	ANKS1B	1.35E-03	4.86E-03	5.51E-01	3.29E-01
147	ARC	1.35E-03	4.87E-03	5.51E-01	1.91E-01
148	NNT	1.37E-03	4.92E-03	5.54E-01	1.49E-01
149	SIRT6	1.39E-03	4.98E-03	5.58E-01	2.87E-01
150	ARHGAP6	1.40E-03	5.03E-03	5.60E-01	2.55E-01

101	HOMER2	6.72E-04	2.45E-03	4.35E-01	3.45E-01
102	HBEGF	6.85E-04	2.50E-03	4.35E-01	4.06E-01
103	C15orf61	6.97E-04	2.55E-03	4.35E-01	3.79E-01
104	NUDT11	6.98E-04	2.55E-03	4.35E-01	1.38E-01
105	ABCB10	6.98E-04	2.55E-03	4.35E-01	4.37E-01
106	PRR23B	7.00E-04	2.56E-03	4.35E-01	3.15E-01
107	RPUSD3	7.02E-04	2.56E-03	4.35E-01	3.86E-01
108	TRAF3IP3	7.09E-04	2.59E-03	4.37E-01	5.30E-01
109	KCNN1	7.21E-04	2.64E-03	4.38E-01	6.22E-01
110	C17orf89	7.29E-04	2.66E-03	4.38E-01	3.43E-01
111	MAN2A1	7.31E-04	2.67E-03	4.38E-01	3.17E-01
112	HIST1H1E	7.37E-04	2.69E-03	4.38E-01	5.28E-01
113	AQP1	7.98E-04	2.90E-03	4.68E-01	5.44E-01
114	FAM155B	8.16E-04	2.95E-03	4.70E-01	2.79E-01
115	IQCF5	8.19E-04	2.96E-03	4.70E-01	5.47E-01
116	CASP4	8.27E-04	2.99E-03	4.70E-01	4.44E-01
117	IGHMBP2	8.38E-04	3.04E-03	4.70E-01	5.65E-01
118	C17orf112	8.46E-04	3.07E-03	4.70E-01	3.58E-01
119	OR2T1	8.50E-04	3.08E-03	4.70E-01	5.73E-01
120	TMEM42	8.53E-04	3.09E-03	4.70E-01	4.83E-01
121	PHF8	8.57E-04	3.11E-03	4.70E-01	5.89E-01
122	ATP5A1	8.71E-04	3.16E-03	4.74E-01	6.71E-01
123	MAPK1	8.76E-04	3.18E-03	4.74E-01	6.35E-01
124	PITRM1	8.98E-04	3.25E-03	4.76E-01	2.98E-01
125	NDUFV2	9.02E-04	3.27E-03	4.76E-01	5.80E-01
126	UNC93A	9.04E-04	3.27E-03	4.76E-01	1.83E-01
127	STOML2	9.25E-04	3.35E-03	4.81E-01	5.09E-01
128	MYC	9.26E-04	3.36E-03	4.81E-01	9.12E-01
129	TRABD	9.51E-04	3.45E-03	4.85E-01	3.41E-01
130	PFDN1	9.56E-04	3.46E-03	4.85E-01	-2.66E-01
131	HMX2	9.67E-04	3.50E-03	4.85E-01	3.20E-01
132	TMEM14E	9.76E-04	3.53E-03	4.85E-01	3.34E-01
133	NDC1	9.80E-04	3.54E-03	4.85E-01	2.93E-01
134	QRICH2	9.94E-04	3.60E-03	4.85E-01	4.42E-01
135	LSM12	1.01E-03	3.64E-03	4.85E-01	5.22E-01
136	PDLIM3	1.01E-03	3.65E-03	4.85E-01	-8.64E-02
137	CALHM1	1.01E-03	3.65E-03	4.85E-01	2.61E-01
138	JADE1	1.03E-03	3.71E-03	4.85E-01	3.43E-01
139	TOMM7	1.03E-03	3.73E-03	4.85E-01	4.79E-01
140	ZNF441	1.04E-03	3.76E-03	4.85E-01	4.84E-01
141	C1orf105	1.04E-03	3.76E-03	4.85E-01	4.08E-01
142	TOR2A	1.04E-03	3.76E-03	4.85E-01	4.11E-01
143	MDM4	1.04E-03	3.77E-03	4.85E-01	8.00E-01
144	IGSF8	1.04E-03	3.79E-03	4.85E-01	3.19E-01
145	LHX1	1.06E-03	3.84E-03	4.90E-01	-4.53E-02
146	MTG1	1.08E-03	3.93E-03	4.97E-01	3.46E-01
147	GADD45B	1.09E-03	3.96E-03	4.98E-01	3.88E-01
148	ASAP3	1.11E-03	4.03E-03	5.04E-01	3.83E-01
149	ATP5B	1.14E-03	4.11E-03	5.08E-01	6.75E-01
150	SCRN1	1.14E-03	4.12E-03	5.08E-01	3.93E-01

Table 2.2 siRNA sequences used for validation experiments

Gene	siRNA #	Target Sequence	Qiagen Cat. No.
CDK2	1	N/A	SI00299775
CASP8	1	GACAAAGTTTACCAAATGAAA	SI02662457
CASP8	2	AAGAGTCTGTGCCCAAATCAA	SI02661946
CASP8	3	AAGTTCCTGAGCCTGGACTAC	SI00299593
CASP8	4	CTGTCTGATCATCAACAATCA	SI04948314
DR4	1	TAGCTCAGCTGCAACCATCAA	SI03111318
DR4	2	CAGGCAATGGACATAATATAT	SI00056749
DR4	3	CCGGGTCCACAAGACCTTCAA	SI00056742
DR4	4	CAGGAACTTTCCGGAATGACA	SI00056728
DR5	1	CTGCAAATATGGACAGGACTA	SI03094063
DR5	2	ACCAGGTGTGATTCAGGTGAA	SI03038665
DR5	3	CCGACTTCACTTGATACTATA	SI00056707
DR5	4	CTGGACAACCTTACAAGTATA	SI00056700
MAPK14	1	CTCAGTGATACGTACAGCCAA	SI00605164
MAPK14	2	CAGAGAACTGCGGTTACTTAA	SI00605157
MAPK14	3	AACTGCGGTTACTTAAACATA	SI00300769
MAPK14	4	CTGGGAGGTGCCCGAGCGTTA	SI03098683
MAP2K3	1	CCGGGCCACCGTGAACTCACA	SI02222976
MAP2K3	2	ACGGATATCCTGCATGTCCAA	SI02222969
MAP2K3	3	TCGACTGTTTCTACACTGTCA	SI03649604
MAP2K3	4	ACCATTGGAGACAGAAACTTT	SI03038910

Table 2.3 sgRNA sequences used for validation experiments

Gene	sgRNA #	Guide Sequence (5'→3')
CTRL	1	GTAGCGAACGTGTCCGGCGT
CDK2	1	TGAGAAGCATTACCTTGATG
CDK2	2	AAGCAGAGAGATCTCTCGGA
CASP8	1	AGGGGACTCGGAGACTGCGA
CASP8	2	CTACCTAAACACTAGAAAGG
DR4	1	ACACACTCGATGTCACTCCA
DR4	2	AGCCTGTAACCGGTGCACAG
DR5	1	AGATACTCACGATCTCATTG
DR5	2	TGTGCCGGAAGTGCCGCACA
MAPK14	1	AAGTAACCGCAGTTCTCTGT
MAPK14	2	CAAGGCGAGTAATACCTGTC
MAP2K3	1	AAGCTGTCGGTGATCCACAG
MAP2K3	2	CTACGGGGCACTATTCAGAG
FAM122A	1	AATGAAATCGATGCGCTTGG
FAM112A	2	ACACCGGCGAAGTGTCACTG

Table 2.4 Primers used in two-step nested PCR for NGS preparation

Step 1 Nested PCR Primers (5'→3')	
Forward	GAGGGCCTATTTCCCATGATTCCTTCA
Reverse	AACTTCTCGGGGACTGTGG

Step 2 Nested PCR Primers (5'→3') (*NNNNNN* = specific NGS barcode)	
Forward	AATGATACGGCGACCACCGAGATCTACACTCTTTCCCTACACGACGCTCTTCCGATCT***NNNNNN***
Reverse	CAAGCAGAAGACGGCATACGAGATGTGACTGGAGTTCAGACGTGTGCTCTTCCGATCT

	NGS Barcode Sequences		
	Screen 1	Screen 2	Screen 3
Day 0 - Replicate 1	ATCACG	ATCACG	ATCACG
Day 0 - Replicate 2	CGATGT	CGATGT	CGATGT
Day 4 - Replicate 1	TTAGGC		
Day 4 - Replicate 2	TGACCA		
Day 4 - Replicate 3	ACAGTG		
Day 14 - Replicate 1		TTAGGC	GCCAAT
Day 14 - Replicate 2		TGACCA	CAGATC
Day 14 - Replicate 3		ACAGTG	ACTTGA

Table 2.5 Primers used for pooled qPCR outgrowth assay

Gene	Forward Primer (5'→3')	Universal Reverse Primer (5'→3')
CTRL	GTAGCGAACGTGTCCGGCGTGTTT	CCCCAACTTCTCGGGGACTGT
CDK2	CGTGAGAAGCATTACCTTGATGGT	CCCCAACTTCTCGGGGACTGT
CASP8	CGCTACCTAAACACTAGAAAGGGT	CCCCAACTTCTCGGGGACTGT
DR4	CGACACACTCGATGTCACTCCAGT	CCCCAACTTCTCGGGGACTGT
DR5	CGAGATACTCACGATCTCATTGGT	CCCCAACTTCTCGGGGACTGT
MAPK14	CGAAGCTGTCGGTGATCCACAGGT	CCCCAACTTCTCGGGGACTGT
MAP2K3	CGAAGCTGTCGGTGATCCACAGGT	CCCCAACTTCTCGGGGACTGT

Chapter 3. Molecular Determinants of CDK4/6 Inhibitor Response in OHNSCC

3.1 Introduction

Following FDA approval of the first CDK4/6 inhibitor for the treatment of ER+ advanced breast cancers in 2015, scientists and oncologists have been exploring its application in a wide variety of other cancer types including ovarian, pancreatic, oral, among others[51,55,90–94]. In many pre-clinical and early phase clinical trials, CDK4/6 inhibitors such as palbociclib show promising results initially, however, tumor resistance and/or recurrent disease ultimately emerges as a frequent problem[52,57,60,95–97]. Understanding the exact mechanisms of CDK4/6 inhibitor resistance will be vital to its proper application for these various cancer types.

As mentioned previously, the most commonly described mechanisms of CDK4/6 inhibitor resistance include *RB1* downregulation or loss, *CDK4/6* amplification, and *CCNE1* upregulation or amplification. In the context of OHNSCC, the most relevant of these changes are pRb loss and cyclin E upregulation. pRb loss in OHNSCC is typically the result of HPV infection wherein the E7 oncoprotein binds to and promotes the degradation of pRb[98–101]. This results in the elimination of the main CDK4/6 substrate and thus negates the primary effect of CDK4/6 inhibitors. Several pre-clinical and clinical studies have demonstrated robust CDK4/6 inhibitor resistance in HPV-positive OHNSCC[61,62]. Intriguingly, one phase I clinical trial showed dramatic response to CDK4/6 inhibition in a patient with HPV+ OHNSCC, however follow-up studies were unable to recapitulate this result[58]. Nonetheless, one-off results like this demonstrate the complexity in forming a unified model for cell cycle drugs and possibly suggest alternate mechanisms at play beyond the prevention of pRb phosphorylation.

CCNE1 gain was first described as a mechanism of CDK4/6 inhibitor resistance in 2015 in the context of ovarian cancer[65]. The following year, a separate group showed that *CCNE1* amplification occurred in breast cancer cell lines that were chronically exposed to palbociclib over the course of 3 to 4 months and thus gained drug resistance over that time[66]. These two studies are the foundation of the now accepted paradigm that cyclin E upregulation results in CDK4/6 inhibitor resistance. Mechanistically, the authors of these studies suggest that upregulated cyclin E complexes with CDK2 to phosphorylate pRb during G1 as a way to bypass CDK4/6 inhibition. This especially makes sense given the functional redundancy between cyclin E and the D-type cyclins that was elegantly demonstrated by Geng *et al*. in 1999[102]. Since 2016, many studies have been published supporting a correlation between high cyclin E and poor CDK4/6 inhibitor response[67,68,103,104]. One of the more notable studies in favor of this resistance mechanism is the ongoing PALOMA-3 clinical trial that is testing the efficacy of combining palbociclib with fulvestrant (ER antagonist) over fulvestrant alone[105]. In this study, the authors show a correlation between high *CCNE1* mRNA expression and low palbociclib efficacy, though other clinical trials like PALOMA-1 and PALOMA-2 previously failed to find this correlation[106,107].

Recently, Guiley *et al*. published their study demonstrating that the primary mechanism by which palbociclib induces cell cycle arrest is through the indirect inhibition of cyclin E-CDK2 complexes[69]. Using crystallography, the authors show that palbociclib binds directly to monomeric CDK4/6 and is otherwise unable to bind the kinase(s) when they are in complex with the D-type cyclins. Furthermore, p27 is known to bind and bring together the D-type cyclins and CDK4/6 to help form the mature complex[108,109]. Phosphorylation of p27 on Y74 yields the active cyclin D-CDK4/6 complex, and this structure prevents the binding of palbociclib. However, when palbociclib binds monomeric CDK4/6 prior to complex formation, p21 and p27 molecules are

shuttled to cyclin E-CDK2 complexes where their primary effect is inhibitory. Challenging the conventionally accepted mechanism of action, Guiley *et al*. argue that this shuttling of p21/p27 to cyclin E-CDK2 complexes is the key event leading to cell cycle arrest upon palbociclib treatment. This proposed mechanism could help explain how high cyclin E levels may outcompete endogenous p21/p27 thus leading to CDK4/6 inhibitor resistance. However, while in our hands we are able to see a slight increase in cyclin E associated p21 and p27 upon palbociclib treatment, it is an insufficient amount to inhibit kinase activity. Thus, our data do not support the model of palbociclib induced arrest through indirect cyclin E-CDK2 inhibition in the setting of OHNSCC.

Cyclin E1 is infrequently altered at the genomic level in OHNSCC, so its contribution to CDK4/6 inhibitor resistance, if present, must be the result of transcript or protein level deregulation. One obvious candidate for cyclin E deregulation in OHNSCC is loss of Fbw7, an E3 ubiquitin ligase responsible for regulating the levels of cyclin E, Myc, Notch, Jun, and a host of other substrates[110,111]. Fbw7 is generally considered a tumor suppressor since the majority of its targets are proto-oncogenes. Thus, inactivating mutations or deletions of the Fbw7 gene, *FBXW7*, usually contribute to carcinogenesis and can be found in approximately 6% of all human cancers, including 5-10% of OHNSCCs[39,72,73]. Since loss of *FBXW7* would result in cyclin E deregulation, we hypothesized that OHNSCCs lacking *FBXW7* would be resistant to CDK4/6 inhibition given the current paradigm of high cyclin E and CDK4/6 inhibitor resistance.

To test this idea, we used CRISPR-Cas9 to knockout *FBXW7* in three OHNSCC cell lines (FaDu, PCI-15A, and SCC1) and examined their response to the CDK4/6 inhibitor, palbociclib. To our surprise, *FBXW7* knockout cells demonstrated only a mild but reproducible resistance phenotype as measured by EdU incorporation and cell proliferation assays. To further examine palbociclib response and resistance, we stably overexpressed cyclin E as a more direct method to

study its effects in response to CDK4/6 inhibition. Furthermore, we used CRISPR-Cas9 once again to knockout *RB1* to create a benchmark for true resistance in previously sensitive cell lines. While cells lacking *RB1* demonstrated the clearest palbociclib resistance phenotype, cells stably overexpressing cyclin E more closely resembled *FBXW7* knockout cells rather than *RB1* knockout cells. Overall, we demonstrate that high cyclin E abundance and activity may drive palbociclib resistance, though to a far lesser extent than what would be expected from a bona fide mediator of resistance such as *RB1* loss. Thus, our results suggest that while high cyclin E levels may contribute to clinical CDK4/6 inhibitor resistance, cyclin E is insufficient on its own to drive resistance and may depend on other pathways to exert its full effect.

3.2 Materials and Methods

3.2.1 Cell lines, plasmids, and drug treatments

All cell lines were maintained in Dulbecco's Modified Eagle Medium (DMEM) supplied with 10% fetal bovine serum (Gibco) and penicillin-streptomycin (Gibco). To generate individual knockouts, the lentiCRISPRv2 vector backbone was obtained from the Paddison lab (originally from the Feng Zhang lab, MIT). The pBABE vector backbone with a hygromycin selection marker was used to stably overexpress full length cyclin E as previously described[112]. All palbociclib (MedChemExpress) treatments were delivered at 500nM unless otherwise noted.

3.2.2 Generating overexpression and CRISPR/Cas9 knockout systems

sgRNA assembly for knockouts of *FBXW7* and *RB1* were completed as previously described (Chapter 2). Guide sequences used to knockout each gene are provided in Table 3.1. Retrovirus and lentivirus generation began by seeding 2-3 million Lenti-X 293T cells into 10cm plates and left to settle and grow overnight. The following afternoon, cells were transfected using 10µg cyclin E retroviral vector or sg*FBXW7*/sg*RB1* CRISPR vector along with 6.5µg pSPAX2

and 6.0µg pMD2.G packaging vectors using the traditional calcium-phosphate transfection protocol. Media was changed the following morning and retrovirus/lentivirus containing media was filtered and harvested the morning after. Viral transduction was completed immediately upon harvest and any excess viral media was stored in -80°C for future use.

One day prior to viral transduction, target cells were plated such that they would reach approximately 25% confluency at the time of virus delivery. Retrovirus/lentivirus was delivered to target cells with 4µg/µL polybrene and left to incubate overnight. Cells were washed the following morning, and puromycin (1µg/mL) or hygromycin (250µg/mL) selection was initiated the morning after. Once cells in the control plates had completely died off (approximately 2-4 days for puromycin or 6-8 days for hygromycin), surviving cells in the target plates were pelleted and successful gene knockout or overexpression was confirmed by western blot. Remaining cells were frozen down in 10% DMSO + DMEM in liquid N_2 for future use.

3.2.3 Immunoblotting, immunoprecipitation, and in-vitro kinase assays

Immunoblotting was completed as described previously (Chapter 2). Immunoprecipitations for cyclin E were done using the anti-cyclin E (HE111) antibody (Santa Cruz Biotechnology). 100µg of lysate from each sample was loaded into a 1.5mL Eppendorf tube containing 1.5µL HE111 antibody and 15µL Protein G agarose beads at a final volume of 400µL. Tubes were left to tumble overnight at 4°C and washed the following day 3 times with 0.5% NP-40 lysis buffer supplemented with protease and phosphatase inhibitors with a 30 second centrifugal spin at 9.5g between each wash. After the final wash, samples were prepared in Laemmli buffer, boiled at 95°C for 10 minutes, spun down for 1 minute at 9.5g, and the supernatants were loaded into immunoblotting gels for electrophoresis. The remainder of the protocol is identical to the steps described for immunoblotting (Chapter 2).

For completion of in-vitro cyclin E kinase assays, immunoprecipitations against cyclin E were conducted as described above. Following the second wash in 0.5% NP-40 lysis buffer, the beads were equilibrated with kinase reaction buffer (50mM HEPES pH7.4, 10mM $MgCl_2$, 1mM DTT), centrifuged, and the supernatant aspirated. Beads were then manually mixed with the kinase reaction buffer (50mM HEPES pH7.4, 10mM $MgCl_2$, 10mM DTT, 30µM cold ATP, 2µCi [γ-^{32}P] ATP and 0.5µg recombinant GST-pRb was used as a substrate (prepared in lab previously)) at a final volume of 20µL. Samples were incubated in a Heat Only Thermal Mixer II (Boekel) at 30°C for 30 minutes shaking at 1500RPM. At the end of the reaction, samples were prepared with Laemmli buffer, boiled at 95°C for 10 minutes, spun down for 1 minute at 9.5g, and the supernatants were loaded into Bolt 4-12% Bis-Tris (Invitrogen) gradient gels, and electrophoresed for approximately 1 hour at 125 volts. Following electrophoresis, kinase reactions on the gel were visualized in the cellular imaging core of the Fred Hutch Cancer Center using the Typhoon Trio Imager (GE). Quantifications of the gel were subsequently completed using ImageJ software.

3.2.4 Antibodies

Antibodies were purchased from suppliers and used as follows: Bethyl: Fbw7 (A301-720A, rabbit polyclonal, 1:1,000); Cell Signaling Technology: Actin (13E5, rabbit monoclonal HRP-conjugated, 1:1,000), p21 (12D1, rabbit monoclonal, 1:1,000), p27 (#2552, rabbit polyclonal, 1:1,000), pRb (4H1, mouse monoclonal, 1:1,000), p-pRb Ser807/811 (D20B12, rabbit monoclonal, 1:1,000); Santa Cruz Biotechnology: Cyclin A1 (H-230, rabbit polyclonal, 1:1,000), Cyclin E IB (HE12, mouse monoclonal, 1:1,000), Cyclin E IP (HE111, mouse monoclonal, 1:250), PCNA (PC10, mouse monoclonal HRP-conjugated, 1:1,000). Sigma: Vinculin (hVIN-1, mouse monoclonal, 1:10,000).

3.2.5 Cell cycle analysis and flow cytometry

Growing cells were pulsed with 10μM 5-ethynyl-2'deoxyuridine (EdU) for one hour prior to harvest. At the end of one hour, cells were washed, harvested by trypsinization, and fixed in 4% paraformaldehyde at room temperature for 15 minutes. Once fixed, cells were washed with PBS and stored in ice cold methanol for at least 24 hours at -20°C. To prepare samples for cell cycle analysis by flow cytometry, fixed cells were washed twice with flow wash buffer (0.3% bovine serum albumin (BSA) and 0.1% tween in PBS) and centrifuged at 300g for 3 minutes in between washes. A third was completed using 3% BSA alone after which a "click" chemistry reaction was performed to conjugate a fluorescent azide to incorporated EdU. Final concentrations of reaction components were carried out in a 100μL reaction as follows: 0.48μM biotin-azide, 11mM ascorbic acid, 2.2mM CuSO4. Fixed cells were incubated in the reaction mixture at room temperature for 45 minutes, washed with flow wash buffer, centrifuged, aspirated, and stained with 1μg/mL DAPI for an additional 10 minutes. After a final wash, cells were resuspended in FBS Stain Buffer (BD Biosciences) and taken to the flow cytometry core at the Fred Hutch Cancer Center for analysis. Flow cytometry was conducted on a BD FACSymphony A5 cytometer and data was analyzed using FlowJo software.

3.2.6 siRNA

siRNA transfections against p21 (Qiagen, Cat. No. SI00604898) and p27 (Cell Signaling Technology, Cat. No. 12324S) were completed using Lipofectamine RNAiMAX Reagent according to manufacturer's protocol (Invitrogen). Target protein knockdown was confirmed via western blot, and all follow up assays were completed within five days of siRNA delivery.

3.2.7 Growth assays

Cells were seeded in 6-well plates at 10,000 cells/well on day 0. The following morning, treatment plates were given 500nM palbociclib and incubated for 48, 96, 144, and 192 hours. At each timepoint, cells from a single treatment and control well were harvested by trypsinization, pelleted, and resuspended in 50-250µL of PBS. 10µL of each sample was then loaded onto a counting slide and cell counts were measured using the TC20 Automated Cell Counter (Bio-Rad). Final analysis of cell count data was completed using Prism software.

3.2.8 Quantitative reverse transcription PCR (RT-qPCR)

Cells were harvested by trypsinization, pelleted, and snap frozen at -80°C until time of assay. Total RNA was extracted from pellets using RNeasy Plus Mini Kit (Qiagen) according to manufacturer's protocol. RNA was quantified using the NanoDrop One^{C} spectrophotometer (Thermo Scientific) and 1µg from each sample was used for the reverse transcription reaction. A 20µL reaction with the iScript Reverse Transcription Supermix (Bio-Rad) was carried out in a Mastercycler Pro S (Eppendorf) according to manufacturer's protocol to generate cDNA. Platinum SYBR Green qPCR SuperMix-UDG with ROX (Invitrogen) was combined with gene specific primers (IDT) and cDNA for RT-qPCR in a QuantStudio 5 instrument. Primer sequences used for RT-qPCR can be found in Table 3.2. Transcripts were normalized to the housekeeping genes *TBP* and *RPLP0* and ΔΔCt analysis was used to detect changes in gene expression between treatment and non-treatment groups.

3.2.9 FUCCI system delivery and live-cell imaging

The FUCCI vectors pCSII-EF-FUCCI-mAG-hGeminin and pCSII-EF-FUCCI-mCherry-hCdt1 were individually transfected into Lenti-X 293T cells along with the lentiviral packaging plasmids psPAX2 and pMD2.G using calcium-phosphate transfection[113]. Cells were washed the

following day and target cells (FaDu WT, CycE, sgFBXW7, and sgRB1) were plated in 10cm plates at approximately 25% confluency. The following morning, lentiviral media was filtered, harvested, and delivered to target cells with 4μg/μL polybrene. After overnight incubation in lentiviral media, cells were washed and allowed to grow until plates were approximately 90% confluent (3-5 days). Cells were then harvested by trypsinization, pelleted, and resuspended in DMEM containing 1% BSA in preparation for flow sorting. Cells were sorted using the Sony MA900 in the Fred Hutch Cancer Center flow cytometry core initially gating for FITC+ (green) cells to confirm expression of the mAG-hGeminin plasmid. Sorted cells were plated into 10cm plates and allowed to recover for 4-5 days until they reached approximately 90% confluency. Cells were again harvested by trypsinization, pelleted, and resuspended in DMEM containing 1% BSA in preparation for flow sorting. Cells were sorted using the Sony MA900 in the Fred Hutch Cancer Center flow cytometry core this time gating for PE+ (red) cells to confirm expression of the mCherry-hCdt1 plasmid. Doubly sorted cells were plated into 10cm plates and allowed to recover for 4-5 days until they reached approximately 90% confluency at which point, they could be used for experiments and/or frozen down for future experiments as needed.

For live-cell imaging, each FUCCI-FaDu genotype (WT, CycE, sgFBXW7, and sgRB1) was seeded into two wells within a 24-well plate at 5,000 cells/well. Cells were treated the following morning with 500nM palbociclib and placed within the IncuCyte ZOOM incubator for the next 5 days. Phase contrast, red fluorescence, and green fluorescence images were taken every hour at 20X magnification over that time. Data files were exported, compiled within ImageJ, and then imported to Imaris Cell Imaging Software for analysis. 50 cells for each condition were manually traced and their red/green fluorescence values were used in Prism for cell cycle length analysis.

3.3 Results

3.3.1 Establishing sensitivity and resistance to CDK4/6 inhibition in OHNSCC

To determine baseline responses to CDK4/6 inhibition, we treated a panel of OHNSCC lines with palbociclib for 24 hours and measured cell cycle inhibition by EdU incorporation and flow cytometry. Since MCF7 is well characterized in the literature as a highly sensitive breast cancer line to palbociclib, we used it as a baseline for comparison against our OHNSCC lines. Indeed, when treated for 24 hours with 500nM palbociclib, MCF7 cells show a strong G1 arrest (>90% decrease in S-phase fraction) when analyzed by flow cytometry (Figure 3.1A). Furthermore, pRb phosphorylation at S807/811 was dramatically reduced showing proper inhibition of the D-type cyclins (Figure 3.3E). Our panel of three HPV-negative OHNSCC lines (FaDu, PCI-15A, SCC1) are each *TP53* mutated, *CCND1* amplified, and *CDKN2A* loss[114–117]. While the role of p53 loss in determining sensitivity or resistance to CDK4/6 inhibition is still an unsettled question in the field, it is generally accepted that cells with high cyclin D and little or no p16 are the most likely to be sensitive to CDK4/6 inhibition, though these biomarkers are also imperfect at predicting drug response in patient tumors[118–120]. In our hands, all three of our HPV-negative cell lines demonstrated similar levels of sensitivity to palbociclib when treated at 500nM for 24 hours (Figure 3.1A).

To understand longer term palbociclib response, we also grew cells in drug containing media for eight days and measured cell growth by counting cells every two days. Wild type MCF7, FaDu, PCI-15A, and SCC1 all demonstrated poor growth in palbociclib containing media (Figure 3.3C). Of note, all cell lines did appear to grow to varying degrees despite being in drug, albeit at a very slow rate, suggesting that not all cells experienced complete cell cycle arrest. This was particularly the case for our panel of OHNSCC lines which were able to complete 1.5-2.5 cell

doublings in that period. On the other hand, while MCF7 cell number did increase over time, the total population failed to double suggesting that these cells are more sensitive to CDK4/6 inhibition than our panel of OHNSCC lines. Other groups have also reported that while cells may appear sensitive to CDK4/6 inhibitors, they may not necessarily exit the cell cycle completely, though their growth rate is dramatically curbed in the presence of drug[121]. This may be critically important in how we understand the mechanism of action for CDK4/6 inhibitors depending on if they truly arrest cells in the cycle or simply slow them down during specific phases.

We also looked at EdU incorporation in three HPV-positive cell lines to confirm that the absence of pRb (due to abrogation by the E7 oncoprotein) truly rendered these cells resistant to CDK4/6 inhibition. Indeed, when treated with varying concentrations of palbociclib up to 1μM, the cell cycles of all three HPV-positive lines were virtually unaffected validating the conventional wisdom that pRb loss is a strong predictor of palbociclib resistance (Figure 3.1B).

3.3.2 *RB1* knockout confers strong palbociclib resistance in HPV-negative OHNSCC

To continue testing the idea that pRb loss predicts palbociclib resistance, we sought to induce resistance in previously sensitive cells by knocking out *RB1* (cells herein referred to as sg*RB1*) (Figure 3.2A). To accomplish this, we used two CRISPR-Cas9 targeting guides to knockout *RB1*, treated those cells with palbociclib, and assayed their cell cycle profiles by EdU incorporation and flow cytometry. Knocking out *RB1* did not significantly change the baseline cell cycle profile, however, sg*RB1* cells demonstrated strong palbociclib resistance as seen by the high level of EdU incorporation as compared to palbociclib treated WT cells (Figure 3.3A-B). While WT cells consistently showed >90% decrease in EdU-positivity after palbociclib treatment, sg*RB1* cells had a far milder decrease, between 10% and 40%, depending on the cell line.

Eight-day outgrowth assays of sg*RB1* cells in palbociclib supported our flow cytometry data showing enhanced capacity for growth in drug as compared to WT cells (Figure 3.3C). While growth was inhibited by up to 98% in WT cells, sg*RB1* growth was only inhibited between 20% to 37% depending on the cell line. We speculate that the higher degree of growth inhibition in FaDu sg*RB1* cells, as compared to PCI-15A sg*RB1* cells for example, may reflect varying degrees of G1/S regulation by the other pocket proteins (p107 and p130) in the different cell lines.

3.3.3 *FBXW7* knockout and stable *CCNE1* overexpression only confer mild palbociclib resistance in HPV-negative OHNSCC

After establishing a baseline resistance phenotype in previously sensitive cells, we began to explore the role of cyclin E in mediating palbociclib response and resistance. To test the idea that high cyclin E confers resistance to CDK4/6 inhibition, we generated two systems of high cyclin E expression in each of our OHNSCC lines. In one system, we stably overexpressed cyclin E using the pBABE vector backbone (cells herein referred to as CycE), and in the other, we knocked out the gene *FBXW7* (cells herein referred to as sg*FBXW7*) to prevent cyclin E turnover thus resulting in high protein accumulation (Figure 3.2B-C). As expected, high cyclin E levels resulted in slightly higher EdU incorporation in untreated CycE and sg*FBXW7* cells across the board (Figure 3.3A).

When treated with palbociclib, CycE and sg*FBXW7* cells failed to demonstrate strong drug resistance as measured by EdU incorporation (Figure 3.3A-B). While we observed a reproducible and statistically significant increase in EdU positive CycE and sg*FBXW7* cells treated with palbociclib at 24 and 48 hours, it was to a far lesser extent than the EdU incorporation we observed in sg*RB1* cells (Figure 3.3A-B). Statistical significance was maintained when controlling for differences in baseline EdU levels for untreated cells (Figure 3.3B).

Interestingly, all of our WT cells showed some degree of S-phase recovery at the 48-hour treatment mark. For example, average S-phase fraction increased from 3.33% in 24-hour treated FaDu WT cells to 16.3% in 48-hour treated FaDu WT cells (Figure 3.3B). A similar pattern was observed in WT PCI-15A cells (3.57% to 12.0%) and to a lesser extent in SCC1 cells (1.07% to 4.47%) (Figure 3.3B). While average S-phase fractions were consistently higher in palbociclib treated CycE and sg*FBXW7* cells, this S-phase "rebound" was also observed in these genotypes. In some cases (e.g., FaDu CycE/sg*FBXW7* and PCI-15A CycE), the 48-hour S-phase fractions were either approaching or surpassing the levels seen in sg*RB1* cells. While this might suggest strong resistance on first glance, these data points need to be considered in context with all others, including the 24-hour S-phase fractions and outgrowth assay numbers, to fully characterize levels of drug sensitivity and resistance. In our experience, the most durable data points indicating true resistance remain the 24-hour timepoint for EdU incorporation and cell count numbers from outgrowth assays.

With that in mind, eight-day outgrowth assays of CycE and sg*FBXW7* cells in palbociclib again demonstrated only a mild degree of drug resistance at best (Figure 3.3C). Doubling times of FaDu CycE cells increased from 29.9 hours (untreated) to 57.2 hours (treated) (91.3% increase) and of FaDu sg*FBXW7* cells from 29.7 hours (untreated) to 59.8 hours (treated) (101.3% increase) (Figure 3.3D). These values are far closer to the doubling time increases seen in FaDu WT cells (30.2 to 83.4 hours, 176.2% increase) than FaDu sg*RB1* cells (27.8 to 30.9 hours, 11.2% increase), and similar patterns were observed across all three OHNSCC lines (Figure 3.3D). Taken together, these results suggest that high cyclin E levels are insufficient in driving strong resistance to CDK4/6 inhibitors and can only contribute to a mild but reproducible degree of resistance on its own.

3.3.4 High cyclin E levels contribute to mild palbociclib resistance by promoting slow S-phase entry after 78 hours of treatment

To examine how cyclin E exerts its effect on the cell cycle in the presence of palbociclib, and to better understand the kinetics of the S-phase rebound, we designed an EdU pulse/chase regimen and compared cell cycle progression across FaDu WT, CycE, and sg*FBXW7* cells (Figure 3.3G). For this assay, we treated cells with 500nM palbociclib for 48 hours and pulsed with 10μM EdU for the final hour of treatment. After one hour of EdU labeling, we washed cells twice with PBS, replenished plates with drug and media, and harvested timepoints for up to 48 hours after EdU washout. After analyzing samples by flow cytometry, we could gate for EdU-positive cells and track their progression through the cell cycle from our first timepoint (2 hours post-EdU washout) to our final timepoint (48 hours post-EdU washout). While the histograms between WT, CycE, and sg*FBXW7* appear largely the same until hour 30, real differences begin to emerge in the final three timepoints between hour 30 and 48. After hour 30, WT cells appear mostly stuck in G1, and CycE/sg*FBXW7* cells appear to slowly transition from G1 to S over the course of those 18 hours (Figure 3.3G). These data suggest that high cyclin E exerts a weak effect on accelerating the G1/S transition, but only after a certain amount of time that cells are incubated in drug (in this case between 78-96 hours).

These results were supported by our live cell imaging FUCCI experiment. Briefly, FaDu WT, CycE, sg*FBXW7*, and sg*RB1* cells were transduced with lentivirus expressing the FUCCI vectors, pCSII-EF-FUCCI-mAG-hGeminin and pCSII-EF-FUCCI-mCherry-hCdt1. This system allows us to measure cell cycle phase length based on the amount of time cells fluoresce green (indicating G1), yellow (indicating G1/S), or red (S-G2-M). We plated cells of each genotype in its own well within a 12-well plate (including control and treatment wells) and let the cells grow

in an Incucyte ZOOM incubator for the next 5 days, taking 1 image every hour for the full duration of the experiment. Average G1 length in untreated WT FaDu cells was 10.8 hours, however, when treated with palbociclib, average G1 length in WT cells increased to 81.1 hours (Figure 3.7A). In contrast, average G1 length in untreated sg*RB1* cells was 9.4 hours and only increased to 17.8 hours when treated with PD (Figure 3.7D). In line with our previous observations, data for CycE and sg*FBXW7* cells more closely mirrored WT than sg*RB1* cells with average G1 lengths increasing with PD treatment from 13.0 hours to 73.9 hours and 12.1 to 72.3 hours, respectively, indicating only limited resistance once again (Figure 3.7B-C).

The most critical observation from this experiment was seen in the difference between the number of WT and CycE/sg*FBXW7* that were able to progress through the G1/S transition and ultimately reach the subsequent mitosis. Every WT cell that we observed transitioning past G1/S while in drug failed to reach mitosis by the end of the experiment. In contrast, a handful of CycE/sg*FBXW7* cells that transitioned past G1/S were observed to reach mitosis, indicated by green dots in the figure, and successfully divide before the end of the experiment (Figure 3.7B-C). These observations suggest that in addition to its role during G1/S, cyclin E may play an additional role either during S, G2, or M that allows cells to divide more readily in the presence of palbociclib.

3.3.5 Palbociclib treatment stabilizes cyclin E, but not through p21/p27 redistribution

One interesting observation from our experiments has been the consistent increase in cyclin E protein levels after palbociclib treatment (Figure 3.3E). This observation has held true across all cell lines irrespective of any genetic manipulations (i.e., protein overexpression and/or knockout). Initially, we suspected that palbociclib induced cyclin E accumulation was due to p21/p27 redistribution as described by Guiley *et al*. In their model, palbociclib binds to monomeric CDK4 or CDK6 thus preventing the formation of active p27-cyclin D-CDK4/6 complexes. As a result,

p27 (and p21) are shuttled to cyclin E-CDK2 complexes resulting in the accumulation of inactive cyclin E-CDK2, and they argue that this inhibitory effect is the true mediator of palbociclib induced cell cycle arrest. To test these ideas, we immunoblotted for cyclin E associated p21 and p27 in palbociclib treated MCF7 cells (Figure 3.4A). We also used siRNAs to knockdown p21 and p27 in these cells. If the redistribution model is correct, then it should predict palbociclib resistance in the absence p21 and p27. In agreement with the redistribution model, we did observe an increase in cyclin E associated p21 upon palbociclib treatment, though cyclin E associated p27 only increased when p21 was knocked down (Figure 3.4A). In opposition to their model, however, knocking down either of the inhibitors alone or in combination did not change the EdU profile of palbociclib treated MCF7 cells (Figure 3.4B). This suggests that these inhibitors do not contribute to palbociclib induced cell cycle arrest as the model predicts.

We extended this observation to FaDu cells, though only examining cyclin E associated p27 since these cells are *TP53* mutated and thus fail to induce p21 appropriately. In this case, we observed only a modest increase in cyclin E associated p27, but it once again failed to induce resistance to palbociclib as measured by EdU incorporation in WT and in CycE cells (Figure 3.4C-D). The redistribution model appears to apply even less in cells lacking p53 as the accumulated cyclin E after palbociclib treatment results in *active* cyclin E complexes as seen in our kinase assays (Figure 3.3F). In the context of intact p53, as is the case in MCF7, cyclin E activity remains relatively constant despite rising levels of protein after palbociclib treatment, most likely due to the effects of p21 (Figure 3.3F). The precise cause of rising cyclin E levels in response to palbociclib remains unsettled, but we have so far ruled out an increase in transcription by measuring mRNA through RT-qPCR. Cyclin E mRNA levels are relatively constant over 24 and 48 hours of palbociclib treatment, while a clear reduction and return of cyclin A mRNA is observed

which closely resembles the pattern seen in cyclin A western blots (Figure 3.6A and Figure 3.3E). It is possible that palbociclib induces an increase in translation of cyclin E due to an observed drop in cyclin E protein levels when cells are co-treated with the mTOR inhibitor rapamycin (Figure 3.6B).

3.4 Discussion

In this study, we have demonstrated that high cyclin E levels (achieved either through stable overexpression or *FBXW7* knockout) fail to induce robust resistance to CDK4/6 inhibition in a panel of HPV-negative OHNSCC lines. This finding was also reproduced in a breast cancer cell line (MCF7) where amplification of *CCNE1* had previously been reported as a mechanism of resistance to palbociclib. In contrast, loss of *RB1* consistently demonstrated strong resistance to CDK4/6 inhibition, and this was seen in HPV-negative cell lines with *RB1* knockout, as well as in HPV-positive cell lines where pRb is abrogated by the E7 oncoprotein. While high cyclin E cells failed to confer resistance to the level of pRb null cells, there was clearly a small but reproducible level of resistance that we observed in our flow cytometry and cell outgrowth assays (Figure 3.3A-D). This suggests that while high cyclin E has been observed clinically in patients with resistance to CDK4/6 inhibitors, it is insufficient on its own to drive that resistance. Thus, we conclude that cyclin E may be dependent on other molecular changes that occur with continuous exposure to CDK4/6 inhibitors in order to contribute to resistance.

An important finding that we have not previously seen discussed in the literature are differences seen in cells treated with palbociclib for 24 hours versus 48 or more hours. In general, we observed high accumulation of cells in G1 measured by EdU incorporation after 24 hours of exposure to drug, but then varying degrees of cell cycle reentry after 48 hours of treatment across our panel of cell lines (Figure 3.3A-B). This result was recapitulated even when new drug was

added after the first 24 hours thus eliminating the possibility that this observation was due to decay of the drug over time (data not shown). This suggests that while cells may exhibit acute sensitivity to CDK4/6 inhibition, they are not necessarily exiting the cell cycle upon exposure to drug. Rather, cells are dramatically slowed down at the G1/S transition as phosphorylation of pRb by the D-type cyclins is prevented. The inability of cyclin E to bypass this inhibition may reflect its dependence on a priming phosphorylation by cyclin D-CDK4/6 in order to fully hyperphosphorylate pRb. As an example, Narasimha *et al*. demonstrated that cyclin E relies on cyclin D mediated mono-phosphorylation of pRb in order to fully hyperphosphorylate the protein[122]. This explanation could be supported by our data that show high cyclin E cells conferring a greater degree of resistance to palbociclib when treated with lower concentrations of drug (Figure 3.5). In other words, at lower concentrations of drug, cells may experience incomplete inhibition of CDK4/6 thus hypophosphorylating pRb to some degree and allowing cyclin E to more effectively hyperphosphorylate pRb and drive the G1/S transition.

In one of the seminal studies that first demonstrated cyclin E amplification as a resistance mechanism to CDK4/6 inhibition, the investigators produced palbociclib resistant MCF7 cells by chronic exposure to drug over three to four months and showed an increase in the copy number for *CCNE1*[66]. While their follow up experiments focused on cyclin E, a number of other genetic changes were also reported, though none were specified outside of an activating mutation to *PIK3CA*. Activation of the PI3K-Akt pathway is known to stabilize cyclin D and has also been implicated in CDK4/6 inhibitor resistance in this study and others[123,124]. Perhaps the increased copy number of *CCNE1* can only contribute to CDK4/6 inhibition resistance in a robust fashion when coupled with activating mutations in pathways such as PI3K-Akt.

Finally, we challenged the redistribution model of p21 and p27 as the mechanism of cell cycle arrest seen with palbociclib. While subtle increases in cyclin E associated p21 and p27 were seen in palbociclib treated MCF7 cells, or just p27 in the case of FaDu, it was an insufficient amount to restore the cell cycle when measured by EdU incorporation (Figure 3.4A-D). These data were in accordance with another group that also demonstrated palbociclib efficacy in cells lacking p21 and p27[125]. Furthermore, the slight accumulation of p27 on cyclin E in FaDu cells did not prevent cyclin E-CDK2 activity, but rather, we saw a dramatic rise in cyclin E levels *and* activity upon palbociclib treatment. Because our panel of OHNSCC lines are p53 deficient and thus fail to induce p21, we consistently observed an increase in cyclin E activity when cells were treated with palbociclib (Figure 3.3E). We determined that this increase was not due to transcription, but might instead be the result of increased translation, however, further studies are required to elucidate this exact mechanism (Figure 3.6A-B). The fact that we observe high cyclin E accumulation and activity in WT backgrounds in response to palbociclib is further evidence that it alone cannot drive resistance to CDK4/6 inhibition. Thus, finding the accompanying molecular and genetic changes that occur in conjunction with cyclin E deregulation will be an important finding of future studies to more accurately predict CDK4/6 inhibitor resistance.

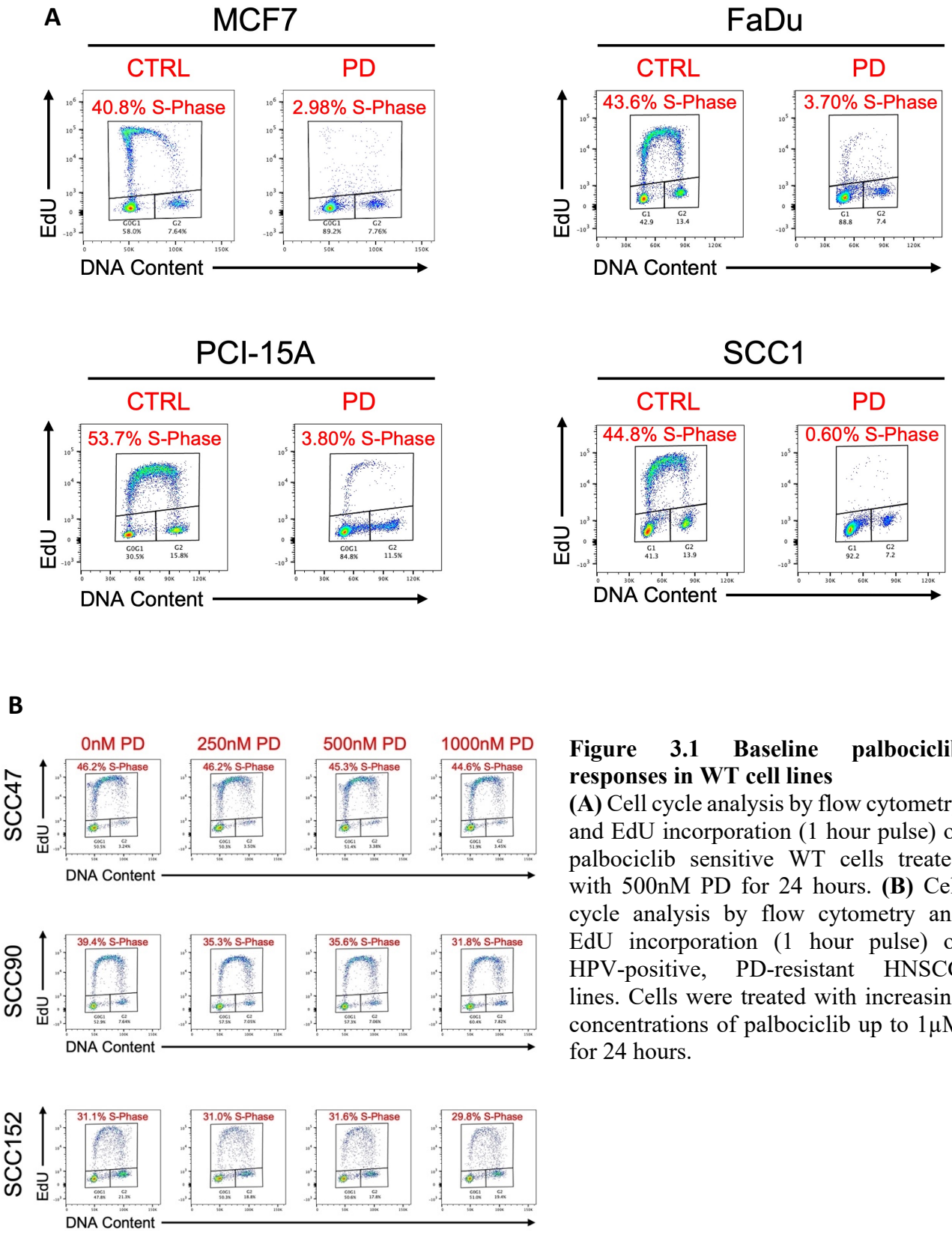

Figure 3.1 Baseline palbociclib responses in WT cell lines
(A) Cell cycle analysis by flow cytometry and EdU incorporation (1 hour pulse) of palbociclib sensitive WT cells treated with 500nM PD for 24 hours. **(B)** Cell cycle analysis by flow cytometry and EdU incorporation (1 hour pulse) of HPV-positive, PD-resistant HNSCC lines. Cells were treated with increasing concentrations of palbociclib up to 1μM for 24 hours.

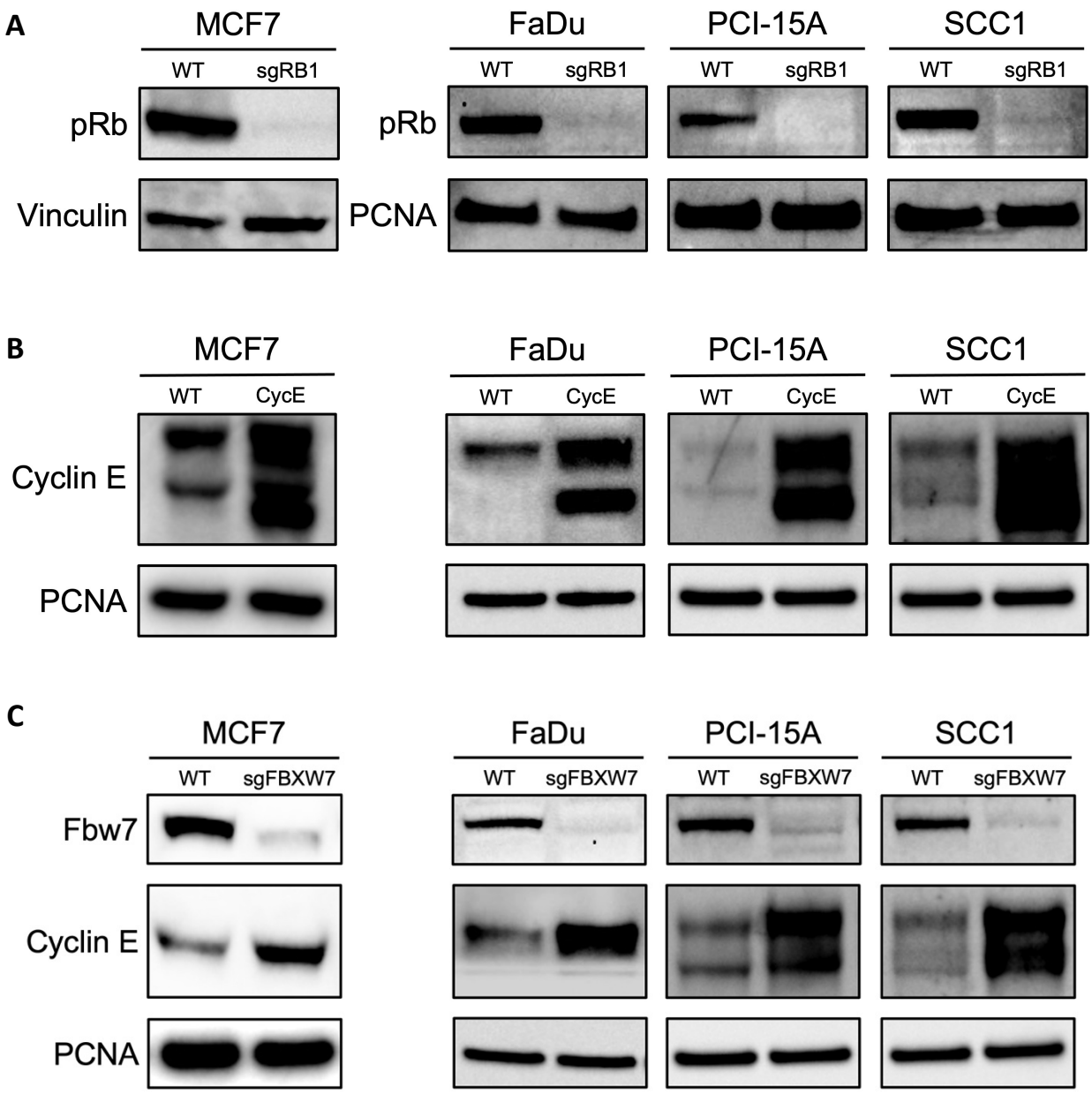

Figure 3.2 Cell line modifications
(A) MCF7, FaDu, PCI-15A, and SCC1 cells were transduced with lentivirus containing sgRNA targeting *RB1*. **(B)** MCF7, FaDu, PCI-15A, and SCC1 cells were transduced with retrovirus to stably overexpress cyclin E. **(C)** MCF7, FaDu, PCI-15A, and SCC1 cells were transduced with lentivirus containing sgRNA targeting *FBXW7*.

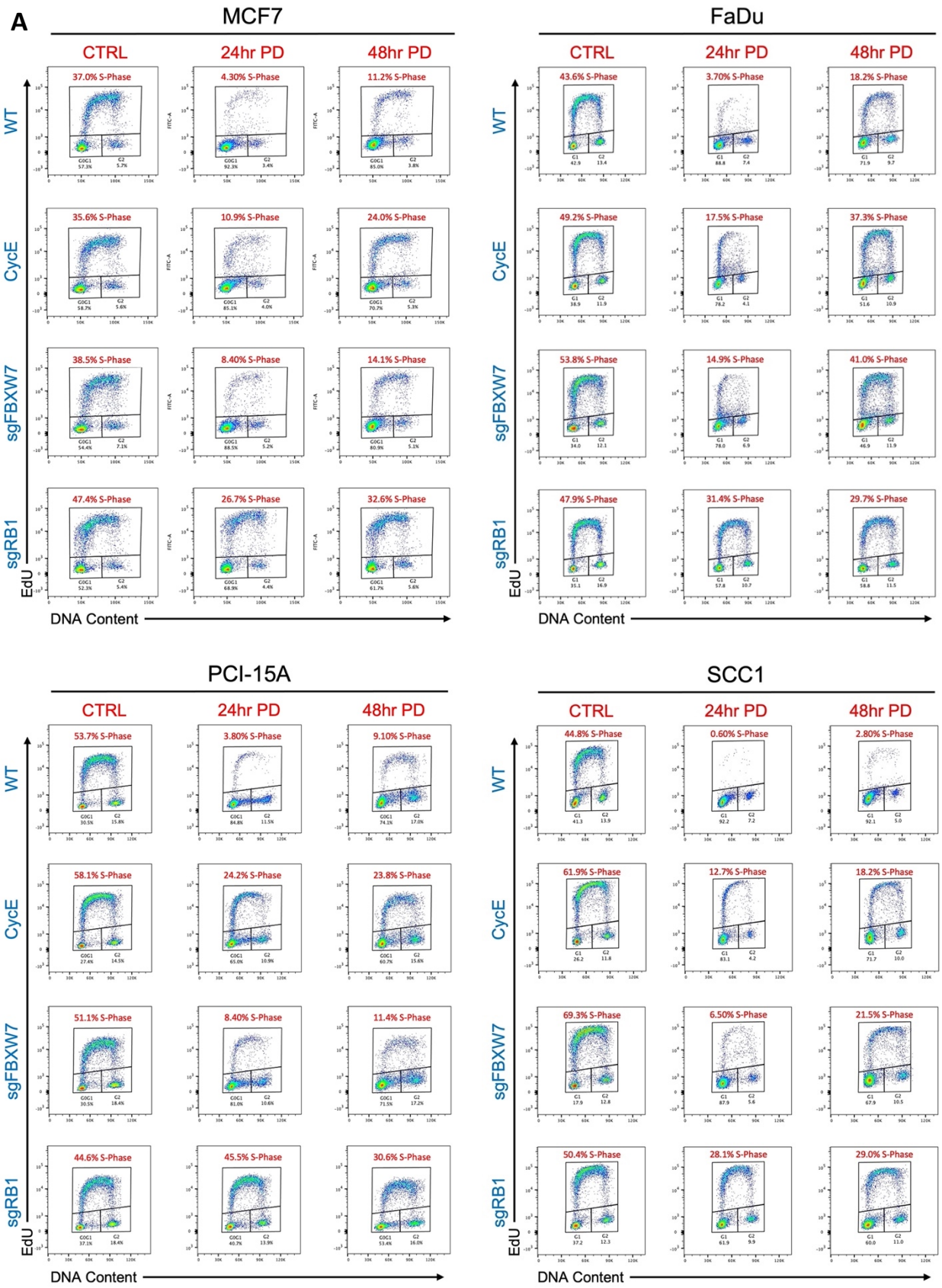
A
MCF7
FaDu
PCI-15A
SCC1
CTRL
24hr PD
48hr PD
WT
CycE
sgFBXW7
sgRB1
EdU
DNA Content
37.0% S-Phase
4.30% S-Phase
11.2% S-Phase
35.6% S-Phase
10.9% S-Phase
24.0% S-Phase
38.5% S-Phase
8.40% S-Phase
14.1% S-Phase
47.4% S-Phase
26.7% S-Phase
32.6% S-Phase
43.6% S-Phase
3.70% S-Phase
18.2% S-Phase
49.2% S-Phase
17.5% S-Phase
37.3% S-Phase
53.8% S-Phase
14.9% S-Phase
41.0% S-Phase
47.9% S-Phase
31.4% S-Phase
29.7% S-Phase
53.7% S-Phase
3.80% S-Phase
9.10% S-Phase
58.1% S-Phase
24.2% S-Phase
23.8% S-Phase
51.1% S-Phase
8.40% S-Phase
11.4% S-Phase
44.6% S-Phase
45.5% S-Phase
30.6% S-Phase
44.8% S-Phase
0.60% S-Phase
2.80% S-Phase
61.9% S-Phase
12.7% S-Phase
18.2% S-Phase
69.3% S-Phase
6.50% S-Phase
21.5% S-Phase
50.4% S-Phase
28.1% S-Phase
29.0% S-Phase

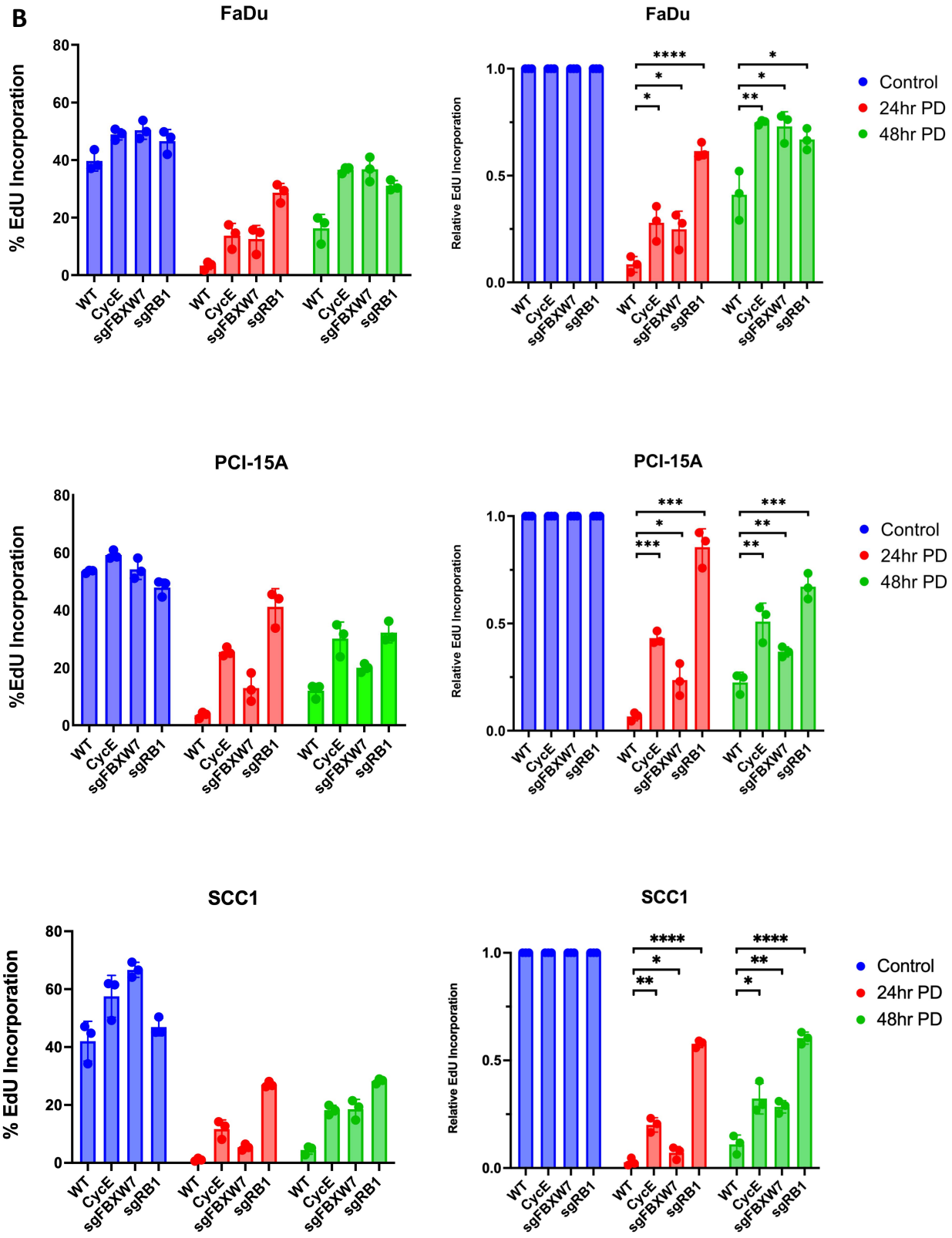
B
FaDu
% EdU Incorporation
Relative EdU Incorporation
Control
24hr PD
48hr PD
WT
CycE
sgFBXW7
sgRB1
PCI-15A
%EdU Incorporation
SCC1

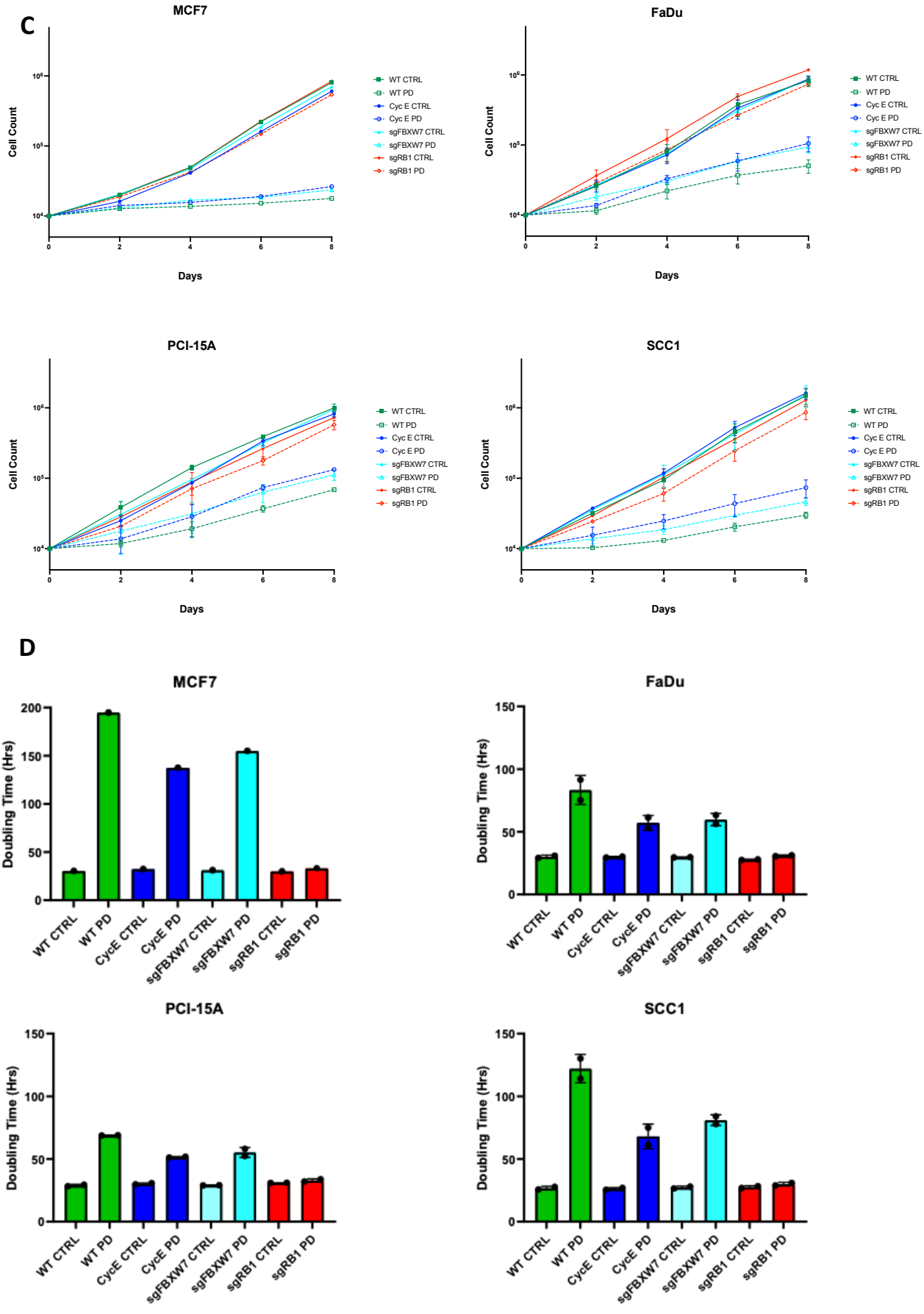
C
MCF7
FaDu
PCI-15A
SCC1
Cell Count
Days
WT CTRL
WT PD
Cyc E CTRL
Cyc E PD
sgFBXW7 CTRL
sgFBXW7 PD
sgRB1 CTRL
sgRB1 PD
D
Doubling Time (Hrs)
CycE CTRL
CycE PD

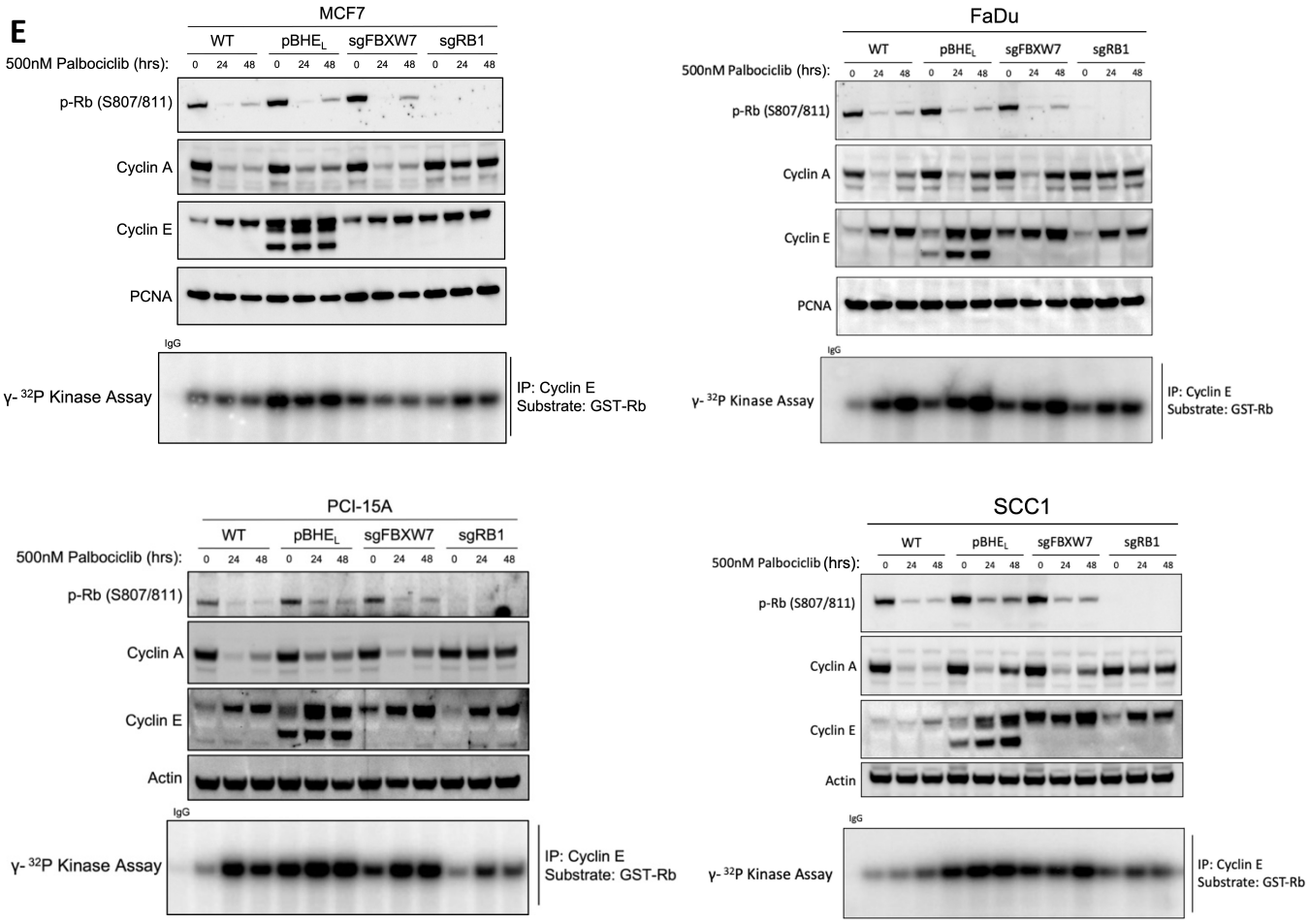
E
MCF7
WT
pBHE$_L$
sgFBXW7
sgRB1
500nM Palbociclib (hrs):
0 24 48 0 24 48 0 24 48 0 24 48
p-Rb (S807/811)
Cyclin A
Cyclin E
PCNA
IgG
γ-^{32}P Kinase Assay
IP: Cyclin E
Substrate: GST-Rb
FaDu
PCI-15A
Actin
SCC1

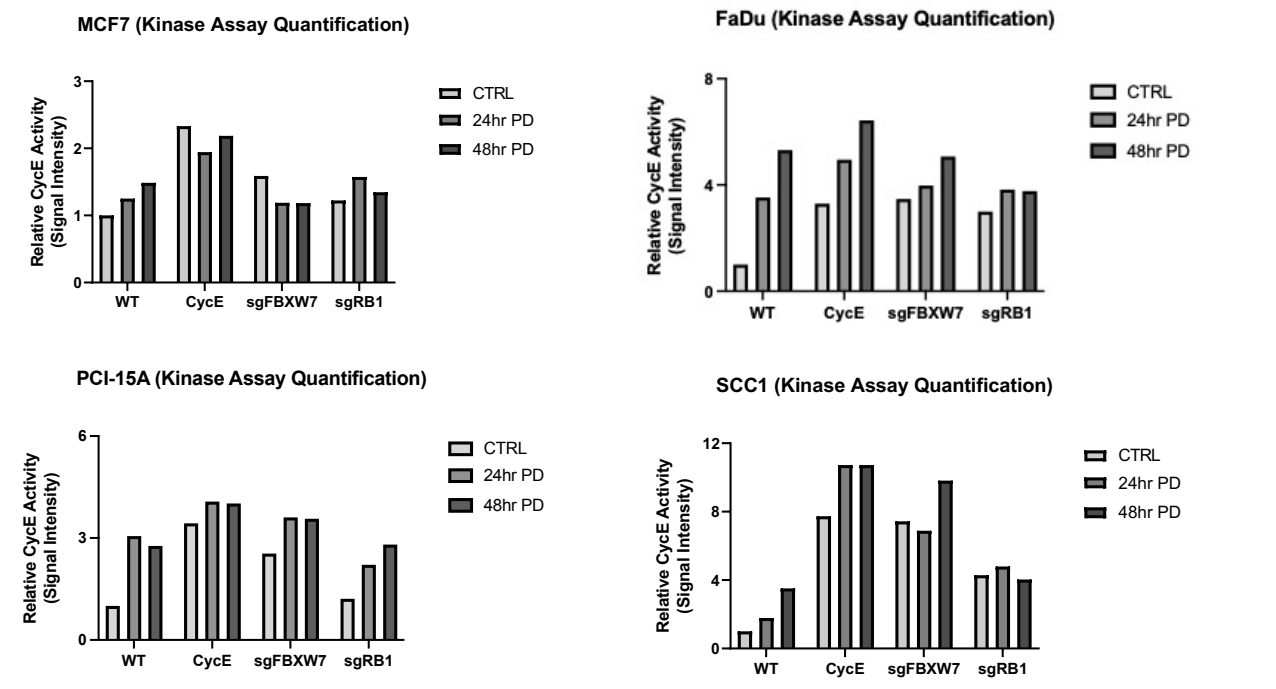
F
MCF7 (Kinase Assay Quantification)
FaDu (Kinase Assay Quantification)
PCI-15A (Kinase Assay Quantification)
SCC1 (Kinase Assay Quantification)
Relative CycE Activity (Signal Intensity)
CTRL
24hr PD
48hr PD
WT
CycE
sgFBXW7
sgRB1

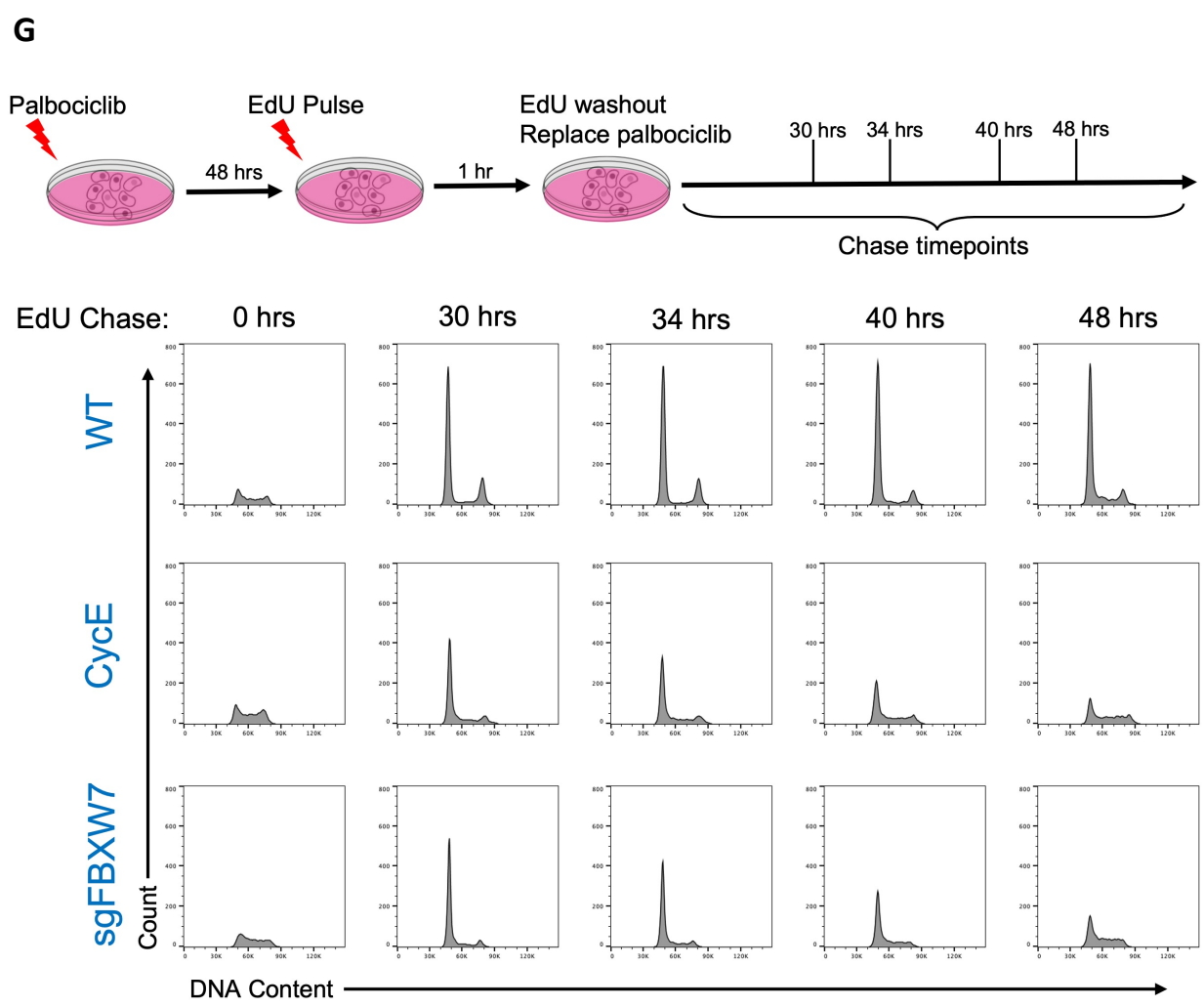

Figure 3.3 Palbociclib responses in modified cell lines
(A) Cell cycle analysis by flow cytometry and EdU incorporation (1 hour pulse) of WT and modified (CycE, sg*FBXW7*, sg*RB1*) MCF7, FaDu, PCI-15A, and SCC1 cells. Cells were treated with 500nM PD for either 24 or 48 hours prior to EdU pulse and analysis. **(B)** Quantification of flow cytometry analyses and relative EdU incorporations for each condition in OHNSCC panel only (n=3) (*=p<0.05; **=p<.005, ***=p<.0005, ****=p<.0001). **(C)** Long term (8-day) outgrowth of each cell line (WT and modified) in 500nM PD. Cell counts were taken every two days (MCF7 cells (n=1), OHNSCC panel (n=2). **(D)** Doubling times of MCF7 and OHNSCC panel with and without palbociclib treatment over 8-day outgrowth. Doubling times were calculated using the following formula: doubling time = (192 hours*log(2))/(log(day 8 cell count) – (log(day 0 cell count)) **(E)** Western blot panel and cyclin E kinase assay of each cell line. Cells were treated with 500nM PD for either 24 or 48 hours prior to harvest. **(F)** Cyclin E kinase assay quantifications all normalized their own untreated WT lanes. **(G)** EdU pulse chase assay in FaDu WT, CycE, and sg*FBXW7* cells. Cells were treated with 500nM PD for 48 hours, pulsed with EdU for 1 hour, washed, and allowed to grow in drug for the indicated timepoints prior to fixation. EdU+ cells were then gated by flow cytometry and their histograms were generated for each timepoint.

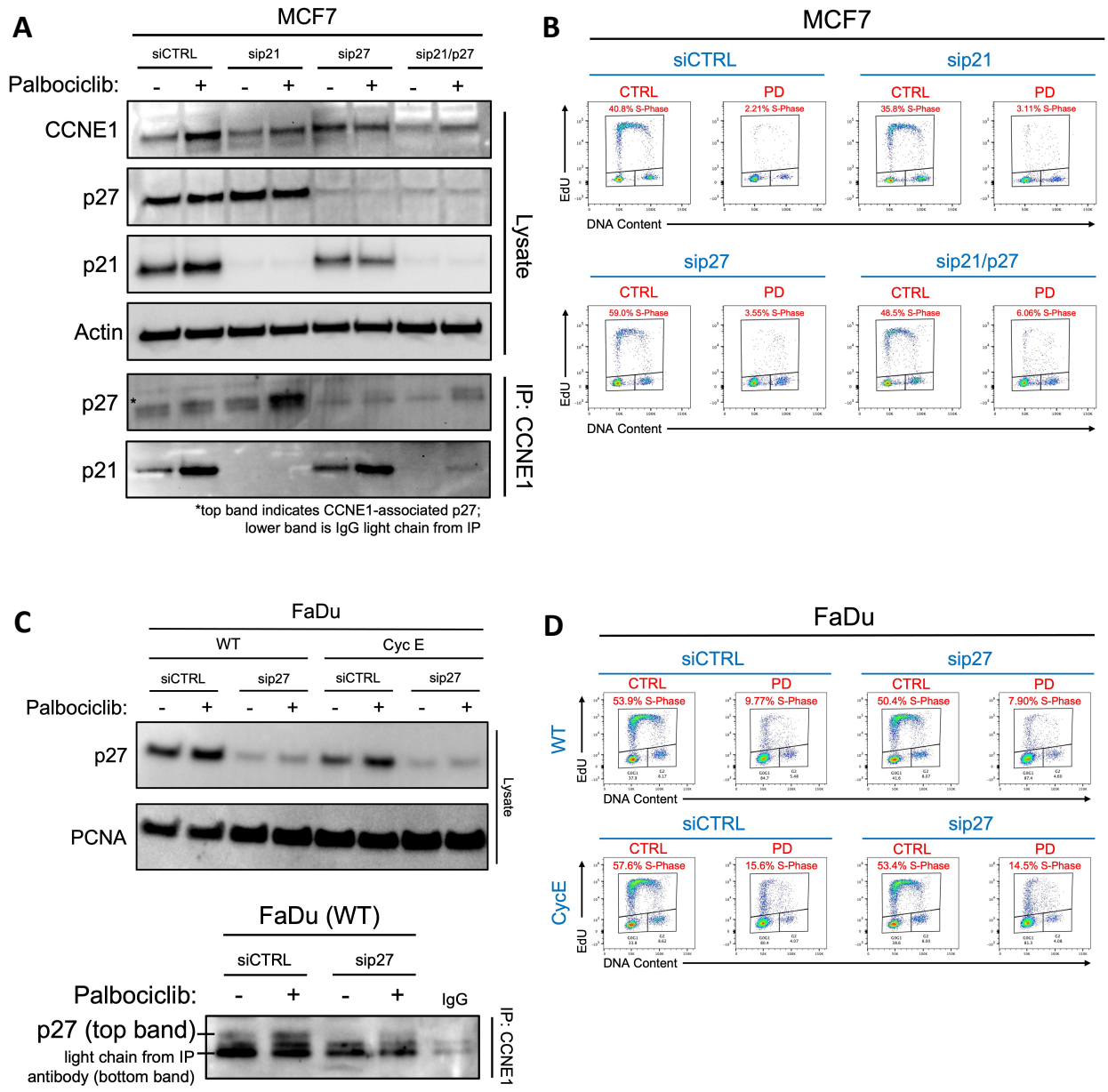

Figure 3.4 p21 and p27 response to palbociclib

(A) MCF7 cells were given siRNAs targeting p21, p27, or both and then treated with 500nM palbociclib overnight. To see changes in cyclin E associated p21 and p27, we immunoprecipitated cyclin E and then blotted for p21 and p27. **(B)** Cell cycle analysis by flow cytometry and EdU incorporation (1 hour pulse) of MCF7 sip21 and/or sip27 cells. **(C)** FaDu WT and CycE cells were given siRNAs targeting only p27 and treated with 500nM palbociclib overnight. To see changes in cyclin E associated p27, we immunoprecipitated cyclin E and then blotted for p27. **(D)** Cell cycle analysis by flow cytometry and EdU incorporation (1 hour pulse) of FaDu WT and CycE sip27 cells.

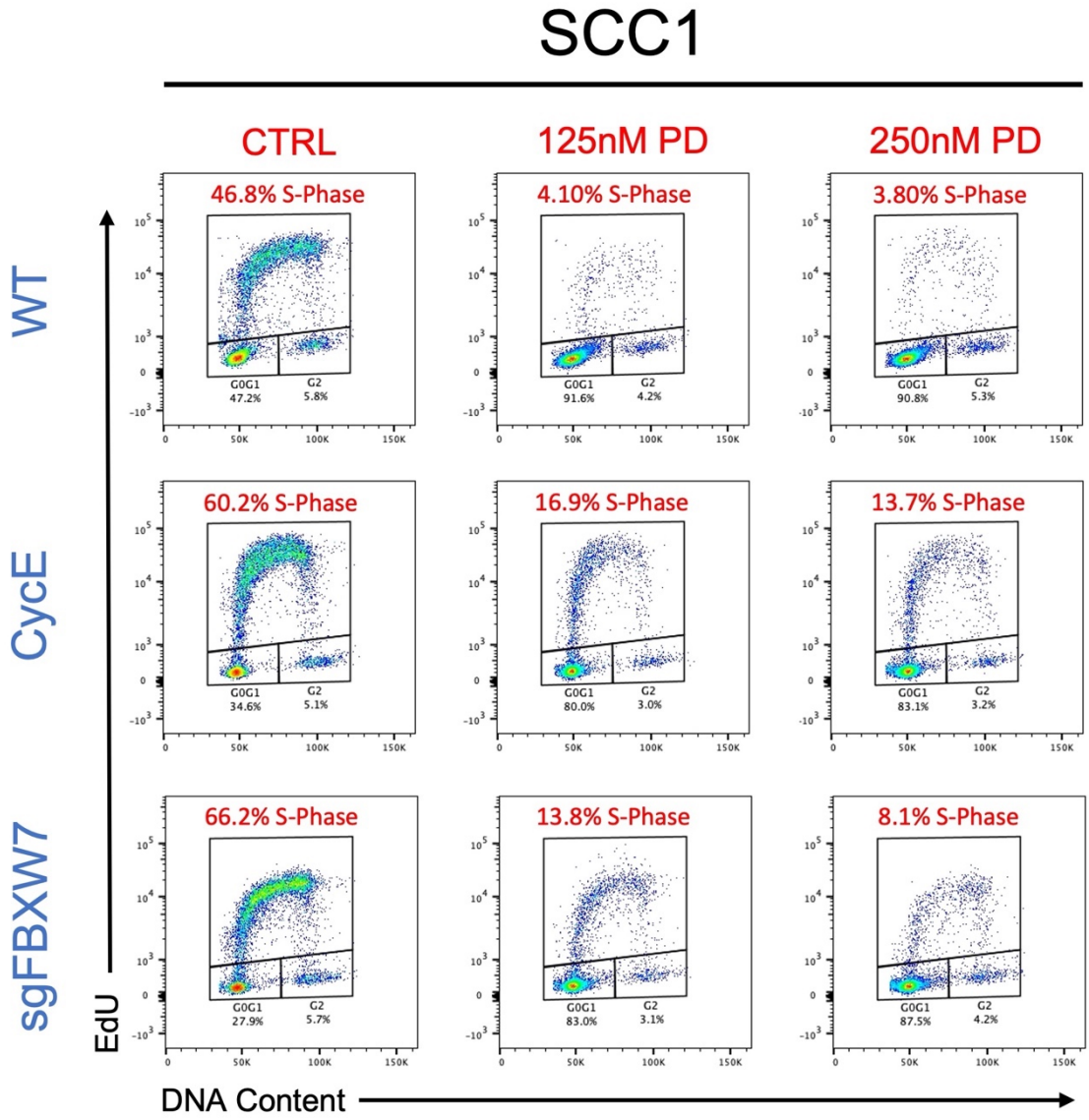

Figure 3.5 Low dose palbociclib treatment in modified SCC1 Cells
Cell cycle analysis by flow cytometry and EdU incorporation (1 hour pulse) of SCC1 cells (WT, CycE, and sg*FBXW7*) treated with 125nM or 250nM palbociclib for 24 hours. S-phase differences between WT and high cyclin E cells are more pronounced at lower concentrations of drug.

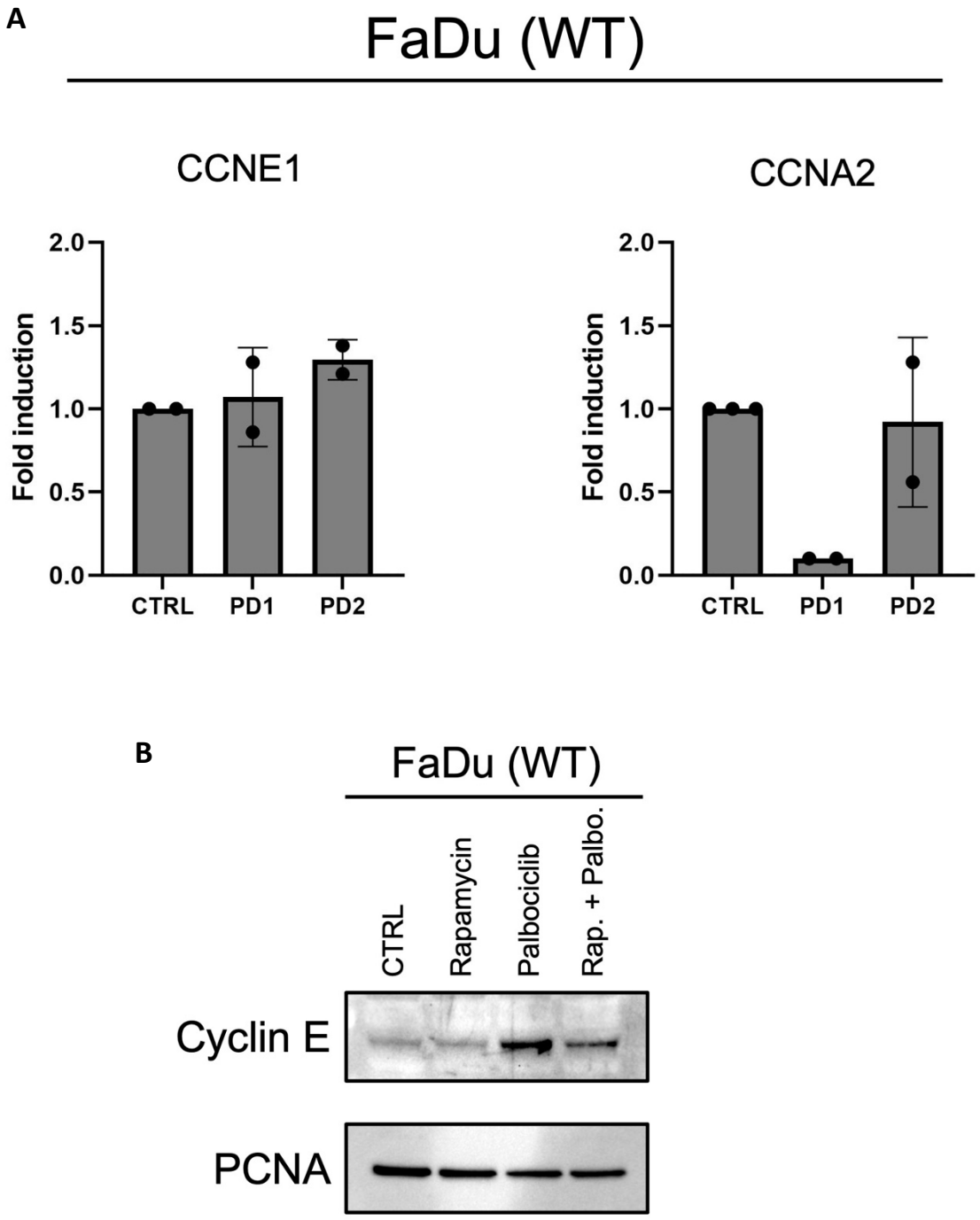

Figure 3.6 Cyclin E response to palbociclib in FaDu cells
(A) RT-qPCR of cyclin E and cyclin A in palbociclib (500nM) treated FaDu WT cells. Note: PD1 = 1-day (24hr) treatment and PD2 = 2-day (48hr) treatment. **(B)** Cyclin E western blot of FaDu WT cells treated with 1μM rapamycin alone, 500nM palbociclib alone, or 1μM rapamycin and 500nM palbociclib in combination.

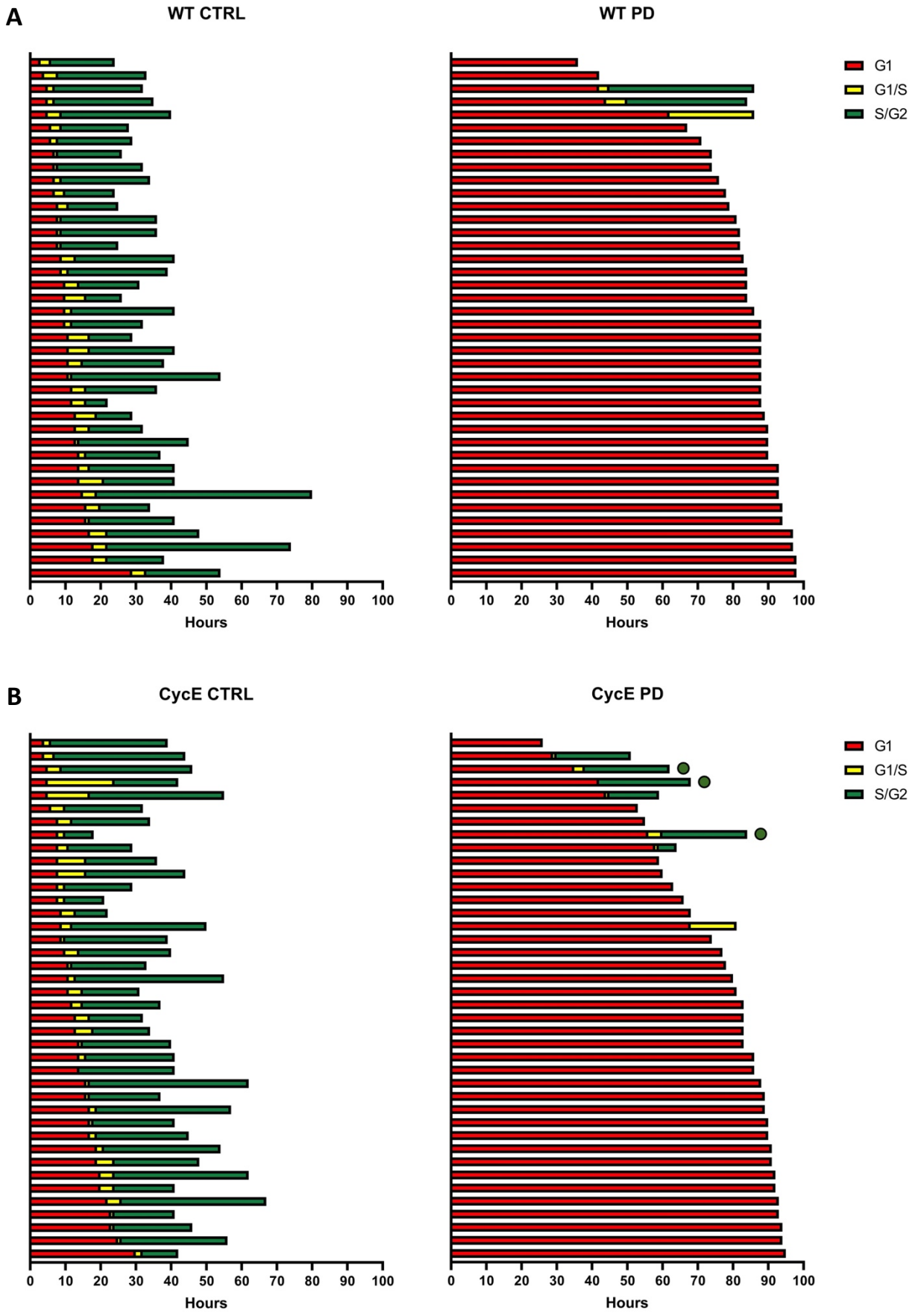
A
WT CTRL
WT PD
G1
G1/S
S/G2
0 10 20 30 40 50 60 70 80 90 100
Hours
B
CycE CTRL
CycE PD
G1
G1/S
S/G2
0 10 20 30 40 50 60 70 80 90 100
Hours

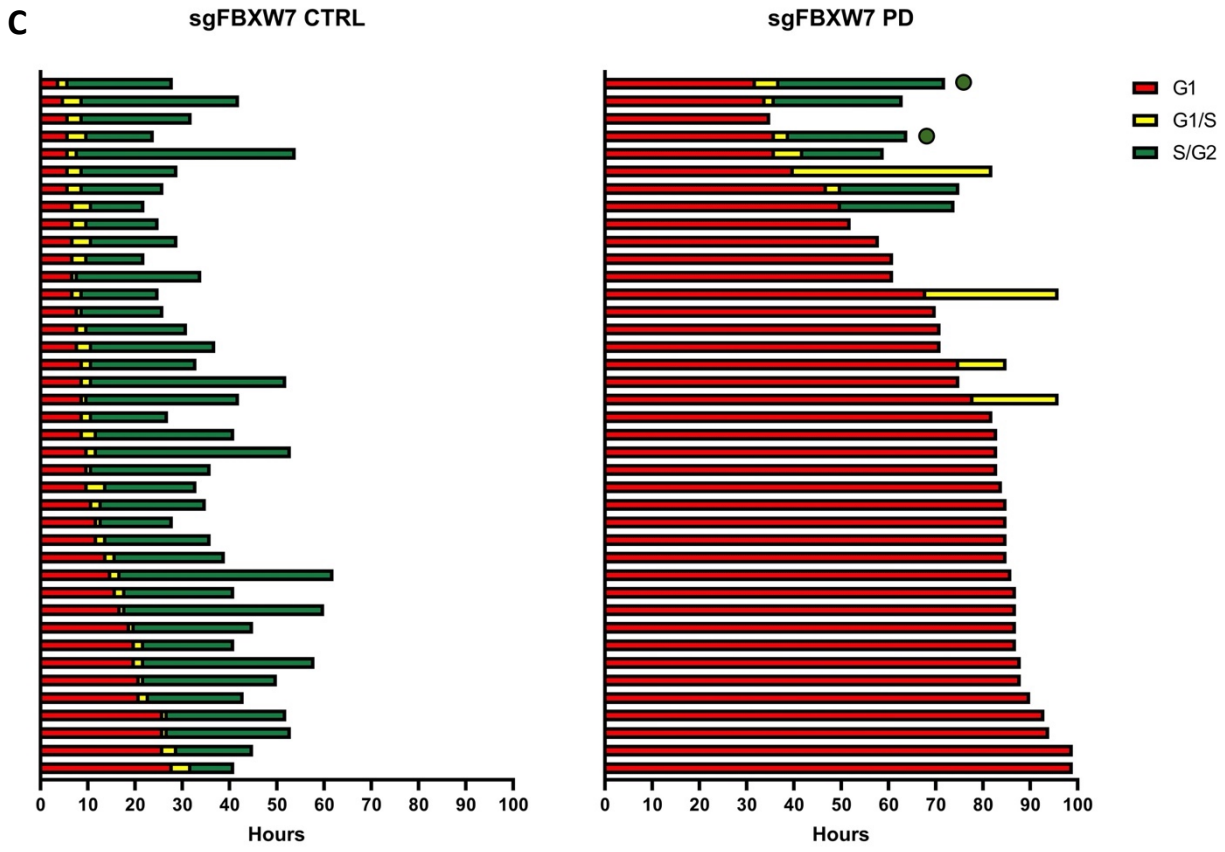
C
sgFBXW7 CTRL
sgFBXW7 PD
G1
G1/S
S/G2
0 10 20 30 40 50 60 70 80 90 100
Hours
0 10 20 30 40 50 60 70 80 90 100
Hours

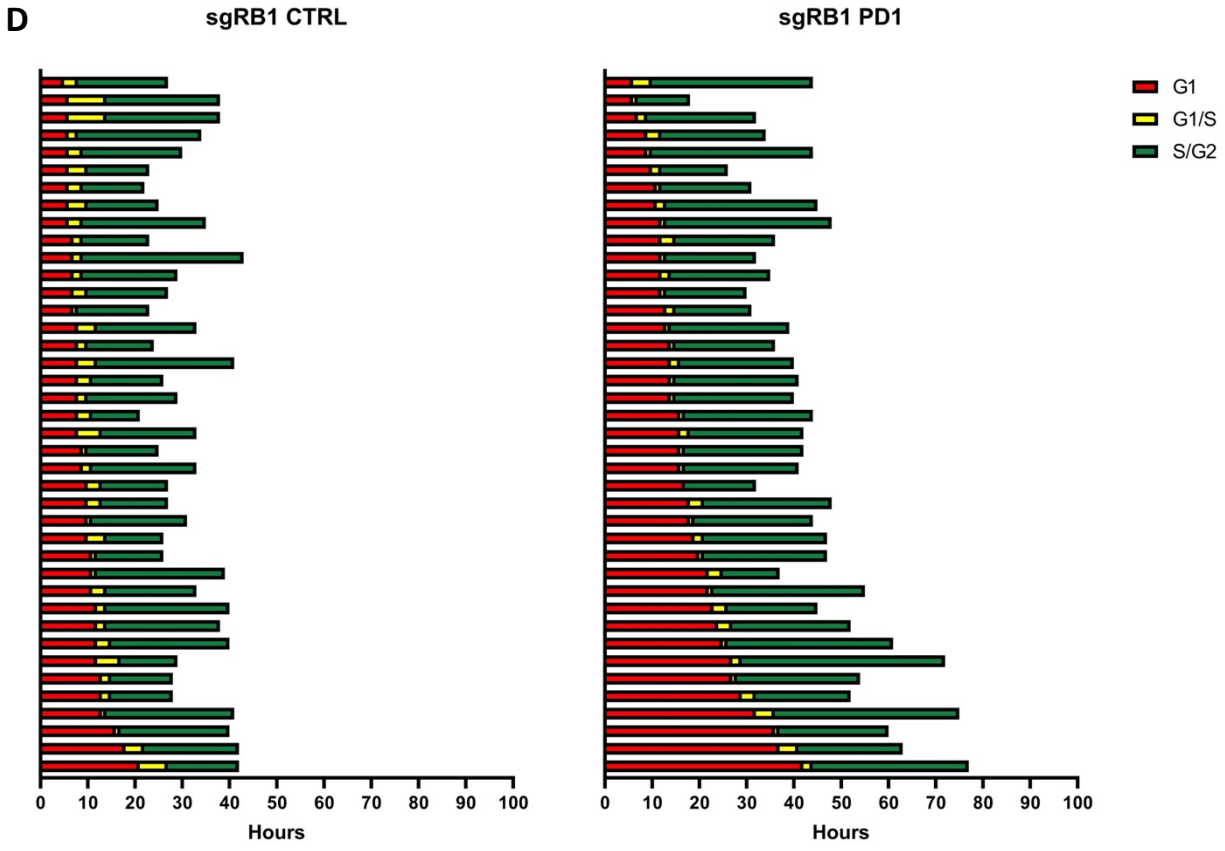
D
sgRB1 CTRL
sgRB1 PD1
G1
G1/S
S/G2
0 10 20 30 40 50 60 70 80 90 100
Hours
0 10 20 30 40 50 60 70 80 90 100
Hours

Figure 3.7 Live cell imaging with FUCCI in FaDu cells
(A) WT **(B)** CycE **(C)** sg*FBXW7* and **(D)** sg*RB1* live cells were tracked (n=40) using the FUCCI system while being treated with 500nM PD over a five-day period. Each row represents a single cell, and the length of each cell cycle phase is denoted by the indicated colors (red = G1, yellow = G1/S transition, green = G2 & M). Note that if cell division was observed in PD treated CycE or sg*FBXW7* cells, they are indicated with a green dot at the end of their row. None of our tracked PD treated WT cells were seen dividing. Note that all of our tracked PD treated sg*RB1* were seen dividing but we omitted the use of green dots to prevent cluttering in the figure. Average G1 lengths were calculated as: WT CTRL: 10.8 hours; WT PD: 81.1 hours; CycE CTRL: 13.0 hours; CycE PD: 73.9 hours; sg*FBXW7* CTRL: 12.1 hours; sg*FBXW7* PD: 72.3 hours; sg*RB1* CTRL: 9.43 hours; sg*RB1* PD: 17.8 hours.

Table 3.1 sgRNA sequences used for CRISPR-Cas9 knockouts

Gene	sgRNA #	Guide Sequence (5'→3')
FBXW7	1	AAGAGCGGACCTCAGAACCA
FBXW7	2	GCAAAGTCTCAGAATATACA
RB1	1	ACATGAATGTAATATAGATG
RB1	2	TCACCTCGAACACCCAGGCG

Table 3.2 Primers used for RT-qPCR

Gene	Forward Primer (5'→3')	Reverse Primer (5'→3')
CCNA2	CGCTGGCGGTACTGAAGTC	GAGGAACGGTGACATGCTCAT
CCNE1	AAGGAGCGGGACACCATGA	ACGGTCACGTTTGCCTTCC
RPLP40	TGACCAGCCCAAAGGAGAAG	CACCATTGAAATCCTGAGTGATGT
TBP	GAGCTGTGATGTGAAGTTTCC	TCTGGGTTTGATCATTCTGTA

Chapter 4. In-Situ Phosphorylation and Mass Spectrometry Screen to Identify Novel CDK Substrates

4.1 Introduction

The classical pocket proteins (i.e., pRb, p107, and p130) have been known as the primary substrates of CDK4 and CDK6 since the early 1990s[16,126]. The importance of these proteins was steadily uncovered in the following years as their role in the cell cycle and deregulation in cancer were outlined in detail. Briefly, the pocket proteins regulate the G1/S transition by binding to and suppressing the E2F family of transcription factors. As cells progress through G1, cyclin D-CDK4/6 activity increases resulting in hypophosphorylation of the pocket proteins. This releases E2F allowing the transcription of S-phase promoting genes like cyclins E & A, which go on to hyperphosphorylate the pocket proteins thus generating a positive feedback loop pushing the cell past the G1 restriction point and into S-phase.

These discoveries revealed an apparent redundancy between cyclin E-CDK2 and cyclin D-CDK4/6 in controlling pocket protein phosphorylation[102]. While much attention was given to the fact that cells could substitute cyclin E function in place of the D-type cyclins, many groups overlooked CDK4 and CDK6 in favor of the more active and seemingly more important kinases, CDK1 and CDK2. Indeed, while CDK1/2 targets have been the subject of many reports over the years, only a handful of studies have identified CDK4/6 substrates outside of the classical pocket proteins such as SMAD3, FOXM1, and CDH1 to name a few[127–129]. This is mainly due to a lack of systemic screens for CDK4/6 substrates like the one conducted by Anders *et al*. in 2011[129]. While this group was successfully able to validate one of their hits (FOXM1), their method was limited by the use of wild-type kinases and screening candidate substrates against a protein

database. A more direct and unbiased approach using analog-sensitive kinases could uncover a broader and more accurate list of candidate substrates.

In 1997, Shah *et al*. engineered a mutant version of the protein tyrosine kinase v-Src to identify its specific substrates[130]. The ATP-binding site was mutated so as to accept a unique, bulky ATP analog (N^6-(cyclopentyl)-ATP) that wild-type kinases were unable to use. By subjecting cell lysates to the mutant, analog-sensitive (AS) kinase and ATP analog, Shah *et al*. would go on to identify novel and specific substrates of v-Src thus laying the groundwork for a new method to identify substrates of other protein kinases.

Members of the Clurman lab later built upon this principle by introducing similar ATP-binding site mutations into the cell cycle kinases CDK2, CDK4, and CDK6. In 2008, Chi *et al*. published their method utilizing AS-CDK2, N6-(2-phenylethyl)-ATP (PE-ATP), and mass spectrometry (MS) to identify over 180 potential substrates[131]. They went on to refine their "in-situ" method by restricting the kinase reaction to isolated cell nuclei so as to maintain more physiologically relevant conditions[132,133]. Once again, over 100 potential substrates were identified, 40% of which were already known, and several novel substrates were validated including LSD1, DOT1L, and Rad54[133].

To further broaden our understanding of CDK functions in the cell cycle, we applied the in-situ phosphorylation method to CDK6 in the context of OHNSCC. In addition to searching for novel CDK6 substrates, another goal of this study was to uncover any secondary effects of CDK4/6 inhibition. The consequences of CDK4/6 inhibitors like palbociclib can sometimes be unpredictable or at odds with data generated between different research groups. One potential reason behind these discrepancies may rise from potentially unknown effects of CDK4/6 inhibition. While it is known that the primary effect of CDK4/6 inhibition is to prevent pRb

phosphorylation, this may be an oversimplification if CDK4 and/or CDK6 are responsible for phosphorylating any number of other substrates. The current scarcity of known CDK4/6 substrates not only provides us an opportunity to fill in this knowledge gap using known methodologies, but it may also help us better understand the global effects of CDK4/6 inhibition.

We conducted three independent AS-CDK6 screens using nuclei isolated from FaDu cells (OHNSCC) and introduced slight modifications to each of the three screens. In the first screen, we transfected cells using only AS-CDK6 and identified 50 potential substrates (Figure 4.2A). In the second screen, we used AS-CDK6 harboring an additional activating mutation (S178P) that mimics the phosphorylated CAK sites on CDK1/2 thereby increasing kinase activity in our experiment (herein referred to as AS-CDK6*) (Figure 4.2B). To our surprise, we identified fewer candidate substrates (38) with this more active kinase, though in this screen we identified an expected substrate, the pocket protein p107 (gene: *RBL1*). And finally in our third screen, we co-transfected cells with AS-CDK6* and cyclin-D to maximize in-vivo kinase activity (Figure 4.2A). This third screen yielded 162 potential substrates and most importantly, it identified the known CDK6 substrate pRb which had been unexpectedly absent in our previous two runs. Within the list of potential substrates, we observed an enrichment for proteins involved cell division, chromatin remodeling, DNA replication initiation and elongation, among others (Figure 4.3B). Intriguingly, the list of potential CDK6 substrates had substantial overlap with the list of potential CDK2 substrates from our lab's previous studies[133]. We speculate that this overlap reflects the functional redundancy observed between the different CDKs, however its biological significance will require further study to understand. Between our three AS-CDK6 screens, eight potential substrates were shared between all three conditions (Figure 4.3A). While those eight substrates served as the starting point in selecting candidates for the validation process, we chose to focus on the candidate

substrate, CDC45 (found only in the cyclin D-AS-CDK6* screen), due to its relevance in the cell cycle and ease of future study.

4.2 Materials and Methods

4.2.1 Cell lines, plasmids, recombinant protein expression/purification

FaDu and Lenti-X 293T cells were grown in Dulbecco's Modified Eagle Medium (DMEM) supplied with 10% fetal bovine serum (Gibco) and penicillin-streptomycin (Gibco). PE-ATP-γ-S was synthesized in the Clurman lab and all CDK phosphosite mutants were generated in the Clurman lab by site-directed mutagenesis as previously described[132]. Plasmids encoding HA-tagged CSNK1D and FLAG-tagged FOXK1 were generated previously in the Clurman lab using the pCMV vector backbone (Markus Welcker). pCMV-FLAG-CDC45 was purchased from SinoBiological. GST-CDC45 was generated using cDNA isolated from pCMV-FLAG-CDC45 vector (SinoBiological) and cloned into a pGEX-4T1 vector backbone (Addgene). The plasmid was expressed in bacteria and purified using glutathione Sepharose beads.

4.2.2 Cell nuclei isolation and in situ kinase assay

FaDu cells transiently overexpressing WT-CDK6, AS-CDK6, AS-CDK6*, or cyclin D-AS-CDK6* were each grown on two 15cm plates for two days after transfections and harvested by trypsinization around 80-90% confluency. Pellets were washed once with PBS and then twice in 1mL cold hypotonic lysis buffer (10mM HEPES pH7.4, 10mM KCl, and 2mM$MgCl_2$) followed by centrifugation for 1min at 0.5g. Pellets were resuspended in 1mL hypotonic lysis buffer and left on ice for 15min to allow cells to swell. Swollen cells were then lysed by repetitive pipetting (5-7 times) using a 1-mL, 26-gauge needle syringe keeping nuclei intact and verified by trypan blue staining (Life Technologies). The remainder of the slurry was added to the surface of 7mL cold hypotonic lysis buffer with 30% sucrose (w/v) in a 15mL Falcon tube. The tube was then

centrifuged for 10min at 1000g, and the supernatant aspirated. The remaining pellet containing only nuclei was washed three times with cold hypotonic buffer and centrifuged for 1min at 0.5g between washes. After a final trypan blue check for intact and isolated nuclei, the final pellet was resuspended in kinase assay reaction buffer containing 500mM PE-ATP-γ-S, 50mM HEPES pH7.4, 10mM $MgCl_2$, 1mM DTT and incubated at 30°C for 30min with continuous shaking in a Heat Only Thermal Mixer II (Boekel). Following the reaction, tubes were centrifuged briefly (0.5g, 30sec), supernatant aspirated, and the pellets were either processed immediately (described below) or flash frozen in liquid nitrogen for future processing.

4.2.3 Purification of thiophosphorylated peptides

Frozen nuclei pellets were resuspended in 400µL of 30mM HEPES pH7.4, 10mM EDTA, and 25U/mL benzonase (Millipore Sigma) and incubated on ice for 30 minutes. After adding Tween-20 for a final concentration of 0.1%, samples were pulse sonicated for 1 second, twenty times each. Sonicated samples were centrifuged for 10 min at 20,000g, and the supernatant was subject to sequencing grade modified trypsin (Promega) at 1:20. Thiophosphopeptides from the mixture were purified by using 40µL Thiopropyl Sepharose 6B disulfide beads (GE Healthcare) at pH 4.0. After washing, beads were eluted with 25mM DTT in 5% acetonitrile in H_2O at room temperature for 30 min. 5mM tris(2-carboxyethyl)phosphine and 0.1% formic acid were added to the eluate for the final acidification step prior to analysis by mass spectrometry.

4.2.4 Mass spectrometry analysis

Samples were submitted to the shared resources proteomics core at the Fred Hutch Cancer Center where they were analyzed by Nanoflow liquid chromatography (NanoLC) and electrospray ionization tandem mass spectrometry (MS/MS) using the LTQ-Orbitrap mass spectrometer (Thermo Scientific) as previously described[133]. Four samples (WT-CDK6, AS-CDK6, AS-

CDK6*, Cyclin D-CDK6*) were analyzed in duplicate runs for a total of eight MS runs. Acquired spectra were searched against a human peptide database with parameters including a precursor tolerance of 20 parts per million. Peptides containing thiophosphate modifications were filtered for and WT samples were compared against AS samples to generate the initial list of CDK6 candidate substrates.

4.2.5 Immunoblotting, immunoprecipitation, and in-vitro kinase assays

Immunoblotting, immunoprecipitations, and validation in-vitro kinase assays were completed as previously described (Chapter 2, 3) with the following modifications: candidate substrates were immunoprecipitated from lysate using the 12CA5 anti-HA antibody and the M2 anti-FLAG antibody.

4.2.6 Antibodies

Antibodies were purchased from suppliers and used as follows: BD Biosciences: Anti-BrdU (3D4, mouse monoclonal PerCP-Cy^{TM}5.5 conjugated, 1:100 for flow cytometry); BioLegend: HA (16B12, mouse monoclonal, 1:1,000 for IB); Santa Cruz Biotechnology: CDK6 (C-21, rabbit polyclonal, 1:1,000), Cyclin D1 (DCS-6, mouse monoclonal, 1:1,000), PCNA (PC10, mouse monoclonal HRP-conjugated, 1:1,000); Sigma: FLAG (M2, mouse monoclonal, 1:1,000 for IB, 1:250 for IP), HA (12CA5, mouse monoclonal, 1:250 for IP).

4.3 Results

4.3.1 Identification of nuclear cyclin D-CDK6 substrates in OHNSCC

We performed a large-scale mass spectrometry screen using WT-CDK6 and three replicates of AS-CDK6 to label substrates in cell nuclei with PE-ATP-γ-S. Each replicate of the AS-CDK6 samples had minor modifications to enhance kinase activity for each run: AS-CDK6, AS-CDK6*, and cyclin D-AS-CDK6*. Our screen identified 5,889 total unique peptides, and 563

of those were unique, proline directed thiophosphopeptides. Of those, 295 belonged to the WT sample and 268 belonged to the AS samples. 499 thiophosphopeptides were shared by both WT and AS samples. 317 total thiophosphopeptides were found across all AS samples (268 unique) and among those, 55 were found in the AS-CDK6 run, 46 were found in the AS-CDK6* run, and 216 were found in the cyclin D-AS-CDK6* run. This corresponded to 49 candidate proteins found by AS-CDK6, 36 candidate proteins found by AS-CDK6*, and 159 candidate proteins by cyclin D-AS-CDK6. Gene set enrichment of candidate proteins from all screens revealed a diverse array of nuclear functions including cell cycle regulation (RB1, CSNK1D, CSNK1E, NUMA1, CHEK1, CDK11A, CDK11B), mRNA processing and transport (NUP214, NUP133, NUP153, POM121), DNA replication (CDC45, ORC1, MCM4, RPA1), and more (Figure 4.3B). Of these candidate proteins, 26 were shared by two of the three runs, while eight were shared by all three (Figure 4.3A). The eight shared proteins included MKI67, SON, TFPT, NOP2, LIG3, KIAA1522, NCL, and LMNB2. A full list of all identified proteins from each screen can be found in Table 4.1.

Of note, the AS-CDK6 and AS-CDK6* returned a noticeably smaller list of thiophosphorylated peptides reflecting the limitation of endogenous cyclin D activity to phosphorylate substrates in our assay. It was only upon co-transfection with exogenous cyclin D that our third run returned the well characterized CDK6 substrate, pRb. Thus, as we proceeded in our selection of candidate substrates for validation, we primarily focused on the list returned by the cyclin D-AS-CDK6* run. Interestingly, the list of candidate proteins returned in our cyclin D-AS-CDK6* sample had considerable overlap (40 out of 162 proteins) with substrates found in a previous AS-CDK2 screen conducted in our lab[133]. This likely reflects the functional redundancy amongst different cyclin-CDKs throughout the cell cycle.

To narrow down our list of candidate substrates for validation, we focused on proteins relevant to the cell cycle. We prioritized candidates containing only a handful of SP/TP sites for ease of future mutagenesis experiments or ones that our lab had previous experience working with. With these factors in mind, we selected the candidates FOXK1, CSNK1D, and CDC45 for in-vitro kinase assay validation.

4.3.2 In-vitro validation of candidate substrates as cyclin-CDK targets

To test whether cyclin D1-CDK6 could indeed phosphorylate our candidate substrates in vitro, we first expressed FLAG-FOXK1, FLAG-CDC45, and HA-CSNK1D in HEK-293A cells by calcium-phosphate transfection and immunoprecipitated each protein using antibodies against FLAG or HA (Figure 4.4A). After confirming expression of each protein, we exposed them to an in-vitro ^{32}P-ATP kinase assay with recombinant cyclin D1-CDK6 (Sigma-Aldrich) and used GST-pRb as a positive control for the reaction. While we confirmed phosphorylation of our GST-pRb positive control, we failed to see in-vitro phosphorylation of CDC45, CSNK1D, or FOXK1 by recombinant cyclin D1-CDK6 (Figure 4.4B).

Concerned that phosphosites of the expressed proteins might be saturated while in the cell, we decided to express and purify one of our candidate substrates, CDC45, in *E. coli* so as to prevent in vivo phosphorylation of our substrate. To accomplish this, we used the pGEX-4T-1 bacterial expression plasmid and cloned in CDC45 cDNA. After purifying GST-CDC45 from bacteria, we exposed the protein to a panel of cyclin-CDK complexes for in-vitro ^{32}P-ATP kinase assays and once again used GST-pRb as positive control. Our GST-pRb positive control was phosphorylated by all cyclin-CDK complexes to varying degrees indicating differential activity of each cyclin-CDK complex (Figure 4.4A). We could only visually confirm phosphorylation of our GST-CDC45 substrate by cyclin A-CDK2 and cyclin D1-CDK6 (previously immunoprecipitated from

mammalian cell lysate) thus providing our first piece of in-vitro validation data (Figure 4.4A). While our substrate may well have been phosphorylated by the additional cyclin D3-CDK6 and commercial cyclin D1-CDK6 complexes, the activity was too low to be observed visually in this assay.

We next wanted to confirm substrate phosphorylation by mass spectrometry and identify the specific peptide(s) being phosphorylated in the reaction. Because signals from the cyclin D-CDK6 in-vitro kinase assays were comparatively weak next to cyclin A-CDK2, we opted to use the latter complex for this validation step. Once again using GST-pRb as a positive control and two separate cyclin A-CDK2 complexes (one commercial and one purified), we ran two kinase assays in parallel: i) a cold ATP kinase assay to submit to mass spectrometry, and ii) a hot ^{32}P-ATP kinase assay to confirm successful reaction. We observed successful ^{32}P-ATP labelling on both GST-pRb and GST-CDC45 with a stronger signal from our purified cyclin A-CDK2 reaction (Figure 4.5B). Thus, we cut out the corresponding band on the cold kinase assay gel (located via Coomassie staining) and submitted for mass spectrometry. Five total phospho-CDC45 peptides were identified in the MS run, and among them only one site was proline directed (S386) (Figure 4.5C). Encouragingly, among the five identified phospho-peptides, the one containing S386 had the greatest number of peptide spectral matches (31 vs. the next highest at 8), and S386 was the site identified in our original screen, thus validating this site as an in-vitro CDK substrate.

4.4 Discussion

The identification of novel CDK4 and CDK6 substrates has historically been a challenge due to the difficulty in untangling target redundancy from the more active kinases, CDK1 and CDK2. With the refinement of chemical genetic techniques beginning with Shah *et al.* in the late 1990s through to Chi *et al*. as recently as 2020, we now have the tools to better identify the

substrates of specific kinases in more physiologically relevant conditions than ever before. In this study, we sought to identify novel CDK substrates by expressing AS-CDK6 in FaDu cells and subjecting nuclear extracts to an in-vivo kinase assay with a bulky ATP analogue, PE-ATP-γ-S. We then isolated thiophosphorylated peptides and generated a list of candidate CDK6 substrates by submitting our samples to mass spectrometry and screening for thiophosphorylation at canonical proline directed CDK phosphorylation sites, i.e., SP/TP. Our three versions of this proteomic screen yielded many candidate CDK6 substrates involved in a variety of cellular processes including cell cycle regulation, mRNA processing, DNA replication, and more.

With an abundance of candidates to select for validation, we chose a substrate involved in cell cycle regulation and DNA replication with only two possible proline directed CDK phosphorylation sites, CDC45. The site identified in our screen (S386) is found within a consensus CDK phosphorylation motif (S/T-P-X-K/R), specifically, SPEK. This candidate was interesting for several reasons including its known role as part of the CMG helicase at the onset of S-phase for proper DNA replication[134]. The CMG helicase consists of CDC45, MCM hexamer, and the GINS complex and is responsible for unwinding DNA prior to replication[135,136]. Formation of the CMG relies on the recruitment of its constituents by DBF4-dependent kinase (DDK) and S-phase CDK activity, but the recruitment of CDC45 is specifically thought to be mediated by DDK activity, not CDK[137]. To our knowledge, until now, direct CDK phosphorylation of CDC45 has never been described or characterized.

Our initial attempts to validate CDC45 by transient expression in HEK-293A cells and in-vitro kinase assays proved unsuccessful (Figure 4.4B). Thus, we constructed a GST-tagged form of CDC45, expressed the protein in *E. coli*, purified GST-CDC45 out of bacterial lysate, and repeated our ^{32}P-ATP in-vitro kinase assay with a panel of cyclin-CDK complexes (Figure 4.5A).

This method proved successful, and we observed the greatest degree of phosphorylation from cyclin A-CDK2 with more limited phosphorylation from cyclin D1-CDK6, thereby validating our candidate as a CDK substrate in-vitro. After submission of our in-vitro kinase assay product to mass spectrometry, we were able to verify the specific site (S386) of CDK phosphorylation which coincided with the peptide identified in the AS-CDK6 screen (Figure 4.5C).

Significance of this phosphorylation in-vivo is currently speculative and characterizing the biological effects will be the basis for future study. As a first step, synthesis of a phospho-S386 CDC45 antibody is currently underway. As noted previously by Chi *et al*., in-situ implementation of AS-CDKs continues to be an effective method for the discovery of novel substrates at near-physiologic conditions. Overall, data from these experiments suggest a more expansive role for CDKs throughout the cell cycle than previously described. Specifically, while it is well established that cyclin D-CDK4/6 complexes primarily act on the pocket proteins to drive the G1/S transition, our proteomic screens indicate their involvement in non-canonical processes such as DNA replication initiation, among others. If confirmed, these non-canonical functions would be highly relevant to the proper application of CDK4/6 inhibitors in the clinic. Predicting tumor sensitivity and/or resistance to this class of drug remains a challenge for clinicians and scientists, and the problem is further complicated by an incomplete understanding of the full network of CDK4/6 substrates. We hope that our work here will serve as the basis for future studies to validate these candidate substrates and provide a more complete understanding of the biological consequences of CDK phosphorylation.

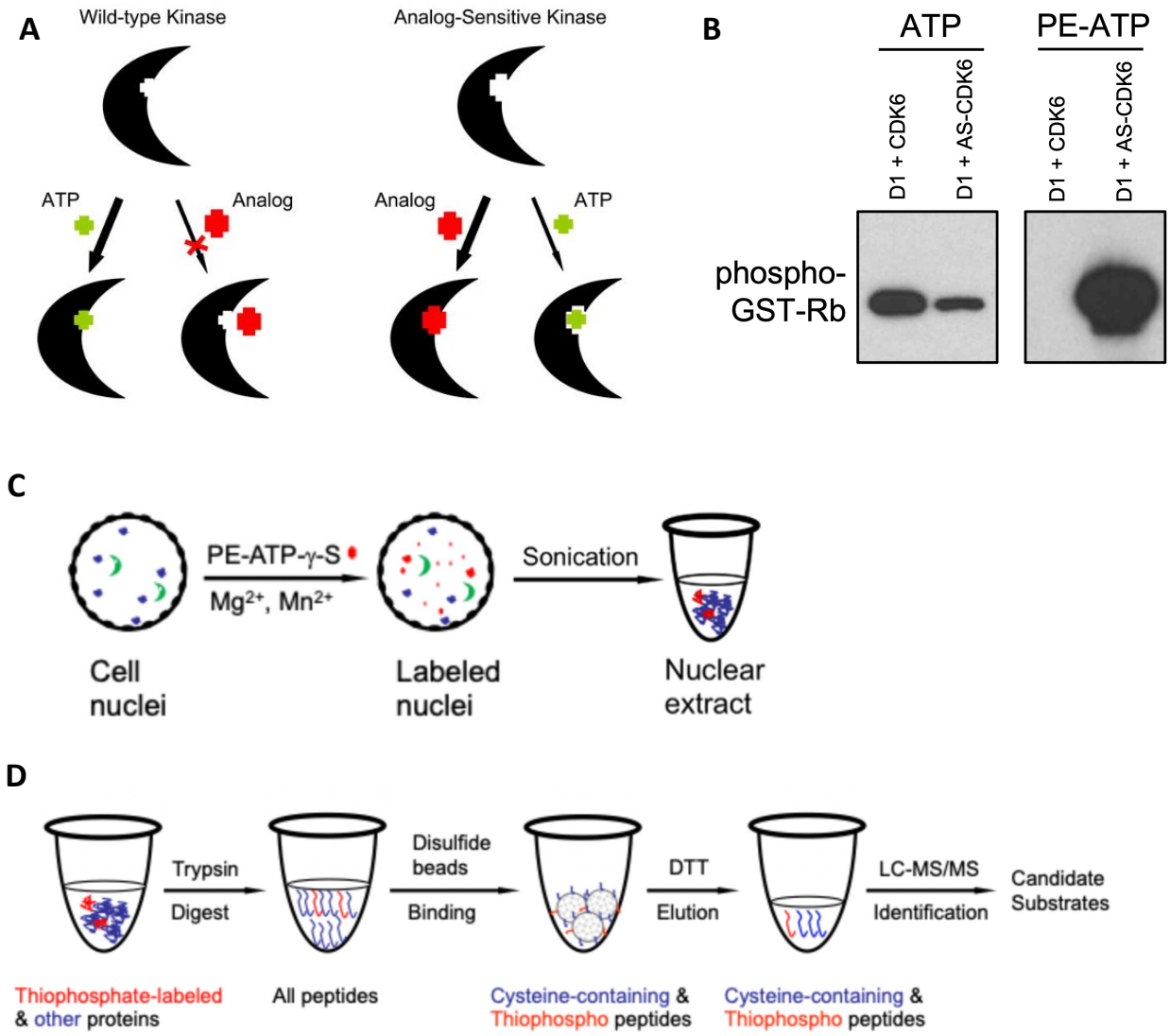

Figure 4.1 Analog sensitive CDK screen design
(A) Schematic depicting the difference between wild-type and analog-sensitive kinases. With a mutation in the ATP-binding site of the AS kinase, it can use bulky ATP analogs that will not fit in the WT binding site (original schematic designed by Chi *et al*. 2010). **(B)** In-vitro ^{32}P-ATP kinase assay demonstrating the specificity of AS-CDK6 using bulky PE-ATP-γ-S compared to WT CDK6 (data originally by Markus Welcker). **(C-D)** Schematic outlining each step of the in-vivo thiophosphorylation and peptide elution process. Cell nuclei expressing AS-CDK6 are incubated in a kinase reaction with PE-ATP-γ-S. Nuclei are then lysed and digested with trypsin to create shorter peptides. Thiophosphorylated peptides are then captured by disulfide beads, eluted with DDT, and submitted for mass spectrometry (original schematic designed by Chi *et al*. 2008).

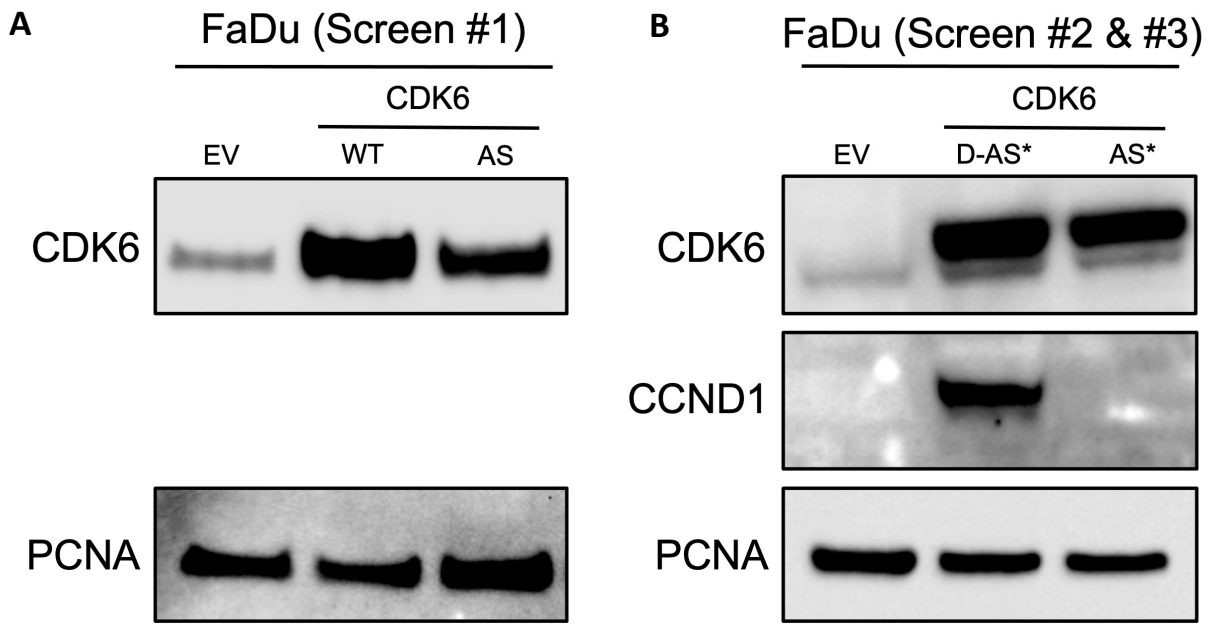

Figure 4.2 Expression of AS-CDK6 in FaDu cells
(A) Expression of WT and AS-CDK6 in FaDu cells for screen #1. **(B)** Expression of cyclin D and/or AS-CDK6* in FaDu cells for screens #2 and #3.

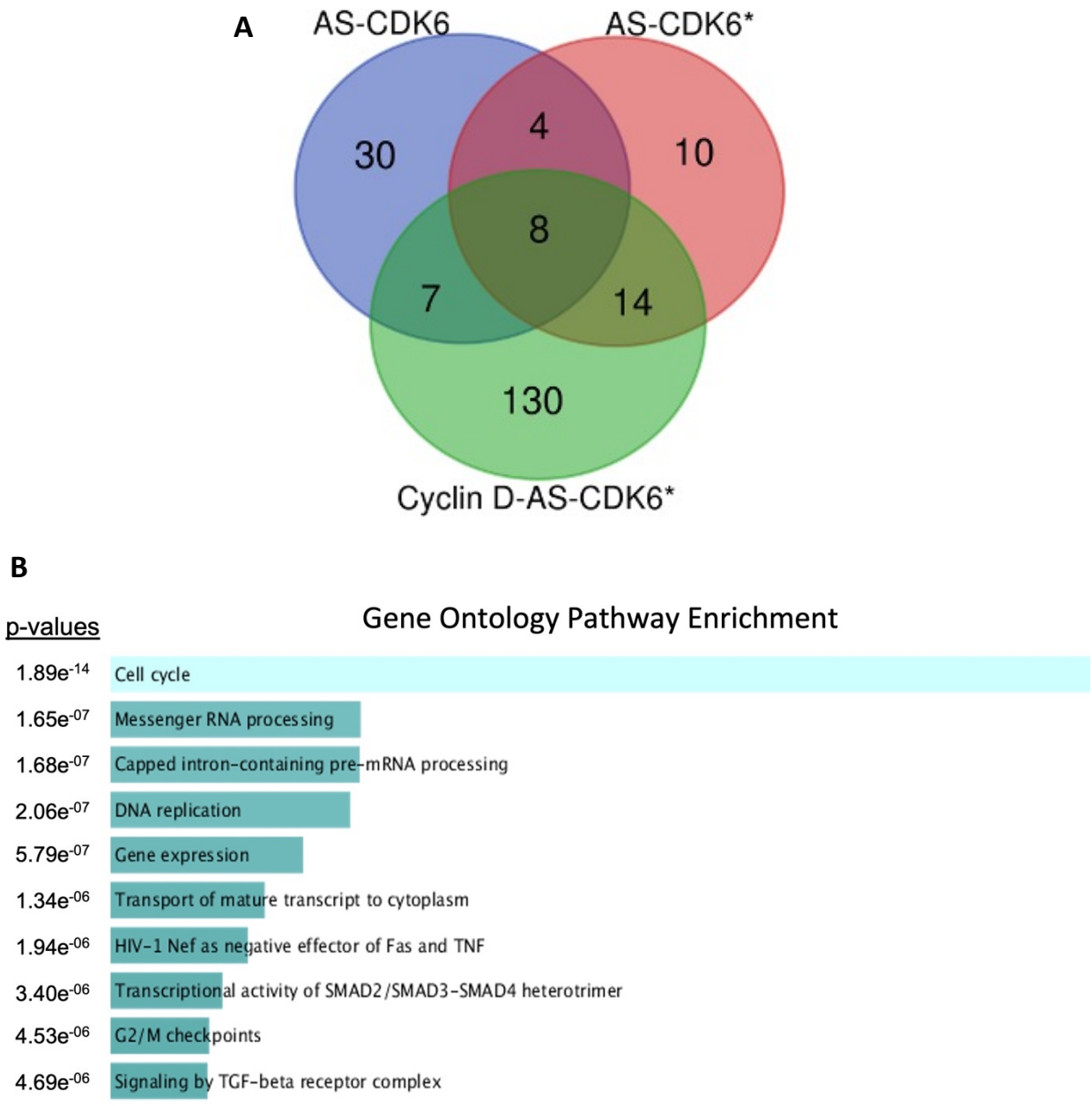

Figure 4.3 AS-CDK6 mass spectrometry screen results
(A) Venn diagram showing overlap of identified proteins from each of the three proteomic screens. **(B)** Gene ontology terms from all screens that were enriched for specific biological functions ranked in order by decreasing p-value.

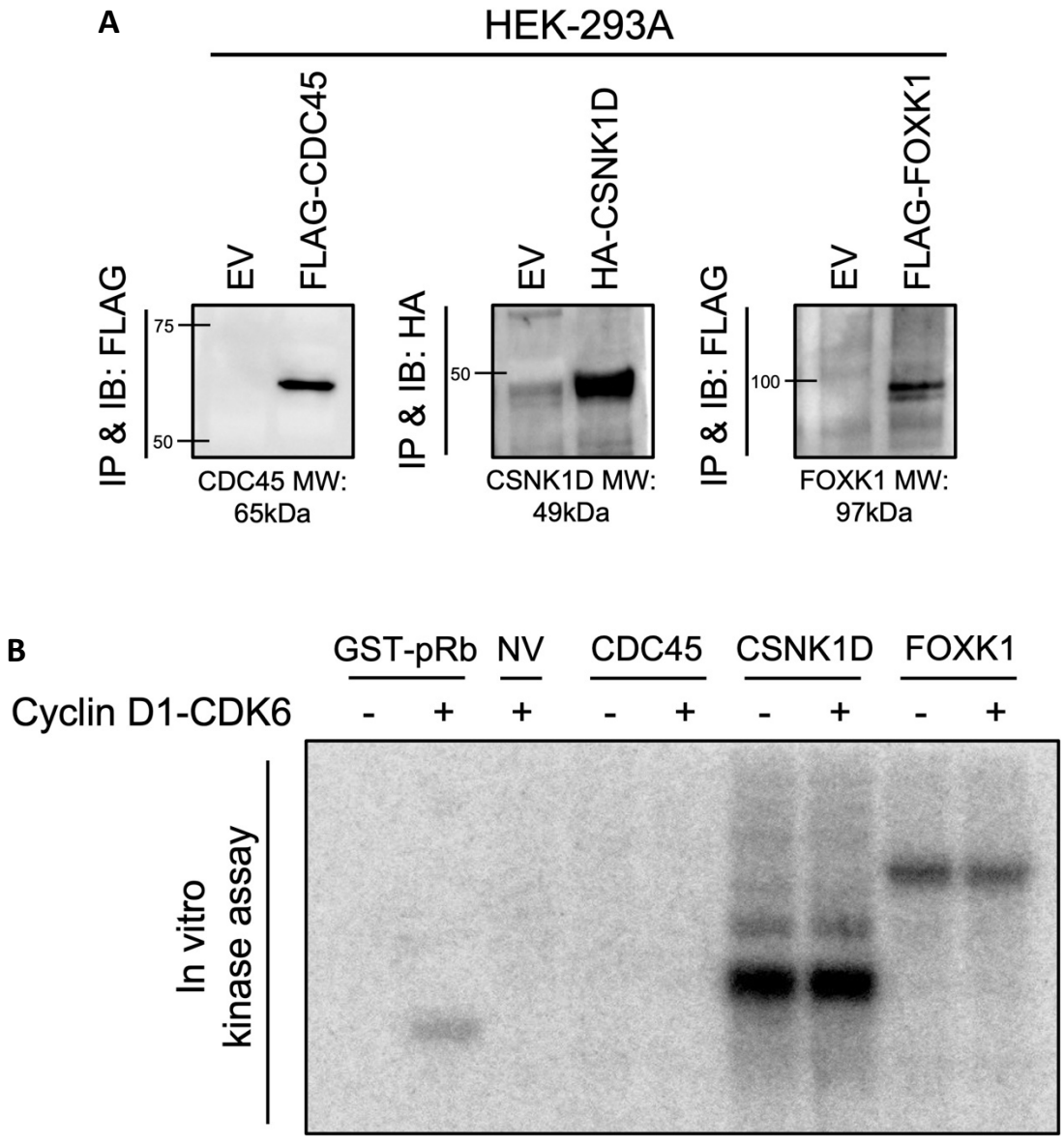

Figure 4.4 In-vitro kinase assay validation of candidate substrates
(A) Expression of three candidate substrates (CDC45, CSNK1D, FOXK1) in HEK-293A cells tagged with either FLAG or HA. Substrates were expressed in HEK-293A via calcium phosphate transfection, immunoprecipitated with antibodies against either FLAG or HA, and then blotted with antibodies against those epitopes. **(B)** In-vitro ^{32}P-ATP kinase assays with commercial cyclinD1-CDK6, immunoprecipitated candidate substrates, and GST-pRb as a positive control substrate. No differences were observed in any of the candidate substrates between +/- cyclin D1-CDK6. Bands outside of the GST-pRb + cyclin D1-CDK6 lane most likely represent non-specific ^{32}P binding.

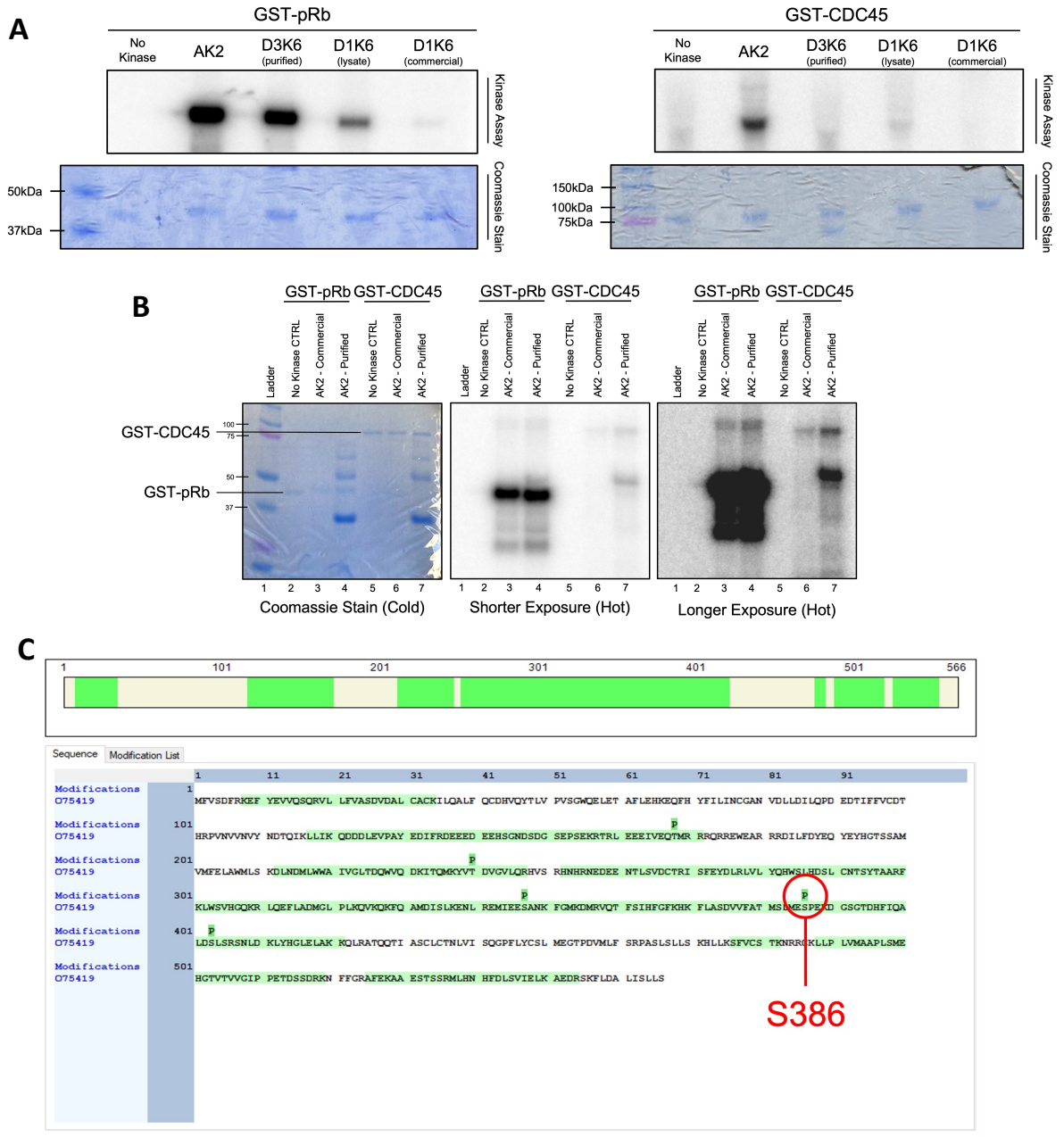

Figure 4.5 In-vitro and mass spectrometry validation of CDC45
(A) In-vitro ^{32}P-ATP kinase assays with a panel of cyclin-CDK complexes and GST-CDC45 purified from *E. coli* (GST-pRb once again used as positive control). Coomassie stains of the kinase assay gels were used to confirm the presence and location of substrates used in the reactions. **(B)** In-vitro ^{32}P-ATP kinase assays with cyclin A-CDK2 and GST-CDC45 used for mass spectrometry submission. After confirming phosphorylation of our substrate with longer exposure of the gel on the phospho-imaging plate, we cut out the corresponding Coomassie stained band and submitted our sample for analysis by mass spectrometry. **(C)** Results from mass spectrometry analysis revealed five phosphorylated peptides including the site identified in our original proteomic screen, S386. Peptide spectral matches at this site (31) were significantly greater than at the next highest site (8).

Table 4.1 Full protein ID list from each mass spectrometry screen

AS-CDK6
ANKLE2
ATP7A
CCDC88C
CDK11A
CDK12
CEP57
CHRM4
DSC3
EDNA1BP2
EZH2
FAM27D1
FANCD2
HNRNPK
INCENP
INO80E
IQSEC2
ITPRID2
JUNB
KCNH6
KIAA1522
KMT5A
KRI1
LIG3
LMNB2
MAP2K7
MIPEP
MKI67
MORN1
MPHOSPH9
MPRIP
MRNIP
NCL
NDRG2
NFATC2
NOP2
NOP58
OCLN
POLR3A
RFX7
SLC12A2
SON
SOX3
SPAG5
SPEN
SRRM2
ST3GAL5
TCOF1
TFPT
VPS26A

AS-CDK6*
ATP7A
BUD13
CCDC88C
CDC5L
CSMD2
DNM1
DNMT1
EFCAB14
ESYT2
FAM27D1
FNDC3A
KIAA1522
KPNA2
LIG3
LMNB2
MED1
MIPEP
MKI67
MUC16
NCL
NOC2L
NOP2
PCIF1
PHF2
PLS1
PSIP1
RBL1
RBM33
RIN1
SON
TAF3
TFPT
TJP2
TMPO
WRNIP1
ZXDC

Cyclin D-AS-CDK6*		
ADAM9	LIG3	RBMXL1
ADAR	LIN9	RFX7
AKIRIN2	LMNB1	RIF1
ARHGAP11A	LMNB2	RNF169
ARID1A	LOXL3	RPA1
ATXN2L	MARK2	RREB1
BAZ2A	MCM4	RRP1B
BCL11A	MED14	SAMD1
BRCA1	MICALL1	SARG
CDC45	MISP	SART1
CDC5L	MKI67	SEPTIN9
CDCA8	MSL3	SF3B1
CDK11B	MTA2	SIPA1L1
CDK12	NCL	SMNDC1
CENPC	NCOR2	SMTN
CENPF	NDE1	SNW1
CHAMP1	NELFA	SNX19
CHEK1	NELFE	SON
CLSPN	NFATC2IP	SPEN
CSNK1D	NFIC	SRSF9
CSNK1E	NOC2L	STAG2
CTTN	NOLC1	SUGP1
DHX38	NOP2	TANC1
DIDO1	NUMA1	TASOR2
DNMT1	NUP133	TCOF1
DNPEP	NUP153	TFDP1
E2F4	NUP214	TFPT
EFCAB14	NUSAP1	TJP2
ELAVL1	OCLN	TMPO
EP400	ORC1	TNKS1BP1
ESYT2	OSBPL9	TONSL
FADS1	PABPN1	TOPBP1
FNDC3A	PATL2	TPR
FOXK1	PBRM1	TPX2
GATAD2A	PDS5A	TRIM29
GTSE1	PHF2	UBN2
HBEGF	PHF8	UNG
HELLS	PKP3	UTP14A
HNRNPK	PLEKHG3	VCPIP1
IFI16	POLDIP3	WIPF2
IK	POM121	WIZ
INCENP	PPFIA1	WRNIP1
IRF2BP2	PPP1CC	WWTR1
KANSL3	PPP1R12A	XRN2
KDM2A	PPP1R13L	YAP1
KDM3B	PRC1	YTHDC2
KDM5A	PRRC2A	ZBTB21
KIAA1522	PSIP1	ZC3H11A
KIF14	RAD18	ZC3H3
KIF22	RAVER1	ZHX2
KPNA2	RB1	ZMYM3
LARP1	RBL1	ZNF385A
LEMD2	RBM33	ZNF609

Chapter 5. Summary and Future Directions

Aberrations in the cell cycle that contribute to carcinogenesis are commonly found in most cancers and OHNSCCs are no exception. These molecular changes in cancer represent an opportunity for researchers to differentially target tumorigenic cells while preserving healthy tissue and minimizing sequelae related to traditional therapies (i.e., chemo, radiation, surgery). Thus, in my dissertation, I sought to uncover mechanisms that cancer cells rely on for replication and how they may adapt to targeted therapies that are currently in the clinical trial pipeline.

First, we conducted a genome-wide CRISPR-Cas9 screen to better understand the mechanisms contributing to replication stress failure in cells with constitutively active CDK2. This project was motivated by previous work completed in the Clurman lab where a colon cancer cell line (HCT-116) was engineered to express a mutant form of CDK2 (CDK2AF) that lacked the inhibitory phosphorylation sites used by Wee1 and Myt1 to regulate its activity. CDK2AF cells showed exquisite sensitivity to drugs that induce replication stress such as HU or APH ultimately resulting in senescence[80]. Adding to those data was a synthetic-lethal model of cancer therapy that demonstrated the vulnerability of p53 deficient OHNSCC to targeted inhibition of the Wee1 kinase[74]. Inhibition of Wee1 prevents regulation of CDK1/2 activity thereby driving these cancer cells toward mitotic catastrophe and apoptosis, especially when paired with low doses of traditional cytotoxic agents like docetaxel and/or cisplatin[78]. To understand why unregulated CDK2 activity induces sensitivity to replication stress, we employed a CRISPR-Cas9 in CDK2AF cells to see what downstream mediators, when knocked out, might rescue growth after HU treatment. Initial data from our screen pointed to specific pathways like apoptosis and MAP kinase signaling, however, validating individual hits proved challenging. After curating a list of screen hits for follow-up experiments that included *CASP8*, *DR4*, *DR5*, *MAPK14*, and *MAP2K3*, we

generated individual knockouts of each gene in CDK2AF cells to study their response to HU. Unfortunately, none of our knockouts successfully rescued CDK2AF cells from HU hypersensitivity when we assayed cell growth and DNA damage accumulation. From these results, we were forced to conclude that CDK2 either does not have a single downstream target that contributes to replication stress failure (but it may have several that act simultaneously to produce the observed phenotype), or that the effect of CDK2 activity in this context is inhibitory in which case our screen would be unable to detect such a target. One interesting finding, however, came about when we revisited the hit *FAM122A*, a highly conserved protein in mammals that inhibits the phosphatase activity of PP2A[88]. When we knocked out *FAM122A* from CDK2AF cells and treated them with HU, we once again failed to rescue post-treatment growth, but we did observe a noticeable drop in DNA damage accumulation. Published literature on FAM122A is sparse, but it has been implicated in regulating Wee1 protein levels[89]. It is therefore possible that CDK2 promotes FAM122A mediated degradation of Wee1 during replication stress thereby preventing proper G2/M checkpoint activation. As a result, cells accumulate DNA damage which is then reversed when we knock out *FAM122A*. Future studies that build on these findings will first have to validate FAM122A either as a direct or indirect target of CDK2 that is activated upon replication stress. Another approach for this line of inquiry might include a CRISPR activation screen rather than the knockout screen we conducted. This would address the possibility that the ultimate effect of CDK2 activity leading to replication stress failure might actually be inhibitory. In other words, CDK2 might be shutting off certain pathways that would otherwise allow, for example, proper DNA damage response. It would therefore be possible to find such mediators by repeating our screen protocol but using a CRISPR activation library in lieu of the knockout library we employed.

The second and third major projects of my dissertation were related to the critical cyclin-CDK complexes that regulate the G1/S transition (cyclin D-CDK4/6 and cyclin E-CDK2). The mutational profiles of HPV-negative OHNSCCs have made these cancers good candidates for the application of CDK4/6 inhibitors such as palbociclib, abemaciclib, and ribociclib. As such, over 15 clinical trials using this class of drug have either been completed or are currently undergoing investigation in OHNSCC. While initial data from these trials looked promising, issues with intrinsic and/or acquired resistance have been reported[58,62]. Resistance to CDK4/6 inhibitors has also been observed in other cancers which has prompted researchers to find potential biomarkers that may predict tumor response. Several mechanisms have been hypothesized such as *RB1* loss and *CCNE1* amplification, but data are often correlational, and some reports are in direct conflict with one another. Of particular interest to our lab is the claim that high cyclin E-CDK2 activity can bypass CDK4/6 inhibition by directly phosphorylating pRb on its own. Because *CCNE1* amplification is rare in OHNSCC, we hypothesized that loss of Fbw7, an E3 ubiquitin ligase that regulates cyclin E degradation, would confer resistance to palbociclib in OHNSCC.

To test this idea, we engineered a panel of OHNSCC cell lines with various genomic modifications including *RB1* knockout, *FBXW7* knockout, and stable overexpression of cyclin E. Cells lacking pRb, including HPV-positive lines, consistently demonstrated strong resistance to palbociclib in EdU incorporation and cell outgrowth assays thus establishing a baseline for comparison against our other modifications. To our surprise, cells with high levels of cyclin E (either through stable overexpression or as a consequence of *FBXW7* knockout) consistently demonstrated a minor but reproducible level of resistance to palbociclib as compared to our pRb null cells. We were unable to demonstrate a bypass effect of cyclin E when the D-type cyclins were inhibited by palbociclib, which stands in stark contrast to the increasingly accepted idea that

high cyclin E levels confer robust resistance to CDK4/6 inhibition. Thus, our data suggest that high cyclin E activity on its own is insufficient to generate CDK4/6 inhibitor resistance, and that it must be accompanied by other molecular changes in order to confer strong resistance. Future studies to uncover co-mutations that accompany high cyclin E activity will more accurately depict the nature of CDK4/6 inhibitor resistance in such cells and tumors. To accomplish this, a CRISPR knockout and/or activation screen in our high cyclin E cell lines can serve as an initial step to find candidate co-mediators of palbociclib resistance. A list of candidate mediators from these screens could then be cross-referenced with patient tumor sample data to identify the most likely pathways that are altered in conjunction with high cyclin E to confer resistance. It is also possible that cyclin E mediated resistance is somehow modulated by the immune system and/or tumor microenvironment. If true, our cell culture and in-vitro experiments would be unable to recapitulate the observed resistance in patient tumors. Therefore, we have initiated a study in mice that will include our engineered cell lines, and we will measure tumor response to palbociclib in a more biologically relevant setting. If we observe more robust palbociclib resistance in cells with high cyclin E, we can then begin exploring changes in tumor microenvironment that would help explain this difference.

Finally, we conducted a proteomic screen to identify novel CDK6 substrates in OHNSCC. Our approach built on the chemical-genetic method developed by Shokat and colleagues who engineered analog-sensitive kinases that could differentially utilize ATP analogs in their assays[130,132]. Our screen revealed over 100 candidate substrates, many of which were unsurprisingly involved in cell cycle regulation. Of particular interest to us was the candidate, CDC45, which is a critical component of the CMG helicase involved in initiating DNA replication. To our knowledge, no group has previously described CDK phosphorylation of CDC45 despite

the presence of a consensus phosphorylation sequence in the protein (SPEK). Using mass spectrometry, we successfully validated CDC45 as a CDK substrate in-vitro and have initiated the development of a phospho-specific antibody on residue S386. With this tool, future studies will be tasked with validating CDC45 as a bona fide CDK substrate in-vivo. The next challenge will then be to understand the biological consequences of CDK phosphorylation on S386. Questions in this line of research will include: which CDK is primarily responsible for phosphorylation on this site? Is phosphorylation on S386 an activating or inhibitory event? And what induces phosphorylation on this site specifically?

Although cell cycle research has been ongoing for many decades, there are an abundance of critical questions that remain unanswered. Particularly as the next generation of targeted therapeutics are developed and deployed, it is essential that we continue to elaborate the mechanistic rationale for the application of these drugs. I believe my work outlined in this dissertation has advanced our understanding of cyclin-CDK biology while also providing a sound basis for future research projects in this field.

References

1. Stallaert W, Kedziora KM, Taylor CD, et al. The structure of the human cell cycle. *Cell Systems*. 2022;13(3):230-240.e3. doi:10.1016/j.cels.2021.10.007
2. Matthews HK, Bertoli C, de Bruin RAM. Cell cycle control in cancer. *Nature Reviews Molecular Cell Biology*. 2022;23(1):74-88. doi:10.1038/s41580-021-00404-3
3. Pardee AB. A restriction point for control of normal animal cell proliferation. *Proceedings of the National Academy of Sciences*.1974;71:1286-1290. doi: 10.1073/pnas.71.4.1286
4. Bartek J, Bartkova J, Lukas J. The retinoblastoma protein pathway and the restriction point. *Current Opinion in Cell Biology.* 1996;8:805-814. doi: 10.1016/s0955-06/S0955-0674(96)80081-0
5. Suski JM, Braun M, Strmiska V, Sicinski P. Targeting cell-cycle machinery in cancer. *Cancer Cell*. 2021;39(6):759-778. doi:10.1016/j.ccell.2021.03.010
6. Hall M, Peters G. Genetic alterations of cyclins, cyclin dependent kinases, and Cdk inhibitors in human cancer. *Advances in Cancer Research*. 1996;(68):67-108. doi: 10.1016/S0065-230X(08)60352-8
7. Lim S, Kaldis P. Cdks, cyclins and CKIs: Roles beyond cell cycle regulation. *Development (Cambridge)*. 2013;140(15):3079-3093. doi:10.1242/dev.091744
8. Malumbres M. Cyclin-dependent kinases. *Genome Biology*. 2014;15(6). doi:10.1186/gb4184
9. Brown NR, Noble MEM, Lawrie AM, et al. Effects of phosphorylation of threonine 160 on cyclin-dependent kinase 2 structure and activity. *Journal of Biological Chemistry*. 1999;274(13):8746-8756. doi: 10.1074/jbs.274.13.8746
10. Liu K, Zheng M, Lu R, et al. The role of CDC25C in cell cycle regulation and clinical cancer therapy: A systematic review. *Cancer Cell International*. 2020;20(1). doi:10.1186/s12935-020-01304-w
11. Denicourt C, Dowdy SF. Cip/Kip proteins: More than just CDKs inhibitors. *Genes and Development*. 2004;18(8):851-855. doi:10.1101/gad.1205304
12. Cánepa ET, Scassa ME, Ceruti JM, et al. INK4 proteins, a family of mammalian CDK inhibitors with novel biological functions. *IUBMB Life*. 2007;59(7):419-426. doi:10.1080/15216540701488358
13. Serra S, Chetty R. p16. *Journal of Clinical Pathology*. 2018;71(10):853-858. doi:10.1136/jclinpath-2018-205216
14. Georgakilas AG, Martin OA, Bonner WM. p21: A two-faced genome guardian. *Trends in Molecular Medicine*. 2017;23(4):310-319. doi:10.1016/j.molmed.2017.02.001
15. Razavipour SF, Harikumar KB, Slingerland JM. p27 as a transcriptional regulator: New roles in development and cancer. *Cancer Research*. 2020;80(17):3451-3458. doi:10.1158/0008-5472.CAN-19-3663
16. Cobrinik D. Pocket proteins and cell cycle control. *Oncogene*. 2005;24(17):2796-2809. doi:10.1038/sj.onc.1208619
17. Rubin SM, Sage J, Skotheim JM. Integrating old and new paradigms of G1/S control. *Molecular Cell*. 2020;80(2):183-192. doi:10.1016/j.molcel.2020.08.020
18. Hume S, Dianov GL, Ramadan K. A unified model for the G1/S cell cycle transition. *Nucleic Acids Research*. 2020;48(22):12483-12501. doi:10.1093/nar/gkaa1002

19. Chung M, Liu C, Yang HW, Köberlin MS, Cappell SD, Meyer T. Transient hysteresis in CDK4/6 activity underlies passage of the restriction point in G1. *Molecular Cell*. 2019;76(4):562-573.e4. doi:10.1016/j.molcel.2019.08.020
20. Cappell SD, Chung M, Jaimovich A, Spencer SL, Meyer T. Irreversible APCCdh1 inactivation underlies the point of no return for cell-cycle entry. *Cell*. 2016;166(1):167-180. doi:10.1016/j.cell.2016.05.077
21. Giacinti C, Giordano A. RB and cell cycle progression. *Oncogene*. 2006;25(38):5220-5227. doi:10.1038/sj.onc.1209615
22. Iyer DR, Rhind N. The intra-S checkpoint responses to DNA damage. *Genes (Basel)*. 2017;8(2). doi:10.3390/genes8020074
23. Bartek J, Lukas J. DNA damage checkpoints: from initiation to recovery or adaptation. *Current Opinion in Cell Biology*. 2007;19(2):238-245. doi:10.1016/j.ceb.2007.02.009
24. Chatterjee N, Walker GC. Mechanisms of DNA damage, repair, and mutagenesis. *Environmental and Molecular Mutagenesis*. 2017;58(5):235-263. doi:10.1002/em.22087
25. Saldivar JC, Hamperl S, Bocek MJ, et al. An intrinsic S/G 2 checkpoint enforced by ATR. *Science*. 2018;361(6404):806-810. doi: 10.1126/science.aap9346
26. Schönthal AH, Stark GR, Taylor WR. Analyzing the G2/M checkpoint. *Methods in Molecular Biology*. 2004;280:51-82. doi: 10.1385/1-59259-788-2:051
27. Schmidt M, Rohe A, Platzer C, Najjar A, Erdmann F, Sippl W. Regulation of G2/M transition by inhibition of WEE1 and PKMYT1 Kinases. *Molecules*. 2017;22(12). doi:10.3390/molecules22122045
28. Hanahan D, Weinberg RA. The hallmarks of cancer. *Cell*. 2000;100(1):57-70. doi: 10.1016/S0092-8674(00)81683-9
29. Kandoth C, McLellan MD, Vandin F, et al. Mutational landscape and significance across 12 major cancer types. *Nature*. 2013;502(7471):333-339. doi:10.1038/nature12634
30. Zhou X, Hao Q, Lu H. Mutant p53 in cancer therapy-the barrier or the path. *Journal of Molecular Cell Biology*. 2019;11(4):293-305. doi:10.1093/jmcb/mjy072
31. Peyressatre M, Prével C, Pellerano M, Morris MC. Targeting cyclin-dependent kinases in human cancers: From small molecules to peptide inhibitors. *Cancers (Basel)*. 2015;7(1):179-237. doi:10.3390/cancers7010179
32. Kourea HP, Orlow I, Scheithauer BW, Cordon-Cardo C, Woodruff JM. Deletions of the INK4A gene occur in malignant peripheral nerve sheath tumors but not in neurofibromas. *American Journal of Pathology*. 1999;155(6):1855-1860. doi: 10.1016/S0002-9440(10)65504-6
33. Migita T, Oda Y, Naito S, Tsuneyoshi M. Low expression of p27Kip1 is associated with tumor size and poor prognosis in patients with renal cell carcinoma. *Cancer*. 2002;94(4):973-979. doi:10.1002/cncr.10338
34. Kirla RM, Haapasalo HK, Kalimo H, Salminen EK. Low expression of p27 indicates a poor prognosis in patients with high-grade astrocytomas. *Cancer*. 2003;97(3):644-648. doi:10.1002/cncr.11079
35. Ferlay J, Colombet M, Soerjomataram I, et al. Estimating the global cancer incidence and mortality in 2018: GLOBOCAN sources and methods. *International Journal of Cancer*. 2019;144(8):1941-1953. doi:10.1002/ijc.31937
36. Johnson DE, Burtness B, Leemans CR, Lui VWY, Bauman JE, Grandis JR. Head and neck squamous cell carcinoma. *Nature Reviews Disease Primers*. 2020;6(1). doi:10.1038/s41572-020-00224-3

37. Siegel RL, Miller KD, Fuchs HE, Jemal A. Cancer statistics, 2021. *CA: A Cancer Journal for Clinicians*. 2021;71(1):7-33. doi:10.3322/caac.21654
38. Stransky N, Egloff AM, Tward AD, et al. The mutational landscape of head and neck squamous cell carcinoma. *Science*. 2011;333(6046):1157-1160. doi:10.1126/science.1208130
39. Lawrence MS, Sougnez C, Lichtenstein L, et al. Comprehensive genomic characterization of head and neck squamous cell carcinomas. *Nature*. 2015;517(7536):576-582. doi:10.1038/nature14129
40. Leemans CR, Snijders PJF, Brakenhoff RH. The molecular landscape of head and neck cancer. *Nature Reviews Cancer*. 2018;18(5):269-282. doi:10.1038/nrc.2018.11
41. Cheng H, Yang X, Si H, et al. Genomic and transcriptomic characterization links cell lines with aggressive head and neck cancers. *Cell Reports*. 2018;25(5):1332-1345.e5. doi:10.1016/j.celrep.2018.10.007
42. Cramer JD, Burtness B, Le QT, Ferris RL. The changing therapeutic landscape of head and neck cancer. *Nature Reviews Clinical Oncology*. 2019;16(11):669-683. doi:10.1038/s41571-019-0227-z
43. Grégoire V, Langendijk JA, Nuyts S. Advances in radiotherapy for head and neck cancer. *Journal of Clinical Oncology*. 2015;33(29):3277-3284. doi:10.1200/JCO.2015.61.2994
44. Nguyen-Tan PF, Zhang Q, Ang KK, et al. Randomized phase III trial to test accelerated versus standard fractionation in combination with concurrent cisplatin for head and neck carcinomas in the radiation therapy oncology group 0129 trial: Long-term report of efficacy and toxicity. *Journal of Clinical Oncology*. 2014;32(34):3858-3867. doi:10.1200/JCO.2014.55.3925
45. Quon H, Leong T, Haselow R, Leipzig B, Cooper J, Forastiere A. Phase III study of radiation therapy with or without Cis-platinum in patients with unresectable squamous or undifferentiated carcinoma of the head and neck: An intergroup trial of the Eastern Cooperative Oncology Group (E2382). *International Journal of Radiation Oncology Biology Physics*. 2011;81(3):719-725. doi:10.1016/j.ijrobp.2010.06.038
46. Burtness B, Goldwasser MA, Flood W, Mattar B, Forastiere AA. Phase III randomized trial of cisplatin plus placebo compared with cisplatin plus cetuximab in metastatic/recurrent head and neck cancer: An eastern cooperative oncology group study. *Journal of Clinical Oncology*. 2005;23(34):8646-8654. doi:10.1200/JCO.2005.02.4646
47. Cohen EEW, Soulières D, le Tourneau C, et al. Pembrolizumab versus methotrexate, docetaxel, or cetuximab for recurrent or metastatic head-and-neck squamous cell carcinoma (KEYNOTE-040): a randomised, open-label, phase 3 study. *The Lancet*. 2019;393(10167):156-167. doi:10.1016/S0140-6736(18)31999-8
48. Leblanc O, Vacher S, Lecerf C, et al. Biomarkers of cetuximab resistance in patients with head and neck squamous cell carcinoma. *Cancer Biology and Medicine*. 2020;17(1):208-217. doi:10.20892/j.issn.2095-3941.2019.0153
49. Kok VC. Current understanding of the mechanisms underlying immune evasion from PD-1/PD-L1 immune checkpoint blockade in head and neck cancer. *Frontiers in Oncology*. 2020;10. doi:10.3389/fonc.2020.00268
50. Kovatcheva M, Liu DD, Dickson MA, et al. MDM2 turnover and expression of ATRX determine the choice between quiescence and senescence in response to CDK4 inhibition. *Oncotarget*. 2015;6(10):8226-8243. doi: 10.18632/oncotarget.3364

51. Knudsen ES, Witkiewicz AK. The strange case of CDK4/6 inhibitors: Mechanisms, resistance, and combination strategies. *Trends in Cancer*. 2017;3(1):39-55. doi:10.1016/j.trecan.2016.11.006
52. McCartney A, Migliaccio I, Bonechi M, et al. Mechanisms of resistance to CDK4/6 inhibitors: Potential implications and biomarkers for clinical practice. *Frontiers in Oncology*. 2019;9. doi:10.3389/fonc.2019.00666
53. Zainal NS, Lee BKB, Wong ZW, et al. Effects of palbociclib in oral squamous cell carcinoma and the role of PIK3CA in conferring resistance. *Cancer Biology and Medicine*. 2019;16(2):264-275. doi:10.20892/j.issn.2095-3941.2018.0257
54. Robinson AM, Rathore R, Redlich NJ, et al. Cisplatin exposure causes c-Myc-dependent resistance to CDK4/6 inhibition in HPV-negative head and neck squamous cell carcinoma. *Cell Death and Disease*. 2019;10(11). doi:10.1038/s41419-019-2098-8
55. Álvarez-Fernández M, Malumbres M. Mechanisms of sensitivity and resistance to CDK4/6 inhibition. *Cancer Cell*. 2020;37(4):514-529. doi:10.1016/j.ccell.2020.03.010
56. Michel L, Ley J, Wildes TM, et al. Phase i trial of palbociclib, a selective cyclin dependent kinase 4/6 inhibitor, in combination with cetuximab in patients with recurrent/metastatic head and neck squamous cell carcinoma. *Oral Oncology*. 2016;58:41-48. doi:10.1016/j.oraloncology.2016.05.011
57. Adkins D, Ley J, Neupane P, et al. Palbociclib and cetuximab in platinum-resistant and in cetuximab-resistant human papillomavirus-unrelated head and neck cancer: a multicentre, multigroup, phase 2 trial. *The Lancet Oncology*. 2019;20(9):1295-1305. doi:10.1016/S1470-2045(19)30405-X
58. Swiecicki PL, Durm G, Bellile E, Bhangale A, Brenner JC, Worden FP. A multi-center phase II trial evaluating the efficacy of palbociclib in combination with carboplatin for the treatment of unresectable recurrent or metastatic head and neck squamous cell carcinoma. *Investigational New Drugs*. 2020;38(5):1550-1558. doi:10.1007/s10637-020-00898-2
59. Adkins DR, Lin JC, Sacco A, et al. Palbociclib and cetuximab compared with placebo and cetuximab in platinum-resistant, cetuximab-naïve, human papillomavirus-unrelated recurrent or metastatic head and neck squamous cell carcinoma: A double-blind, randomized, phase 2 trial. *Oral Oncology*. 2021;115. doi:10.1016/j.oraloncology.2021.105192
60. Pandey K, An HJ, Kim SK, et al. Molecular mechanisms of resistance to CDK4/6 inhibitors in breast cancer: A review. *International Journal of Cancer*. 2019;145(5):1179-1188. doi:10.1002/ijc.32020
61. van Caloen G, Schmitz S, Baroudi M el, et al. Preclinical activity of ribociclib in squamous cell carcinoma of the head and neck. *Molecular Cancer Therapeutics*. 2020;19(3):777-789. doi:10.1158/1535-7163.MCT-19-0695
62. Oppelt P, Ley JC, Worden F, et al. Palbociclib and cetuximab in cetuximab-resistant human papillomavirus-related oropharynx squamous-cell carcinoma: A multicenter phase 2 trial. *Oral Oncology*. 2021;114. doi:10.1016/j.oraloncology.2020.105164
63. Olanich ME, Sun W, Hewitt SM, Abdullaev Z, Pack SD, Barr FG. CDK4 amplification reduces sensitivity to CDK4/6 inhibition in fusion-positive rhabdomyosarcoma. *Clinical Cancer Research*. 2015;21(21):4947-4959. doi:10.1158/1078-0432.CCR-14-2955
64. Yang C, Li Z, Bhatt T, et al. Acquired CDK6 amplification promotes breast cancer resistance to CDK4/6 inhibitors and loss of ER signaling and dependence. *Oncogene*. 2017;36(16):2255-2264. doi:10.1038/onc.2016.379

65. Taylor-Harding B, Aspuria PJ, Agadjanian H, et al. Cyclin E1 and RTK/RAS Signaling Drive CDK Inhibitor Resistance via Activation of E2F and ETS. *Oncotarget*. 2015;6(2):696-714. doi: 10.18632/oncotarget.2673
66. Herrera-Abreu MT, Palafox M, Asghar U, et al. Early adaptation and acquired resistance to CDK4/6 inhibition in estrogen receptor-positive breast cancer. *Cancer Research*. 2016;76(8):2301-2313. doi:10.1158/0008-5472.CAN-15-0728
67. Guarducci C, Bonechi M, Benelli M, et al. Cyclin E1 and Rb modulation as common events at time of resistance to palbociclib in hormone receptor-positive breast cancer. *NPJ Breast Cancer*. 2018;4(1). doi:10.1038/s41523-018-0092-4
68. Chandarlapaty S, Razavi P. Cyclin e mRNA: Assessing cyclin-dependent kinase (CDK) activation state to elucidate breast cancer resistance to CDK4/6 Inhibitors. *Journal of Clinical Oncology*. 2019;37(14):1148-1150. doi:10.1200/JCO.19.00090
69. Guiley KZ, Stevenson JW, Lou K, et al. P27 allosterically activates cyclin-dependent kinase 4 and antagonizes palbociclib inhibition. *Science*. 2019;366(6471). doi:10.1126/science.aaw2106
70. Cerami E, Gao J, Dogrusoz U, et al. The cBio cancer genomics portal: An open platform for exploring multidimensional cancer genomics data. *Cancer Discovery*. 2012;2(5):401-404. doi:10.1158/2159-8290.CD-12-0095
71. Gao J, Arman Aksoy B, Dogrusoz U, et al. Integrative analysis of complex cancer genomics and clinical profiles using the cBioPortal. *Science Signaling*. 2013;6(269):1-19. doi: 10.1126/scisignal.2004088.
72. Stafford ND, Ashman JNE, Macdonald AW, Ell SR, Monson JRT, Greenman J. Genetic Analysis of Head and Neck Squamous Cell Carcinoma and Surrounding Mucosa. *JAMA Archives of Otohinolaryngology-Head & Neck Surgery*. 1999;125(12):1341-1348. doi: 10.1001/archotol.125.12.1341
73. Yokobori T, Mimori K, Iwatsuki M, et al. Copy number loss of FBXW7 is related to gene expression and poor prognosis in esophageal squamous cell carcinoma. *International Journal of Oncology*. 2012;41(1):253-259. doi:10.3892/ijo.2012.1436
74. Moser R, Xu C, Kao M, et al. Functional kinomics identifies candidate therapeutic targets in head and neck cancer. *Clinical Cancer Research*. 2014;20(16):4274-4288. doi:10.1158/1078-0432.CCR-13-2858
75. Kao M, Green C, Sidorova J, Méndez E. Strategies for targeted therapy in head and neck squamous cell carcinoma using WEE1 inhibitor AZD1775. *JAMA Otolaryngology - Head and Neck Surgery*. 2017;143(6):631-633. doi:10.1001/jamaoto.2016.4563
76. Xu C, Nikolova O, Basom RS, et al. Functional precision medicine identifies novel druggable targets and therapeutic options in head and neck cancer. *Clinical Cancer Research*. 2018;24(12):2828-2843. doi:10.1158/1078-0432.CCR-17-1339
77. Mendez E, Rodriguez CP, Kao MC, et al. A phase I clinical trial of AZD1775 in combination with neoadjuvant weekly docetaxel and cisplatin before definitive therapy in head and neck squamous cell carcinoma. *Clinical Cancer Research*. 2018;24(12):2740-2748. doi:10.1158/1078-0432.CCR-17-3796
78. Diab A, Kao M, Kehrli K, Kim HY, Sidorova J, Mendez E. Multiple defects sensitize p53-deficient head and neck cancer cells to the Wee1 kinase inhibition. *Molecular Cancer Research*. 2019;17(5):1115-1128. doi:10.1158/1541-7786.MCR-18-0860

79. Diab A, Gem H, Swanger J, et al. FOXM1 drives HPV+ HNSCC sensitivity to WEE1 inhibition. *Proceedings of the National Academy of Sciences*. 2020;117(45):28287-28296. doi:10.1073/pnas.2013921117
80. Hughes BT, Sidorova J, Swanger J, Monnat RJ, Clurman BE. Essential role for Cdk2 inhibitory phosphorylation during replication stress revealed by a human Cdk2 knockin mutation. *Proceedings of the National Academy of Sciences*. 2013;110(22):8954-8959. doi:10.1073/pnas.1302927110
81. Sanjana NE, Shalem O, Zhang F. Improved vectors and genome-wide libraries for CRISPR screening. *Nature Methods*. 2014;11(8):783-784. doi:10.1038/nmeth.3047
82. Li W, Xu H, Xiao T, et al. MAGeCK enables robust identification of essential genes from genome-scale CRISPR/Cas9 knockout screens. *Genome Biology*. 2014;15(12):554. doi:10.1186/s13059-014-0554-4
83. Doench JG, Fusi N, Sullender M, et al. Optimized sgRNA design to maximize activity and minimize off-target effects of CRISPR-Cas9. *Nature Biotechnology*. 2016;34(2):184-191. doi:10.1038/nbt.3437
84. Henry CM, Martin SJ. Caspase-8 Acts in a Non-enzymatic Role as a Scaffold for Assembly of a Pro-inflammatory "FADDosome" Complex upon TRAIL Stimulation. *Molecular Cell*. 2017;65(4):715-729.e5. doi:10.1016/j.molcel.2017.01.022
85. Monie TP, Bryant CE, Bryant C. Caspase-8 functions as a key mediator of inflammation and pro-IL-1b processing via both canonical and non-canonical pathways. 2015;265(1):181-193. doi: 10.1111/imr.12284
86. Cuollo L, Antonangeli F, Santoni A, Soriani A. The senescence-associated secretory phenotype (Sasp) in the challenging future of cancer therapy and age-related diseases. *Biology (Basel)*. 2020;9(12):1-16. doi:10.3390/biology9120485
87. Anerillas C, Abdelmohsen K, Gorospe M. Regulation of senescence traits by MAPKs. *Geroscience*. 2020;42(2):397-408. doi:10.1007/s11357-020-00183-3
88. Fan L, Liu MH, Guo M, et al. FAM122A, a new endogenous inhibitor of protein phosphatase 2A. *Oncotarget*. 2016;7(39):63887-63900. doi: 10.18632/oncotarget.11698
89. Li F, Kozono D, Deraska P, et al. CHK1 inhibitor blocks phosphorylation of FAM122A and promotes replication stress. *Molecular Cell*. 2020;80(3):410-422.e6. doi:10.1016/j.molcel.2020.10.008
90. Fassl A, Geng Y, Sicinski P. CDK4 and CDK6 kinases: From basic science to cancer therapy. *Science*. 2022;375(6577). doi:10.1126/science.abc1495
91. Ammazzalorso A, Agamennone M, de Filippis B, Fantacuzzi M. Development of CDK4/6 inhibitors: A five years update. *Molecules*. 2021;26(5). doi:10.3390/molecules26051488
92. van Caloen G, MacHiels JP. Potential role of cyclin-dependent kinase 4/6 inhibitors in the treatment of squamous cell carcinoma of the head and neck. *Current Opinion in Oncology*. 2019;31(3):122-130. doi:10.1097/CCO.0000000000000513
93. Konecny GE, Winterhoff B, Kolarova T, et al. Expression of p16 and retinoblastoma determines response to CDK4/6 inhibition in ovarian cancer. *Clinical Cancer Research*. 2011;17(6):1591-1602. doi:10.1158/1078-0432.CCR-10-2307
94. Franco J, Witkiewicz AK, Knudsen ES. CDK4/6 Inhibitors Have Potent Activity in Combination with Pathway Selective Therapeutic Agents in Models of Pancreatic Cancer. *Oncotarget*. 2014;5(15):6512-25. doi: 10.18632/oncotarget.2270

95. Gomatou G, Trontzas I, Ioannou S, Drizou M, Syrigos N, Kotteas E. Mechanisms of resistance to cyclin-dependent kinase 4/6 inhibitors. *Molecular Biology Reports*. 2021;48(1):915-925. doi:10.1007/s11033-020-06100-3
96. Dean JL, Thangavel C, McClendon AK, Reed CA, Knudsen ES. Therapeutic CDK4/6 inhibition in breast cancer: Key mechanisms of response and failure. *Oncogene*. 2010;29(28):4018-4032. doi:10.1038/onc.2010.154
97. O'leary B, Cutts RJ, Liu Y, et al. The genetic landscape and clonal evolution of breast cancer resistance to palbociclib plus fulvestrant in the PALOMA-3 trial. *Cancer Discovery*. 2018;8(11):1390-1403. doi:10.1158/2159-8290.CD-18-0264
98. Munger K, Werness BA, Dyson N, Phelps WC, Harlow E, Howley PM. Complex formation of c-myc papillomavirus E7 proteins with the retinoblastoma tumor suppressor gene product. *EMBO Journal*. 1989;8(13):4099-4105. doi:10.1002/j.1460-2075.1989.tb08594.x
99. Levine M, Noll M, Dyson NA, Howley PM, Monger K, Harlow ED. The human papilloma virus-16 E7 oncoprotein is able to bind to the retinoblastoma gene product. *Science*. 1989;243(4893):934-937. doi: 10.1126/science.2537532
100. Boyer SN, Wazer DE, Band2 V. E7 Protein of human papilloma virus-16 induces degradation of retinoblastoma protein through the ubiquitin-proteasome pathway. *Cancer Research*. 1996;56(20):4620-4624. PMID: 8840974
101. Gonzalez SL, Stremlau M, He X, Basile JR, Münger K. Degradation of the retinoblastoma tumor suppressor by the human papillomavirus type 16 E7 oncoprotein is important for functional inactivation and is separable from proteasomal degradation of E7. *Journal of Virology*. 2001;75(16):7583-7591. doi:10.1128/jvi.75.16.7583-7591.2001
102. Geng Y, Whoriskey W, Park MY, et al. Rescue of Cyclin D1 Deficiency by Knockin Cyclin E. *Cell*. 1999;97(6)767-777. doi: 10.1016/s0092-8674(00)80788-6
103. Min A, Kim JE, Kim YJ, et al. Cyclin E overexpression confers resistance to the CDK4/6 specific inhibitor palbociclib in gastric cancer cells. *Cancer Letters*. 2018;430:123-132. doi:10.1016/j.canlet.2018.04.037
104. Turner NC, Liu Y, Zhu ; Zhou, et al. Cyclin E1 expression and palbociclib efficacy in previously treated hormone receptor-positive metastatic breast cancer. *Journal of Clinical Oncology*. 2019;37(14):1169-1178. doi: 10.1200/JCO.18.00925
105. Cristofanilli M, Turner NC, Bondarenko I, et al. Fulvestrant plus palbociclib versus fulvestrant plus placebo for treatment of hormone-receptor-positive, HER2-negative metastatic breast cancer that progressed on previous endocrine therapy (PALOMA-3): final analysis of the multicentre, double-blind, phase 3 randomised controlled trial. *The Lancet Oncology*. 2016;17(4):425-439. doi:10.1016/S1470-2045(15)00613-0
106. Finn RS, Crown JP, Lang I, et al. The cyclin-dependent kinase 4/6 inhibitor palbociclib in combination with letrozole versus letrozole alone as first-line treatment of oestrogen receptor-positive, HER2-negative, advanced breast cancer (PALOMA-1/TRIO-18): A randomised phase 2 study. *The Lancet Oncology*. 2015;16(1):25-35. doi:10.1016/S1470-2045(14)71159-3
107. Finn RS, Cristofanilli M, Ettl J, et al. Treatment effect of palbociclib plus endocrine therapy by prognostic and intrinsic subtype and biomarker analysis in patients with bone-only disease: a joint analysis of PALOMA-2 and PALOMA-3 clinical trials. *Breast Cancer Research and Treatment*. 2020;184(1):23-35. doi:10.1007/s10549-020-05782-4

108. Labaer J, Garrett MD, Stevenson LF, et al. New functional activities for the p21 family of CDK inhibitors. *Genes and Development*. 1997;11(7):847-862. doi: 10.1101/gad.11.7.847
109. Larrea MD, Liang J, da Silva T, et al. Phosphorylation of p27 Kip1 regulates assembly and activation of cyclin D1-Cdk4 . *Molecular and Cellular Biology*. 2008;28(20):6462-6472. doi:10.1128/mcb.02300-07
110. Welcker M, Clurman BE. FBW7 ubiquitin ligase: A tumour suppressor at the crossroads of cell division, growth, and differentiation. *Nature Reviews Cancer*. 2008;8(2):83-93. doi:10.1038/nrc2290
111. Yeh CH, Bellon M, Nicot C. FBXW7: A critical tumor suppressor of human cancers. *Molecular Cancer*. 2018;17(1). doi:10.1186/s12943-018-0857-2
112. Minella AC, Swanger J, Bryant E, Welcker M, Hwang H, Clurman BE. p53 and p21 form an inducible barrier that protects cells against Cyclin E-Cdk2 deregulation. *Current Biology*. 2002;12(21):1817-1827. doi: 10.1016/s0960-9822(02)01225-3
113. Sakaue-Sawano A, Kurokawa H, Morimura T, et al. Visualizing spatiotemporal dynamics of multicellular cell-cycle progression. *Cell*. 2008;132(3):487-498. doi:10.1016/j.cell.2007.12.033
114. Lin CJ, Grandis JR, Carey TE, et al. Head and neck squamous cell carcinoma cell lines: Established models and rationale for selection. *Head and Neck*. 2007;29(2):163-188. doi:10.1002/hed.20478
115. Barretina J, Caponigro G, Stransky N, et al. The Cancer Cell Line Encyclopedia enables predictive modelling of anticancer drug sensitivity. *Nature*. 2012;483(7391):603-607. doi:10.1038/nature11003
116. Forbes SA, Bindal N, Bamford S, et al. COSMIC: Mining complete cancer genomes in the catalogue of somatic mutations in cancer. *Nucleic Acids Research*. 2011;39:D945-950. doi:10.1093/nar/gkq929
117. Rouillard AD, Gundersen GW, Fernandez NF, et al. The harmonizome: a collection of processed datasets gathered to serve and mine knowledge about genes and proteins. *Database (Oxford)*. 2016. doi:10.1093/database/baw100
118. Sriraman A, Dickmanns A, Najafova Z, Johnsen SA, Dobbelstein M. CDK4 inhibition diminishes p53 activation by MDM2 antagonists. *Cell Death and Disease*. 2018;9(9). doi:10.1038/s41419-018-0968-0
119. Wang B, Varela-Eirin M, Brandenburg SM, et al. Pharmacological CDK4/6 inhibition reveals a p53-dependent senescent state with restricted toxicity. *The EMBO Journal*. 2022;41(6). doi:10.15252/embj.2021108946
120. DeMichele A, Clark AS, Tan KS, et al. CDK 4/6 Inhibitor palbociclib (PD0332991) in Rb+ advanced breast cancer: Phase II activity, safety, and predictive biomarker assessment. *Clinical Cancer Research*. 2015;21(5):995-1001. doi:10.1158/1078-0432.CCR-14-2258
121. Crozier L, Foy R, Mouery BL, et al. CDK4/6 inhibitors induce replication stress to cause long-term cell cycle withdrawal. *The EMBO Journal*. 2022;41(6). doi:10.15252/embj.2021108599
122. Narasimha AM, Kaulich M, Shapiro GS, Choi YJ, Sicinski P, Dowdy SF. Cyclin D activates the Rb tumor suppressor by mono-phosphorylation. *Elife*. 2014;3. doi:10.7554/elife.02872

123. Chang F, Lee JT, Navolanic PM, et al. Involvement of PI3K/Akt pathway in cell cycle progression, apoptosis, and neoplastic transformation: A target for cancer chemotherapy. *Leukemia*. 2003;17(3):590-603. doi:10.1038/sj.leu.2402824
124. Clark AS, Makhlin I, DeMichele A. Setting the pick: Can PI3K inhibitors circumvent CDK4/6 inhibitor resistance? *Clinical Cancer Research*. 2021;27(2):371-373. doi:10.1158/1078-0432.CCR-20-3624
125. Pennycook BR, Barr AR. Palbociclib-mediated cell cycle arrest can occur in the absence of the CDK inhibitors p21 and p27. *Open Biology*. 2021;11(11). doi:10.1098/rsob.210125
126. Weinberg RA. The retinoblastoma protein and cell cycle control. *Cell*. 199581(3):323-330. doi: 10.1016/0092-8674(95)90385-2
127. Zelivianski S, Cooley A, Kall R, Jeruss JS. Cyclin-dependent kinase 4-mediated phosphorylation inhibits Smad3 activity in cyclin D-overexpressing breast cancer cells. *Molecular Cancer Research*. 2010;8(10):1375-1387. doi:10.1158/1541-7786.MCR-09-0537
128. Anders L, Ke N, Hydbring P, et al. A systematic screen for CDK4/6 substrates links FOXM1 phosphorylation to senescence suppression in cancer cells. *Cancer Cell*. 2011;20(5):620-634. doi:10.1016/j.ccr.2011.10.001
129. The I, Ruijtenberg S, Bouchet BP, et al. Rb and FZR1/Cdh1 determine CDK4/6-cyclin D requirement in C. elegans and human cancer cells. *Nature Communications*. 2015;6. doi:10.1038/ncomms6906
130. Shah K, Liu YI, Deirmengian C, Shokat KM. Engineering unnatural nucleotide specificity for rous sarcoma virus tyrosine kinase to uniquely label its direct substrates. *Proceedings of the National Acadmy of Sciences*. 1997;94(8):3565-3570. doi: 10.1073/pnas.94.8.3565
131. Chi Y, Welcker M, Hizli AA, Posakony JJ, Aebersold R, Clurman BE. Identification of CDK2 substrates in human cell lysates. *Genome Biology*. 2008;9(10). doi:10.1186/gb-2008-9-10-r149
132. Chi Y, Clurman BE. Mass spectrometry-based identification of protein kinase substrates utilizing engineered kinases and thiophosphate labeling. *Current Protocols in Chemical Biology*. 2010;2(4):219-234. doi:10.1002/9780470559277.ch100151
133. Chi Y, Carter JH, Swanger J, Mazin A v, Moritz RL, Clurman BE. A novel landscape of nuclear human CDK2 substrates revealed by in situ phosphorylation. 2020;6(16):1-10. doi: 10.1126/sciadv.aaz9899
134. Fragkos M, Ganier O, Coulombe P, Méchali M. DNA replication origin activation in space and time. *Nature Reviews Molecular Cell Biology*. 2015;16(6):360-374. doi:10.1038/nrm4002
135. Simon AC, Sannino V, Costanzo V, Pellegrini L. Structure of human Cdc45 and implications for CMG helicase function. *Nature Communications*. 2016;7. doi:10.1038/ncomms11638
136. Köhler C, Koalick D, Fabricius A, et al. Cdc45 is limiting for replication initiation in humans. *Cell Cycle*. 2016;15(7):974-985. doi:10.1080/15384101.2016.1152424
137. Heller RC, Kang S, Lam WM, Chen S, Chan CS, Bell SP. Eukaryotic origin-dependent DNA replication in vitro reveals sequential action of DDK and S-CDK kinases. *Cell*. 2011;146(1):80-91. doi:10.1016/j.cell.2011.06.012